Melting of Ice and Formation of Lateral Cavity during *In Situ* Burning in Ice-Infested Waters

Hamed Farmahini Farahani

A Dissertation

Submitted to the Faculty

of the

WORCESTER POLYTECHNIC INSTITUTE

in partial fulfillment of the requirements for the

Degree of Doctor of Philosophy

in

Fire Protection Engineering

December 2017

Approved:

_____

Professor Ali S. Rangwala, Worcester Polytechnic Institute, Advisor

_____

Professor Grunde Jomaas, Denmark Technical University, Co-Advisor

_____

Professor Vasudevan Raghavan, Indian Institute of Technology, Committee Member

_____

Professor Morris R. Flynn, University of Alberta, Committee Member

_____

Professor Tahar El-Korchi, Worcester Polytechnic Institute, Committee member

Preface

This dissertation is submitted for the degree of Doctor of Philosophy at the Worcester Polytechnic Institute (WPI). The Ph.D. study was conducted between January 2014 and December 2017 at the Department of Fire Protection Engineering, under the supervision of:

Ali S. Rangwala, principal supervisor, Professor, Department of Fire Protection Engineering, Worcester Polytechnic Institute, USA

Grunde Jomaas, co-supervisor, Professor, Department of Civil Engineering, Technical University of Denmark, Denmark and School of Engineering BRE Centre for Fire Safety Engineering, University of Edinburgh, United Kingdom

The following articles have been published or were under review at the time of submitting this dissertation:

1. **Hamed Farmahini Farahani**, Grunde Jomaas, Ali Rangwala, "Effects of convective motion in n-octane pool fires in an ice cavity", Combustion and Flame 162 (12), 4643-4648, 2015. (Presented in Chapter 3).
2. **Hamed Farmahini Farahani**, Ali Rangwala, Grunde Jomaas, "Convection-driven melting in an n-octane pool fire bounded by an ice wall", Combustion and Flame, 179, 219-227, 2017. (Presented in Chapter 4).
3. **Hamed Farmahini Farahani**, Grunde Jomaas, Ali Rangwala, A study on burning behavior and convective flows in Methanol pool fires bound by ice, International Oil Spill Conference Proceedings, 2017 (1), 1983-1998.
4. **Hamed Farmahini Farahani**, Yanyun Fu, Grunde Jomaas, Ali Rangwala, "Convection-driven cavity formation in ice adjacent to externally heated flammable and non-flammable liquids", (Presented in Chapter 5).
5. **Hamed Farmahini Farahani**, Jose Torero, Grunde Jomaas, Ali Rangwala, Estimating lateral cavity length in oil spill cleanup operations (Presented in Chapter 6).

Abstract

The ice melting and lateral cavity formation caused by *in situ* burning (ISB) of liquid fuels in ice-infested waters was studied in order to improve predictions on the removal efficiency of this oil spill mitigation method. For this purpose, several experimental studies were conducted to increase the fundamental understanding of the mechanisms that lead to ice melting and lateral cavity formation. The findings of the experimental studies provided the required knowledge to mathematically formulate the ice melting problem. Mathematical scaling analysis of ice melting during burning of oils in the vicinity of ice was performed to create a tool to estimate the extent of melting that occurs during ISB in ice-infested waters.

A series of lab-scale experiments were designed to systematically investigate the ice melting problem. The first set of experiments were conducted in cylindrical shaped ice cavities with a 5.7 cm diameter. Burning of n-octane from ignition to natural extinction and the subsequent geometry change of the ice, fuel thickness, and fuel temperature were measured. The preliminary experimental observations showed that the melting of the ice walls was higher in areas where the fuel layer was in contact with ice compared with places of flame exposure. Based on these observations, a hypothesis that suggested the convective flows in the liquid fuel (driven mainly by surface tension and buoyancy) were contributing in melting of the ice was proposed to explain the origins of the lateral cavity. To evaluate this hypothesis, two dimensionless numbers (Marangoni and Rayleigh) were calculated as the indicators of the mechanisms of convection in the fuel layer. The comparison between the melting speed and these dimensionless numbers indicated surface tension driven flow was dominant while the role of buoyancy was negligible.

In another set of experiments, Particle Image Velocimetry (PIV) was used to study the flow structure within the liquid-phase of n-octane pool fire bound on one side by an ice wall. Experiments were conducted in a square glass tray (9.6 cm × 9.6 cm × 5 cm) with a 3 cm thick ice wall placed on one side of the tray. Burning rate, flame height, and melting front velocity were measured to analyze the effect of heat feedback on melting of the ice. The melting rate of the ice increased from 0.6 cm/min for the first 50 seconds after ignition to 1 cm/min for the rest of burning period. Meanwhile, the measurement of the burning rates and flame heights showed two distinctive behaviors; a growth period from self-sustained

ignition to the peak mass loss rate (first 50 seconds after ignition) followed by a steady phase from the peak of mass loss rate until the manual extinguishment. Similarly, the flow field measurements by a 2-dimensional PIV system indicated the existence of two different flow regimes. In the moments before ignition of the fuel, coupling of surface tension and buoyancy forces led to a combined one roll structure in the fuel. This was when a single large vortex was observed in the flow field. After ignition the flow field began transitioning toward an unstable flow regime (separated) with an increase in number of vortices around the ice wall. As the burning rate/flame height increased the velocity and evolving flow patterns enhanced the melting rate of the ice wall. Experimentally determined temperature contours showed that a hot zone with thickness of approximately 3 mm was present below the free surface, corresponding to the multi-roll location. The change in the flow field behavior was found to relate to the melting front velocity of ice.

To further study the lateral cavity phenomena, a parametric experimental study on melting of ice adjacent to liquids exposed from above to various heat fluxes was conducted in order to understand the role of liquid properties in formation of cavities in ice. Multiple liquids with wide variety and range of thermophysical properties were used in order to identify the key influential properties on melting. The melting rate of the ice and penetration speed of the liquid in a transparent glass tray (70 mm × 70 mm × 45 mm) with a 20 mm thick ice wall (70 mm × 50 mm × 20 mm) was measured. The melting front velocities obtained from experiments were then compared to surface flow velocities of liquids obtained through a scaling analysis of the surface flow to elucidate the influence of the various thermophysical properties of the liquids on ice melting. The surface velocity of the liquids correlated well to the melting front velocities of the ice which showed a clear relationship between the flow velocity and melting front velocity.

As the final step of this work, to extend the findings of the experimental studies conducted herein to larger sizes comparable to realistic situations in the Arctic, an order of magnitude scaling analysis was performed to obtain the extent of ice melting. The scaling considered the heat feedback from the flame to fuel surface, the convective heat transfers toward the ice, and the melting energy continuity of ice. The existing experimental data on the size of lateral cavity were also collected and were correlated to the results of the scaling analysis using a nonlinear regression fitting technique. The mathematical correlation that was obtained by the scaling analysis can be used to predict the size of the lateral cavity for a

given fuel, pool fire diameter, and burning time. This correlation will provide a predictive tool to estimate the size of a potential lateral cavity formed during ISB of a given spill scenario.

In general, the ability to predict the ice melting caused by burning of spilled oil in ice-infested waters is of great practical importance for assessment of the response outcome. This would assist with quantifying the geometry change of the burning medium which in turn will define oil burning rate and extinction condition. Knowledge of burning behavior and extinction condition indicate the burned volume which can directly be used to define the removal effectiveness of ISB. Nevertheless, this analysis was conducted on a generic interaction of oil and ice and the specific details that are observed in actual application of ISB in ice-infested waters were neglected for simplicity. Extending the outcome of this study to more specific (scenario-based) oil-in-ice situation and improving the predictability of the melting correlation with large-scale experiments are the next steps to develop this work.

Acknowledgments

My Acknowledgment to the Danish Council for Independent Research for funding this study as a part of the DDF-1335-00282 grant and also Fire Protection Engineering department of WPI for funding the last year of the program.

I would like to express my gratitude to my advisor, Professor Ali S. Rangwala for his supervision, patience, and providing the means for doing research. Also I like to thank my co-advisor, Professor Grunde Jomaas for his guidance and hosting me during my visit to Technical University of Denmark in Fall of 2015. It is a sincere pleasure to thank Professor Jose L. Torero who provided useful insight during my research visit at University of Maryland in the summer of 2017.

There are many others whom I have worked with or interacted with on a daily basis. These individuals are the friends I have found in Combustion lab of WPI, Fire Lab of DTU, and Fire Protection department of University of Maryland. It will be very hard for me to name each of them but I want to thank them all here.

Finally, I would also like to thank my lovely parents, beautiful sister and her family, and two awesome brothers. They are amazing in any possible way and their support has encouraged me to keep on going.

Contents

List of Tables

List of Figures

1 Introduction

1.1 Overview of oil spill response

An *oil spill* is the accidental discharge of a liquid petroleum hydrocarbon into the environment, due to human activity, and is a form of pollution. The term is usually applied to marine oil spills, where oil is released into the ocean or coastal waters, but spills may also occur on land. Oil spills have become a frequent occurrence because of heavy use of oil and petroleum products. Spilled oil can have a broad range of environmental (destroying marine and coastal ecosystems) and socioeconomic (fishing and tourism) ramifications. Thus, the prevention of oil spills has become an important part of protecting the environment, and as a result government and industry funded programs have been in place to research and reduce accidents that lead to spills [1]. Despite the intensive efforts in minimizing the risk of spills, experts estimate that 30% to 50% of oil spills are either directly or indirectly caused by human error, with 20% to 40% of all spill caused by equipment failure [2].

Although it is critical to prevent oil spills from happening, methods for containing and cleaning them must also be effectively determined. Oil spills vary in size and impact, and they require established response plans and sufficient technical knowledge for successful remediation. An effective response plan will prevent dire damages to the environment and is intended to countermeasure the spill in three steps: 1) stopping the flow of oil, 2) containing the oil, and 3) cleaning the oil [3, 4]. Depending on the cause for the spill, steps 1 and 2 may be unnecessary, but the cleanup stage (step 3) is the primary step and the most important part of every response plan. In cases where natural processes such as oil-eating bacteria and wave action disperse and degrade oil more effectively than human intervention and if the spill is well offshore and is considered to have limited environmental impact, a "no action except for monitoring" plan may also be adopted [5].

The three main cleanup strategies developed for recovery of a marine oil spill are categorized as follows [6-8]:

- Mechanical recovery (booms, skimmers, oil-waste separators, adsorbents)
- Chemical treatment agents (dispersants, emulsion breakers)
- *In situ* burning (ISB)

Mechanical recovery operation involves the physical containment of the oil within natural or man-made barriers and then removal of the oil from the water surface. It can involve two or more large ships, trained responders, hundreds of meters of containment boom, skimming systems, pumping equipment, temporary storage devices and disposal systems [9]. The objective of containment is to concentrate oil to a thickness that will permit recovery. Mechanical recovery systems involve three major components: containment barriers, recovery systems, and secondary storage for the recovered oil and water [2]. Except for rare occasions, mechanical recovery operations seldom exceed 20% efficiency and that is with heavy deployment of equipment and personnel [6]. After the Macondo (Deepwater Horizon) oil spill, a total of 24% was cleaned up, and only 3% was by mechanical recovery [10].

Dispersants is a common term used for chemical agents (containing three components: surfactants, solvents, and other additives) sprayed or applied onto oil slicks on water to accelerate the process of natural dispersion. The solvent components reduce viscosity of the slick and surfactants promote emulsification and formation of tiny oil droplets in the water column and prevent the re-coalescence of droplets into slicks because of their surfactant content [11]. In Deepwater Horizon about 2,900,000 liters of dispersant were used at the well head and on the surface and 16% of the oil is claimed to be cleaned with this method [9]. In an oil spill response plan, the dispersants method is chosen to reduce the amount of the floating oil to minimize the damages to shorelines, wildlife, and other sensitive resources. In general, oil pollution of shorelines is environmentally less desirable than dispersing the oil into the water column, where effects are limited and short-lived [3]. Nevertheless, dispersants remain to be a controversial cleanup method as their effectiveness is not clear [12] and its use is promoted by biased entities such as research centers associated with oil companies [13].

Mechanical recovery and use of dispersants for large spills are expensive and labor intensive [14, 15]. In addition to the numerous and different types of equipment that may be required, a mixture of oil, water and debris is generated during the recovery process that pose choices for disposal (recycling, landfill or incineration). Despite the costly equipment and low efficiency, public perception is in favor of mechanical recovery because it is seen as a safe and clean way of spill cleanup.

In situ Burning (ISB) is another method to fight oil spills, and it dates back to 1958 [16]. It involves the intentional and controlled burning of the oil that has spilled, at the location of the spill. The first major attempt to cleanup accidental spills by ISB method was in association with the Exxon Valdez spill in 1989 [17] with an estimated 57,000-114,000 liters of North Slope crude oil being removed. ISB is a countermeasure technique that has infrequently been used on marine oil spills but its successful use during the Deepwater Horizon spill demonstrated a rather high potential with removal of 220,000 to 310,000 barrels of oil which accounted for about 5% of the total oil spill [18, 19]. Compared to the other cleanup methods, higher removal efficiencies are proclaimed for ISB, especially with the development of fire-resistant oil containment booms [20]. However, there are limitations due to environmental conditions both operationally and as a result of the changes in oil characteristics over time (weathering and formation of water-in-oil emulsions).

In summary, the most effective cleanup method is dependent on a number of parameters such as the spilled product, location of the spill, response time, environmental conditions and availability and capability of the response technologies.

1.2 Oil spill cleanup in the Arctic

The area above the Arctic Circle is underlain by sedimentary basins and continental shelves that hold enormous oil and natural gas resources [21]. Overall, the Arctic is estimated to contain between 44 and 157 billion barrels of the recoverable oil which can be about 13% of the world's undiscovered oil [22]. The evaluated gas and oil reservoirs in the Arctic are mostly offshore under less than 500 meters of water. As a result, the Arctic is of interest for oil exploration. But, remoteness and technical difficulty, coupled with the current abundance of low-cost petroleum, have minimized the explorations offshore of the Arctic

[21]. Although recent retreat of polar ice is changing the ecosystem and improving the prospect of easier petroleum exploration and development [23], most of the oil producers have tentatively withdrawn from exploring the Arctic in the past few years due to the high extraction costs and relatively low price of oil. Nevertheless, activities related to the oil industry (polar and sub-polar vessel traffic and oil and gas exploration) are expected to grow in future [24] and the risk for pollution due to the oil spills will therefore increase. For the fragile Arctic ecosystem that is already affected by the climate change [25], an oil spill could result in devastating long term consequences and a proper response plan must be sought.

The Arctic waters are among the most challenging regions for oil spill recovery. In addition to the presence of ice in different conditions (drift/pack ice, fast ice, ice fractures, etc.), heavy winds and limited daylight conditions during winter impose severe limitations on the response plans to oil spills. Another obstacle is the difficult working conditions in the Arctic due to low temperatures that will negatively affect both human efficiency and equipment [26]. Apart from the environmental challenges, there are logistical issues to consider as well. The lack of support facilities (road access, storage and disposal facility, manpower) is one of the limiting variables caused by the remoteness of the area. Generally, ice and weather conditions determine practical strategies and control the eventual outcome [27]. Because of these issues, the response time to a spill incident will be increased and personnel safety will be decreased. If the response to an oil spill is not prompt, the effectiveness of any cleanup technic is reduced [24]. Therefore, developing a response plan for oil spill recovery in the Arctic offshore requires a more comprehensive planning compared to recovery in open waters.

The operational challenges for oil recovery that are introduced by the cold weather and ice vs. the temperate situation in open waters are summarized in the Short State-of-the-Art report by SINTEF and ARCOP [8, 28] as the followings:

- Freezing of equipment
- Limited access to the spill site
- Difficult detection of the oil slick

Because of these significant challenges, and the high stakes of oil spills in cold climates extensive research has been devoted to understand behavior of oil in ice and the applicability of different cleanup strategies to the spills [29]. Nevertheless, not every aspect of the Arctic spill situation is negative and there are few positive outcomes with ice as well. The increased viscosity of the oil due to low temperatures and the ice will act as natural containment and inhibit the spread of oil spill. As a consequence, the oil will maintain a larger thickness which will aid the cleanup operation. Also, because of low temperatures the weathering process will diminish and expand the window of opportunity to respond, especially with ISB [30].

Mechanical recovery is the primary cleanup technic selected by the Arctic Council member states (United States of America, Canada, Greenland, Iceland, Norway, Sweden, Finland and Russia) while the use of dispersing agents and ISB are considered as alternative methods for cleanup [31]. Spilled oil in the Arctic can penetrate in ice/snow or enter the open pools between ice floes. It can spill in the open channels created by vessels or even go under the ice. In these situations, the traditional use of booms and skimmers can be difficult. In particular, for skimming machineries the problems will include limited flow of the oil to the skimmer, separation of oil from ice and water, contamination of ice/cleaning of ice, and the increased oil viscosity [9]. There are new solutions that have Arctic-specific designs [32, 33], but the recovery capabilities of mechanical equipment are still very low.

Similar to mechanical recovery methods, use of dispersing agents is also constrained in the Arctic spill scenarios. The low temperature of water and air, and damping of waves by the ice floes will decrease the energy level below what is required to disperse the oil [34]. Another limiting aspect of dispersing agents in ice is the reduced accessibility and sporadic placement of oil slicks between ice floes, especially at high ice concentrations [33]. Therefore, dispersants have been viewed as having the potential for only limited success.

A large number of studies [35, 36] argue over the suitability of ISB in ice conditions. There are many advantages as well as limitations for use of this method in the Arctic. The trade-off between the benefits of using ISB to remove the oil from ice-infested waters and the potential side-effects of burning is usually in favor of employing ISB. In the next section, an overview explaining the key advantages of this method and its operational challenges is presented.

1.3 *In situ* burning (ISB) in ice-infested waters

After the initial attempt with *in situ* burning in the late 1950s, added interest for using the method in ice-infested waters was fueled by the struggle to find ways to adapt mechanical recovery methods to the Arctic environment. As the results of research in 1970s fire booms were developed [35].

Many researchers and spill responders believe that ISB is especially suitable for ice conditions in the Arctic [20, 33, 37-42]. Early field experiments in the Canadian Beaufort Sea successfully used ISB on oil in spring melt pools after being released beneath the ice surface [42, 43]. Large scale experiments of ISB in the ice also have shown high potentials for oil removal (up to 90% removal efficiency) [44-46]. More recently, ISB field experiments of ISB were carried out by *Arctic Oil Spill Response Technology Joint Industry Programme* (JIP) for spills of various concentrations in pack ice and especially in slush and brash ice [39]. The technique was proven to be very effective for thick oil spills in high ice concentrations and has been used successfully to remove oil spills accidents in ice-covered waters in Alaska, Canada and Scandinavia. Yet, this method has not been used in any spill recovery operation in icy environments. Thereby, the lack of practical knowledge on ISB in the Arctic has pressed for more research projects in the recent years [37, 39].

Examples of important influential parameters for ISB operation in ice include ice thickness, ice concentration and to a lesser degree ice bearing capacity. Sea ice will act as a containing barrier for the oil and also as a platform to execute the operation [47]. Depending on the location and time of the year, ice thickness determines the accessibility and load bearing capacity for staging equipment, and surface travel to and from the spill site. Support recovery equipment, such as pumps and tanks for temporary storage and/or transport of burn residue from the icy water [48]. Given the light equipment required for ISB, ice pathways will be available to support oil spill cleanup operations from December to May [49]. By late May the ice surface is normally too deteriorated to maintain the ice surface in a usable condition. However, the ice sheet itself usually maintains enough stability until early June to support light loads at the spill site. ISB operation on ice from June to breakup will depend on the day to day conditions and may require access from air or below the water surface for ignition [27]. As ice condition continues to change throughout the year, the sea ice may not be feasible to perform as a platform for response plans. A helicopter carrying

a heli-torch is one of the new technologies developed to expand the oil spill response toolbox for this region [50].

ISB involves simpler logistics compared to other cleanup methods. In the simplest form and in an ideal situation, a gasoline-soaked rag can be used to ignite a fresh thick slick of oil without the need for further equipment. In general, if the oil slick is not thick enough to sustain flaming then containment logistics (fire booms and boom-towing vessels) are needed too [51]. In ice conditions, the containment may often be provided by the ice itself, depending on how dense the ice distribution is. Normally, ice coverage of more than 60% provides natural containment [38]. In case of light ice coverage (< 30%) which demands the use of containment equipment to increase the thickness of the oil slick, it is possible to capture and thicken the oil with fire booms. Another positive prospect in ice is the slow weathering process that is caused by the low temperatures of the oil surroundings [48]. This effect assists in expanding the window of time for successful ignition and flame spread of the oil [52]. The other processes involved in spill recovery (transfer, storage, treatment and disposal of oil) also will reduce to only a small fraction of the initial amount of spilled oil when removal effectiveness of ISB is high.

High removal rate is another feature of ISB that appeals to spill responders. As a rule of thumb, the removal efficiency of ISB for oil slicks of 1 cm thickness or more is above 90% as stated by Allen et al. [17]. The total of tar-like residue left as the results of ISB in *Exxon Valdez* recovery operation was as low as 300 gallons, which gives a 98% removal rate based on the initial volume of 15000 gallons before the burning. High elimination rates have also been reported for ISB during *Deep Water Horizon* incident [53]. ISB removed almost twice the oil removed by skimming, and in a much shorter time span.

However, ISB has not been carried out in an Arctic spill cleanup operation yet. Nevertheless, many field and laboratory scale experiments have been conducted to evaluate the efficiency of ISB in ice condition [41, 54, 55]. Field experiments of ISB in ice-covered waters have claimed high removal efficiency [44]. The projects conducted at the *Oil and Hazardous Materials Simulated Environmental Test Tank* (OHMSETT) facility in New Jersey between 1984 and 1987 on burning of crude oil in varying ice concentrations examined the possibility of ISB [54, 56, 57]. The major conclusion was that a minimum of 2.5 mm slick is needed for sustained flaming on cold water and that the ice concentration and burn efficiencies are inversely related. The experiments conducted in the OHMSETT

tank within a 46.5 m^2 boomed area with varying ice coverage of 45-60% and fuel layer thickness of 2-4 mm [58], burned fresh and lightly weathered Prudhoe Bay crude oil with removal efficiencies of over 85%. The thicker oil slick and moderate ice coverage (4 mm and 40%) resulted in a higher efficiency (95%).

The cost associated with cleanup is another advantage of ISB. The cleanup cost is influenced by the condition surrounding the spill; mainly the oil type and location of the spill [59]. The choice of cleanup methodology also strongly influences the cleanup cost. The cost data on over 200 spill cases with respect to the primary cleanup technics were analyzed in the study of Etkins et al. [60]. Their study showed an average cleanup cost of $8.64 and $5.06 per liter of oil for mechanical recovery and dispersants, while ISB had the lowest cost, $2.81 per liter. The relatively low cleanup cost of ISB is accompanied by the fact that it has the highest removal efficiency. Their cost data was extracted from cleanup of spills in open water situations. However, the cost for Arctic situations is not expected to increase as much for ISB in the Arctic given the fact that some spills will be naturally contained.

During *in situ* burning surface oil is removed by transferring most of it into the atmosphere in the form of combustion products and soot [61]. Although ISB reduces the environmental threat imposed by the oil slick, the environmental threat posed by the airborne plume would remain a concern. In both the burned and unburned scenarios, a weathered residue is left on the surface to pollute water-surface resources or shorelines. The amount of residual oil would be much greater without burning and is considerably less weathered. Decision makers need to compare the effects of burning versus not-burning and choose the option that provides the greater net benefit to the environment. Therefore, an analysis on the environmental impact of ISB is essential.

The versatile nature of ISB makes it suitable to be used in different situations and in particular in ice-infested waters. However, there are controversial public perceptions over combustion by-products (such as CO, SO_2, and NO_x) that may negatively affect the responders and human habitations [39, 62]. The formed soot could cause pollution of nearby snow and ice after it deposits on land [23]. In addition, the residue that is left after the ISB needs to be removed manually, which can be difficult in high coverage of ice.

The major technical issue associated with ISB is the problem of ignitibility (capability of the oil slick to maintain burning) [63]. This is especially the case for ice-infested waters where cold boundaries and ice inversely affect the ignitibility of the oil slick and thereby reducing the removal efficiency of ISB. Oil which is thicker than about 2 millimeters is claimed that can be ignited and burned with reasonable efficiency [64, 65]. However, the ignition process is more complicated and many parameters govern it [66]. The presence of ice and cold water generally support greater equilibrium thickness of the oil compared to open water spills [67]. This natural effect may not be sufficient to maintain an ignitable thickness of 2 mm unless solid ice is containing the oil. Arctic spills can occur in different geographical conditions in terms of oil-ice-water configuration. Spills may be in the open waters in warmer seasons, under conditions of partial ice coverage in freeze-up/thaw season, or in solid fast or pack ice in cold season [67].

In summary, there are two parameters that are crucial to the Arctic response plan and are required to be looked at more carefully. The first parameter is the behavior of oil in ice environments and the second parameter is related to the different ice configurations or oil-in-ice situations [68]. The mentioned parameters are discussed in the following sub-sections as the knowledge related to the ice environment and interactions of oil and ice is pertinent to this study.

1.3.1 Fate and behavior of oil in ice-infested waters

The fate and behavior of oil in ice-infested waters has been examined through field tests, laboratory tests, and numerical studies over the past 40 years to understand the interactions of oil when it is discharged in cold waters with presence of ice. Spreading and weathering of the oil are the main factors that determine the fate of the oil in ice environments [48, 69]. A summary of existing knowledge on the fate of oil in the Arctic condition is presented herein.

When oil is discharged into the ice environments, it spreads and expands the contaminated area. Spreading can occur on or under ice, on or in snow, and spreading on water with presence of ice [70]. There are four distinctive forces that govern spreading and retarding of an immiscible liquid fuel. Gravity causes sideway spreading of an oil slick on a surface by creating an imbalance in the pressure distribution of the oil slick, though with

diminishing effect as the slick gets thinner. The other force assisting the spreading of the oil is surface tension force that is predominant for thin spreading and will not vary with oil slick thickness [71]. These spreading forces are retarded by inertia and viscos force of the oil. The inertia dominates when the oil slick is thick and it diminishes as the oil thins. Similarly, as the oil becomes thin the viscos force counterweights the inertia. The dynamic of spreading of oil are characterized by three successive regimes that are dominated by a retarding force. These regimes (gravity-inertia, gravity-viscosity, and surface tension-viscosity) have been used to determine spreading equations. Spreading tests have shown that warm oil spreads very fast and at oil temperature of -19 °C spreading stops due to the increased oil viscosity [72]. Generally, in cold climates with presence of ice the spreading is delayed by the increase in viscosity of the oil. Spreading on ice surface is found to be driven by gravity initially and then by ice surface smoothness. The natural surface irregularities halts further spreading and causes the oil to contain in a small area [73].

Spreading of oil on water with presence of ice has been more attractive to researchers as the possibility of spill on water with ice coverage in the Arctic is higher [74]. In addition to causing larger viscos resistance for spreading, the physical presence of ice obstructs the flow as well. It has been shown that for light ice coverage (less than 30-40%) the oil movement will not include the ice and is similar to that in open waters. If the ice coverage goes beyond 60-70% the oil would drift with ice [75]. The spreading of oil is generally reduced in the presence of ice, where much of the oil absorbs to the frazil ice present, often resulting in oil slick thickness of few centimeters. In high concentrations of ice, where ice concentrations preclude the effective use of traditional containment booms, the oil is effectively confined by the ice itself [76]. The possible natural containment of oil against ice edges/walls leads to thicker oil layers that generally enhance the effectiveness of burning.

Weathering is the combination of processes that break down the spilled oil mainly through evaporation, emulsification, and dissolution. These mechanisms act simultaneously from the moment of oil discharge but their relative importance varies with time. Behavior of the oil is largely dependent on its degree of weathering as it increases the oil viscosity. The window-of-opportunity for any response technic and specially ISB is dependent on the weathering condition of the oil. In the Arctic, the weathering degree of oil is reduced due to the low temperatures (less evaporation) and damping of the sea waves by the action of

floating ice (lower energy to emulsify the oil) [77]. The rate of evaporation of oil is controlled by the ambient condition (wind, temperature) and by the slick thickness. As such, the thicker oil slicks evaporate at a comparatively much slower rate in freezing conditions. In particular, in the study of Brandvik and Faksness [78], the evaporation and emulsification processes of Statfjord crude with different ice coverage (slush ice, 30% and 90% ice coverage) were examined. They reported that evaporative loss by volume was estimated to be 30% for no ice, 25% for the lighter ice coverage, and 19% for the heavier ice coverage. In addition, their experiments at various current and wave height conditions with different air temperatures (-15 to -5 °C) showed reduced water uptake, viscosity, and pour point in dense ice conditions that extend the operational window for response compared to oil spills in open waters.

Aside from the oil, the burn residue fate is also of importance. Similar to individual oil types with varying physical properties, ISB burn residues also have different characteristics and behavior depending upon the initial chemical composition and physical properties of the oil and burning efficiency of ISB [79]. Burn residues may either sink or float. It is recognized now that residue of heavier oils which have burned more effectively are more likely to sink after they have cooled [80]. Residue that sinks is obviously more difficult to recover than floating residue. Chemical composition of the residue and its toxicity is also has been a subject of research [81]. Although most studies have shown that the burn residue is no more toxic than the oil itself, floating residues can be stranded and harm wildlife.

Although the relevant physical and chemical changes of spilled oil in Arctic conditions are in favor of cleanup strategies and especially in favor of ISB, the different oil-in-ice configurations vary considerably from one to another. As this is mainly due to the numerous forms of ice in the Arctic, knowledge of oil and ice situations is necessary for an effective ISB operation.

1.3.2 Oil and ice situations

The Arctic environments adds an additional level of complexity to the problem of oil spill cleanup by introducing ice as a spill substrate that appears in very dynamic forms and geometries. Generally, the different forms of the Arctic ice and coastal environments present a wide range of oil in ice configurations that must be considered for effective

cleanup operation. This is especially the case for ISB operation as the mutual influence of the burning oil and the ice is not understood well [82]. Oil spill accidents can be classified in relation to three main types of oil activities; shipping, offshore extraction of oil, and transport of oil in pipelines.

Global Climate Model simulations indicate a continuing retreat of sea ice during the second half of the 20th century and early 21st century, but also show that the winter sea ice cover will remain intact [49]. This means that the disappearance of the ice is only to be expected for a short durations in summer, even with the current climate change patterns. Nevertheless, an oil spill in the Arctic is a possibility, and a situation to consider and prepare for. Spill incidents may occur on land, on water surface with presence of ice, or below the surface as a results of well blowout. Spillage of oil by vessel accidents in Arctic leads to oil on the water surface situations where ice is present. Therefore, any accidental or illegal discharge of the oil by ships in the Arctic marine environment remains to be tied with ice except for a short summer period. The discharged oil as an outcome of a well blowout also migrates and eventually appears on the icy water surface. In case of a spill in the Arctic, disregarding the type of accident, the oil can be on top/inside or underneath the ice surface, or be incorporated in an area of drifting ice (floes, brash, frazil) on water [33]. In these situations, depending on the shape and concentration of the ice on water, numerous forms of oil-in-ice interactions develop. The concentration of the ice will vary depending on the season and the location of the spill too. Therefore, it is rather difficult to integrate and explain all the ice forms with an analogous term. The Handbook of Oil Spill Science and Technology [83] contains an ice nomenclature to give definition of the relevant oil-in-ice terms. It is essential to discern the definition of these terms in order to appreciate the diversity of the ice forms. The ice configurations that lead to possible oil-in-ice situations that are relevant to this study are summarized in Table 1.1.

Table 1.1: Ice situations relevant to this study based on ref [83].

No.	Name	Definition
1	Fast ice	Sea ice that forms along the coast and is attached to a shore, to an ice wall/front, between shoals, or grounded icebergs.
2	Floe ice	Flat pieces of sea ice 20 m across.
3	Brash ice	Floating ice made up of fragments less than 2 m across
4	Frazil ice	Fine spicules of ice suspended in water
5	Fissure	Ice breaks or ruptures between floes or old ice
6	Ice channels/fracture	Narrow space between ice floes
7	Ice lead	A passageway in ice navigable by surface vessels

Offshore well blowouts or pipeline breakdown in icy waters will also result in unique interaction of oil and ice. For the oil that is discharged below the ice encapsulation and migration is another factor in determining the fate of the oil [29]. Oil that is spilled under young ice is likely to become encapsulated by new ice within 12 to 24 hours of release. After a few months of static condition during winter, it would start to migrate up using the brine channels in the spring [29]. Most of the encapsulated oil (80%) would migrate in brine channels and form melt pools of fresh crude oil on ice surface. The exposure to light and air will evaporate as much as 30% of the oil by volume. The oil in the melt pools on top of the ice (undergone the evaporation loss) is claimed to be burned with the removal efficiency of 96% [8]. However, some of the removal efficiencies reported in literature of ISB are unrealistically high but it is safe to assume that in ideal conditions efficiencies north of 80% are feasible.

There is also a possibility for oil to spill on solid ice and snow conditions. Terrestrial oil pipelines in Alaska and Canada have seen minor and major leakages [84] in the last few decades. Although the burning of such spill is not desired in many of the terrain conditions, unwanted burning of that oil is considered as a safety concern. Thus, the knowledge of burning oil and ice/snow interactions with fire are helpful to prepare for the outcomes of burning on ice from a safety point of view.

Figure 1.1 shows a graphical overview of oil-in-ice situations resulting from spills occurring in different locations. The top row, separated by the solid horizontal line, indicates the type of accidents and the possible location of the discharge (on land, on water surface, and below water surface). The lower side of Figure 1.1 shows the possible scenarios of oil-in ice situations demarked with a dashed line. It should be noted that the oil that is discharged below the water surface will eventually reach the surface thus shaping oil-in-ice scenarios that are similar to those of discharge on the water surface.

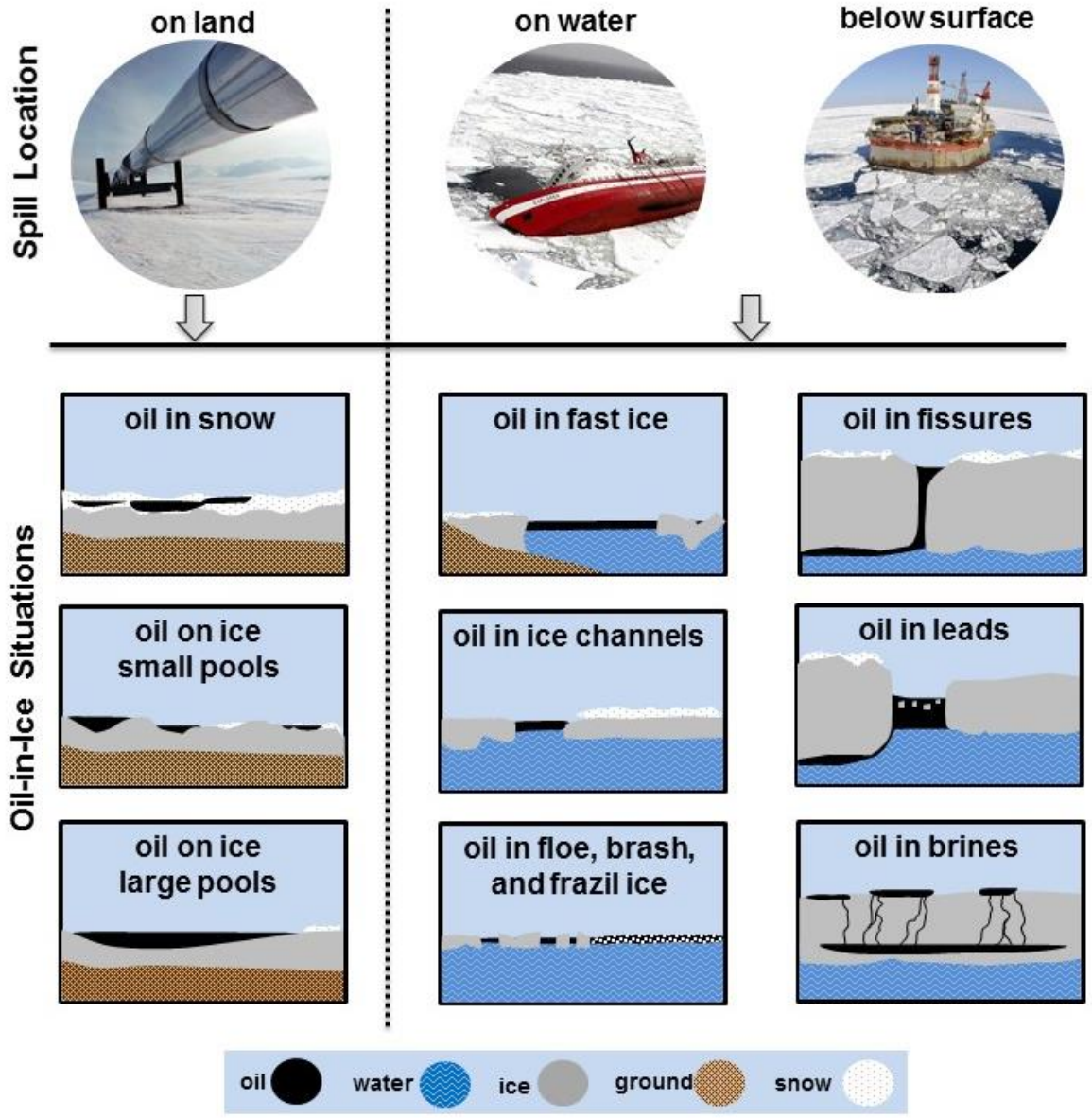

Figure 1.1: Graphical overview of oil-in-ice situations. Adapted from [33].

In the next section the implications of performing ISB in icy condition are discussed. The melting of the ice by the heat that is produced by the flame is one of the consequences of

burning adjacent to ice bodies. Specifically, the melting of ice by the burning oil can lead to a unique situation by penetration of the oil into the ice.

1.3.3 Melting of ice and *lateral cavity* formation

Almost all of the different oil-in-ice situations that were described in the previous section have one common feature; that is the bordering of the oil by the ice. This is the condition in which oil is surrounded by ice bodies. The likely natural containment of the oil against ice edges/walls may lead to thicker oil layer, which is a positive prospect for ISB. However, ice is unstable when exposed to the heat by the combustion of oil and it will melt. Melting of ice causes early extinction by reducing the oil slick thickness and in some case overflow of oil from its containment. Figure 1.2 illustrates two cases where the fires have extinguished due to reduction of oil thickness (a) and overflow from its containment (b).

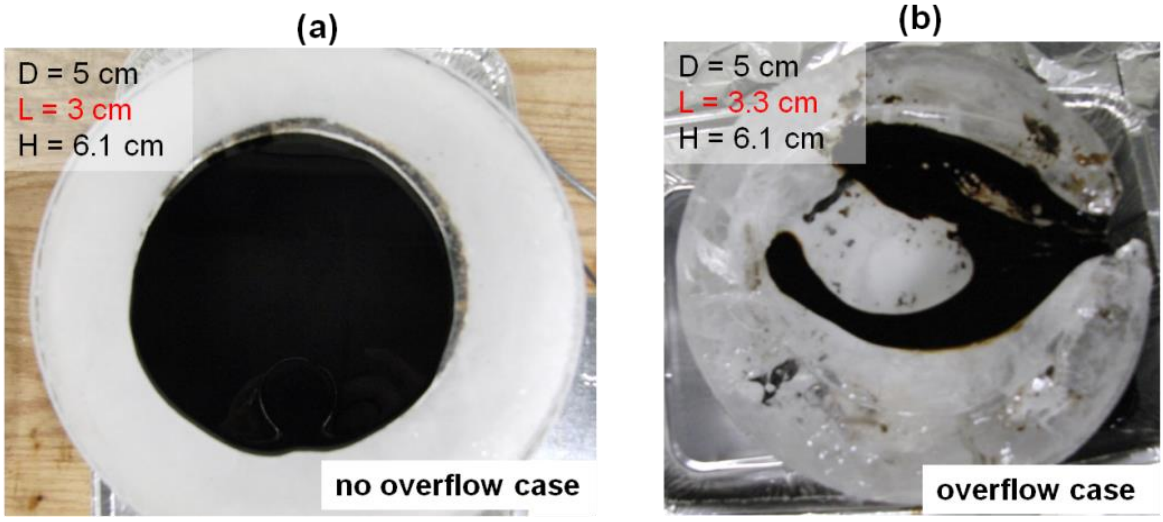

Figure 1.2: Extinction scenarios: a) where oil is confined in the cavity and extinguished because of reaching a critical thickness (~3mm), and (b) extinction observed due to overflow (adapted from [82]).

As explained, there is a common feature in different oil-in-ice situations and that is the adjoining of oil layer to an ice body. Burning of the oil layer in these situations provide the heat for the ice to melt. Therefore, it is expected for every oil-in-ice scenario to follow the change shown in Figure 1.3 in a relative manner. Figure 1.3 illustrates the condition where oil is adjacent to an ice wall (a) and the consequential melting of ice caused by the burning (b) that leads to formation of *lateral cavity*. Note that the distance from oil surface to ice

top surface (*F*) in Figure 1.3 (a), also known as ullage, will determine if a void will be made in the ice wall (for relatively large ullage distances) or the liquid pool would simply widen on its ends (for relatively low ullage distances). This effect is discussed later in this section.

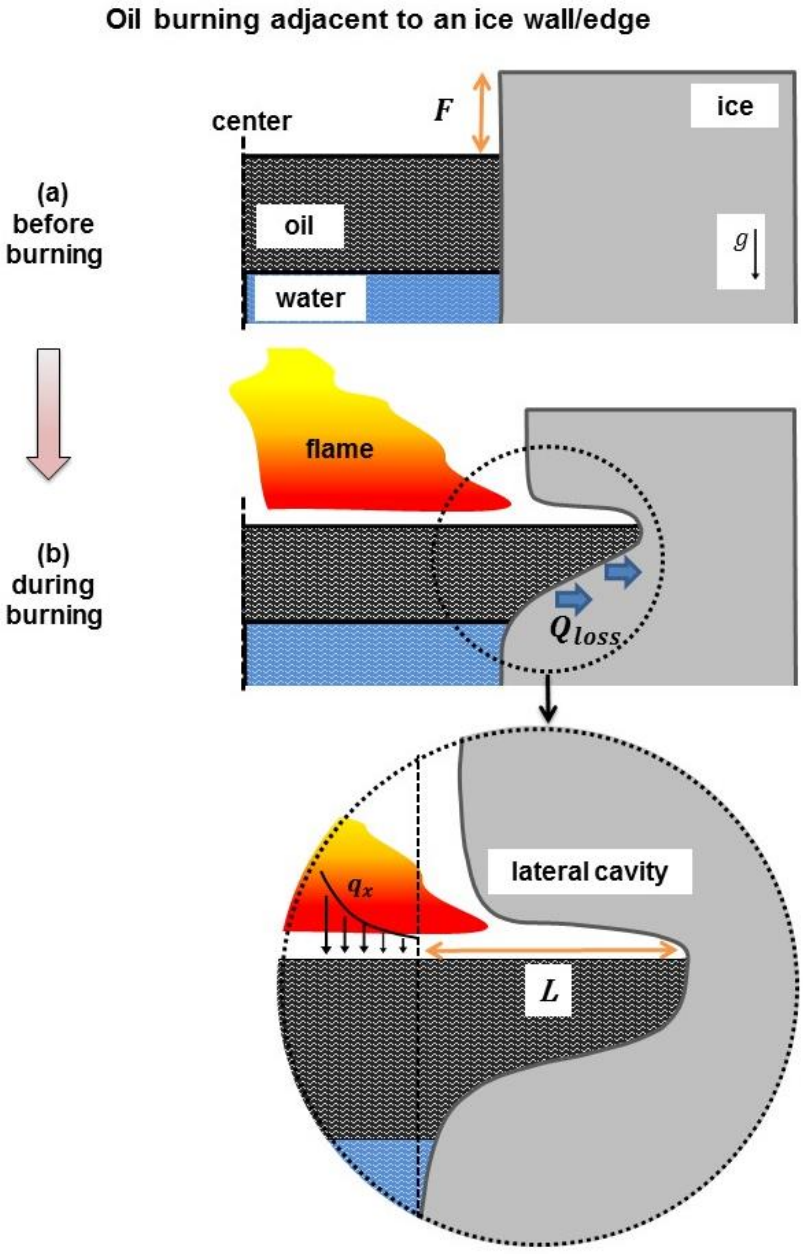

Figure 1.3: Schematic of oil adjacent to an ice wall (a) and burning of the oil causing the lateral cavity formation (b).

The previously performed lab-scale studies, investigating the use of ISB in icy conditions have shown the phenomenon of *"lateral cavity"* formation. [82, 85, 86]. In recent experimental studies of burning liquid fuels in ice cavities and ice channels the burning fuel was observed to penetrate radially into the ice. The melted ice created a void/pocket inside

and around the circumference of the ice. Also, it was mentioned, without providing evidence that the rate of melting of the ice walls were higher in areas where the fuel layer was in contact with ice as compared with places where the flame was present. Formation of lateral cavity is the case where oil is surrounded by walls of ice and its top surface is considerably lower compared to that of ice. If the oil surface is in same level with the ice surface the lateral cavity would not form. However, one should expect the lateral melting to occur regardless of the oil and ice level.

The intrusion length of the oil into/on the ice, denoted by *L* in Figure 1.3 (b), is assumed to be one of the key characteristics of the lateral cavity problem. The length of the lateral cavity, *L*, is defined as the horizontal distance (near the top surface of the oil) between initial and final location of the ice wall. The increase in the intrusion length may be a potential setback for the success of ISB depending on the extent of penetration of the oil into the ice. For example, the ice deformation will allow a portion of the oil to drift underneath the lateral cavity. This is presumed to be a potential factor in reducing the removal efficiencies of fire by preventing the exposure of air to the trapped oil. A decrease in the removal efficiency leads to larger amounts of oil residue. In addition, the confined residue in the cavity would be harder to collect and, as a result, increase the cost of the post-burn cleanup during ISB operations. In particular, if the residue stays untreated, it could be encapsulated due to freezing of the water in colder seasons and potentially remain in the ecosystem for years. Experiments have shown that the residue trapped in lateral cavity can be as high as 10% [85].

There are two main alterations in the ISB process where ice is present. First, the geometrical parameters related to the ice and the oil changes due to melting of the ice (parameters such as diameter of the pool, thickness of the oil layer, and ullage). The expansion of the pool is shown in Figure 1.4. Second, the presence of ice with low temperatures, compared to the burning oil, brings about thermal instabilities that influence the burning of the fuel. The flame and a portion of heat that is fed back to the oil layer from the flame melt the surrounding ice and change the geometry of ice. As the ice melts, the melt water flows down due to its higher density compared to oil. Thus, the oil replaces the melted part of the ice and the pool of oil expands. Although the burning rate increases due to an increase of the burning surface area, the expansion usually causes the oil layer to become thinner and thus extinguish faster. This effect will be more significant for smaller (<1 m) oil pools [87].

Hence, the ultimate consequence of the burning area expansion is the reduction of the removal efficiency.

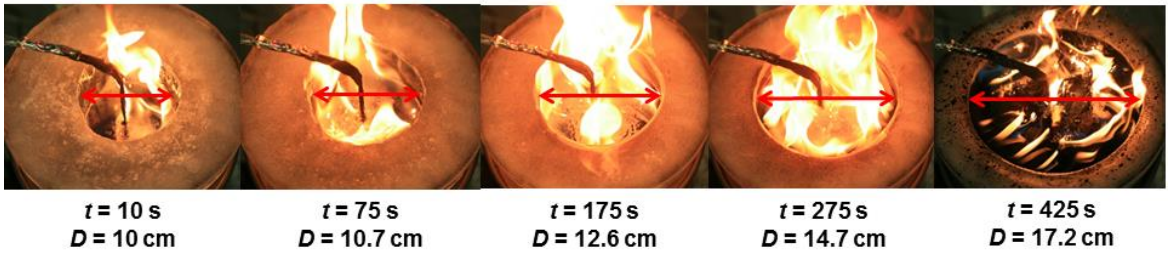

Figure 1.4: Showcasing cavity expansion for crude oil burn in 10 cm ice cavity. Adapted from [82].

The formation of lateral cavity and melting of the ice alongside a burning liquid fuel is suspected to negatively impact the net outcome of ISB. The anticipated positive and negative effects of melting on ISB outcome are summarized herein. The expansion of the pool of burning oil adds to the burning surface area and increase the burning rate of the oil. This effect is potentially a positive prospect for the ISB success, if the oil is being continuously fed to the pool. For a fixed amount of oil spilled in ice, the expansion of the oil causes an early extinction of the flame by thinning the oil layer to its critical limits. The melting of the ice deforms the oil-in-ice configuration by accumulation of melt-water under the oil that displaces the fuel layer. For a closed bottom pool (e.g. spills in melt pools), the oil layer elevates if the amount of melt-water is more than the amount of oil that is removed by burning and vice versa. In general, the smaller size pool brings more melting and less burning of the oil that translates to faster accumulation of the melt-water and more vertical displacement of the fuel layer. A larger pool, however, tends to have higher burning and less melting thus the oil level will not vary significantly during the ISB. This condition increases the chance of having a deep lateral cavity.

The consequences of such vertical movements in oil pools can vary from extinguishments because of overflow or causing a secondary unwanted fire. However, if the oil is in open bottom pools (e.g. spill in frazil, brash, drift and pack ice), then the level of the oil will not be affected by the ice melting or regression of the oil. In this case, the lateral cavity is likely to reach its maximum length.

Ice melting is not entirely a negative aspect of ISB in ice-infested waters. In a setting where multiple small melt-pools are formed near each other, ignition of one of the melt pools and

the subsequent expansion of the burning area may result in connection of the adjacent pools and spread of the flame to the other pools. The joining of melt pools would increase the removal efficiency to desired levels, where single oil pools hardly yield effective removal on their own.

1.3.4 Knowledge gap on melting during ISB

Most ISB studies in ice include field experiments that have focused on operational issues concerning factors such as oil type, degree of weathering (specifically emulsification), and the atmospheric conditions [29, 33, 43, 88]. These field experiments usually report on the ignitibility and removal efficiency as a measure to assess the cleanup success. Besides, only a small number of articles have focused on oil spills in the Arctic conditions where ice and reduced temperatures are included as additional variables. The accumulated results from such field experiments normally lack fundamental examination of the relevant physics and of the fire science behind the burning of oil in icy condition. Therefore, they fail to provide answers related to the effect of the ice. This lack of scientific research has led to establishment of a number of rule-of-thumbs to predict the ignitibility or regression rate of oil for ISB operation in temperate regions [6, 65, 89]. Nevertheless, despite the numerous field experiments and research over the past 45 years, only a few studies have addressed/mentioned the melting that occurs during ISB in ice-infested waters.

There are two brief mentions of melting in the reports published from ISB field experiments in the Arctic region. The first mention is by the report of the NORCOR project in Beaufort Sea [42]. In NORCOR experiments, simulating a subsurface well blowout, 54 m^3 of fresh crude oil was released under landfast sea ice. The oil came up in the spring to form the melt pools containing about 22 m^3 of oil. The melt pools were observed to grow slightly in size as the ice deteriorated naturally by warming of the ambient. ISB was used on the melt pools of oil and it was reported that in several locations, the oil and tidal flush had cut trenches in ice over 30 cm deep between pools. Unfortunately, no more information on the configurations of the trenches is recounted.

In another brief mention in the report of Glaeser and Vance [90], it was observed that oil pools which were burning on ice would provide enough heat to the surroundings to form channels which drained water and burning oil to lower areas. The leakage out of the melt

pool extinguished the fire. They concluded that it is important to know the rate of melting to determine what length of time the ice will contain the oil after a spill. Though, no further ISB related studies on ice melting are conducted.

There are also three studies in other fields where a melting phenomenon similar to lateral cavity is addressed. Figure 1.5 shows the sketches that were used to describe the lateral intrusion into the solid in these studies. In study of Komatiite lava ascent and flow on the ground [91], it was observed that the flowing lava melted the ground to form deep thermal erosion channels. The erosion channels, shown on the left side of Figure 1.5, widened at their base as the channels became deeper. The melting of the ground was found to be related the lava temperature being higher than ground's melting temperature and the low viscosity of lava which facilitated turbulent flow.

In a flame spread study on fuel-soaked snow layers on asphalt roads by Ishida et al.[92], a development similar to the lateral cavity was reported. Their schematic illustration of this phenomenon, shown in the middle of Figure 1.5, presented an expanding fire base throughout and a lateral intrusion in the snow toward the end of the burning duration. A general interpretation was provided to explain the melt development in which heat flux from the flame was responsible for melting the snow. But, no specific explanation is provided to detail the way heat flux melts the snow to produce the unique final shape.

In the third study, lab-scale experiments on burning of an oil mixture in ice channels by Bellino et al. [86] were performed to measure mass loss rates of the oil in ice channels of varying widths. This study presented the unique way that ice melted during burning of the oil in ice. The change in geometry of the ice channel was depicted in the work of Bellino et al. and it was stated that the lateral cavity was formed towards the end of the burning phase. The temperature profiles along the centerline of the oil layer were used to explain the reason for the formation of the lateral cavity.

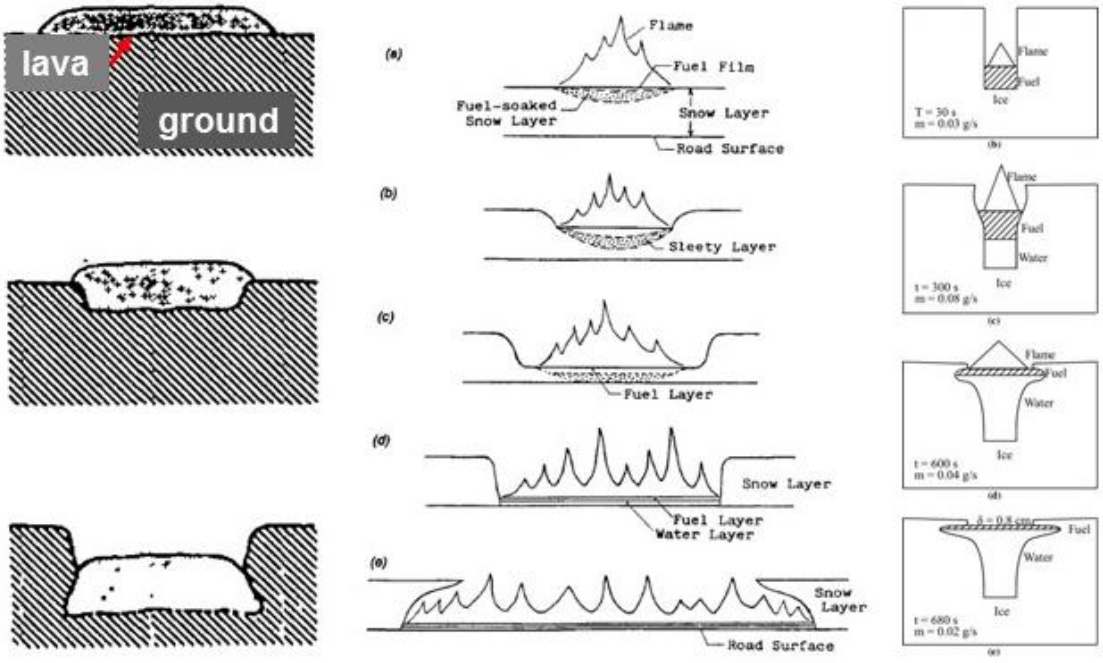

Figure 1.5: Cross sectional sketches of the lateral intrusion of (left) flowing lava in the ground [91], (middle) burning gasoline in the snow [92], and (right) an oil mixture fire in the ice [93].

The changes in the geometry of ice, referred as lateral cavity, were also described in the article by Farahani et al. [87]. In their study, Alaskan North Slope (ANS) crude oil was burned in circular ice cavities (5-25 cm in diameter) to study the burning behavior of the oil. Although, the lateral cavity formation was reported to occur in the ice cavity tests, but the cause for this formation was not discussed in details.

In two recent studies by Shi *et al.* [85, 94] that were published during completion of this work, ANS crude oil was burned in meso-scale size ice cavities. In their first study, crude oil with initial thickness of 0.5 to 1.5 cm in ice cavities with size of 65 cm × 16 cm (a channel) and 110 cm × 110 cm and depths of 10–25 cm were burned. The results of three experiments in ice channels with the same initial ice channel dimension, but different initial oil layer thickness, showed expansion from width of 16 cm to 27.5 cm, 30 cm, and 33.5 cm for the initial oil thicknesses of 0.5 cm, 1 cm and 1.5 cm, respectively. Therefore, the melted length of the lateral cavities on one side was 5.5 cm, 7 cm, and 8.75 cm respectively. The shape of the lateral cavities (and specifically their width) that was formed during these experiments was found to be similar except for their length. This was presumed as an indication that the oil thickness did not directly affect the lateral cavity sizes. Though, the

difference in the lateral cavity lengths can be explained by different burn durations of these tests. For the test in 110 cm by 110 cm square ice cavity, a melting length of 12 cm (on one side) was measured even though the burn duration was shorter. In their second study, five tests were conducted comprising of two indoor tests with freshwater ice and three outdoor tests within an artificial saltwater ice pond. The square ice cavity where the oil was burned had initial dimensions ranging from 100 cm × 100 cm to 150 cm × 150 cm. Table 1.2 is provided here to summarize the data from their experiments and the resulting cavity sizes. For the tests in the outdoor test area, the wind direction significantly changed the amount of melting on different sides of the cavity.

Table 1.2: Cavity expansion during burning of ANS crude oil in ice. Adapted from Shi *et al.* [94].

Test No.	Cavity size (cm^2)	Oil thickness (cm)	Burn rate (mm/min)	Burn time (s)	Final cavity size (cm^2)
2	105 × 101	1.0	2.68	200	112 × 110
3	103 × 101	1.3	2.97	251	113 × 111
4*	100 × 100	1.5	2.91	305	120 × 120 (± 1)
5*	150 × 150	1.3	3.02	227	170 × 170 (± 4)
6*	100 × 100	1.7	2.62	367	128 × 128 (± 6)

* Outdoor test with saltwater ice and ambient winds.

Shi et al. concluded that ullage to diameter ratio had a key role in determining the lateral cavity length and that saltwater ice melts at a faster rate compared to fresh water ice, and a larger cavity expansion was observed.

A survey of literature related to problem of ice melting and lateral cavity formation was presented in this section. This literature search identified that very few published articles have addressed the ice melting during ISB. The dynamic interactions of the oil and ice is also left out of discussions. Furthermore, there is no concrete explanation for the mechanisms that lead to lateral cavity formation. This study is aimed to fill this gap in knowledge of the processes and conditions that result in ice melting during burning of oil slicks in ice-infested waters.

1.4 Research objectives

In the previous section the gap in understanding of ice melting and the lateral cavity phenomenon during ISB was explained. The mechanisms that lead to the lateral cavity formation are not known or studied systematically and potentially many parameters such as fuel properties, size of the fire, and geometric configurations of the ice and oil could be influential on these mechanisms. The melting and the subsequent change in the geometry of the ice in pool fires contained by ice, caused by the intrusion of the oil in ice, has been found to contribute to the alterations of the fuel burning parameters such as the surface area of the fuel, fuel thickness, and ullage distance. As a consequence, burning behavior of the pool of oil will change in such conditions.

The expansion of the fuel surface area, caused by lateral cavity formation, is one of the key factors in determining the removal efficiency that contributes to burning enhancement and simultaneously leads to faster extinction. Therefore, modelling of pool fires in ice conditions is dependent on the knowledge related to the size of the burning area. On an operational scale, fuel burning parameters may be used to determine the suitability of the ISB in the Arctic waters. Therefore, the knowledge on cavity formation phenomenon is essential so as to enhance the chances for successful implantation of ISB.

This study is mainly focused on one parameter and that is the increase of the surface area of the fuel because of melting of the ice. For a fixed volume of oil, the slick thickness is a function of slick surface area, which defines the extinction conditions of the liquid fuel fire. Lateral cavity formation causes an increase in the slick surface area and consequently reduction of slick thickness in a faster rate compared to ISB in temperate waters and inside booms. The amount of oil residue is increased when the fire extinct faster. Therefore, removal efficiency is reduced significantly and cleanup costs are increased. In addition, because of the ice melting, the oil may overflow from the ice containment and stop burning (See Figure 1.2). To that end, the current work is aimed to provide the necessary knowledge and understanding on the mechanisms that lead to the melting of the ice and address the consequences of the penetration of the oil into the ice during ISB operation. As a result of lateral cavity formation, the burning efficiency, which is a key success criterion for ISB, will decrease. Also, the increase in the fuel surface area affects the burning rate and the remaining amount of oil. Further, it is important to know the rate of melting to determine

what length of time the ice will contain the oil in case containment is of importance. Therefore, the knowledge provided by this study will help to understand the ice melting and its effects on suitability of ISB in ice-infested waters. Specifically, the study will address the following questions:

1. How the lateral cavity forms as the result of the ice contact with the burning fuel and the flame?
2. What are the mechanisms that contribute to the melting of ice and which parameters (fuel properties and fire size) are influential in determining the melting rate of the ice?
3. How can the intrusion length for a given spill scenario be estimated?

Observations have shown that the melting is most significant in the area of fuel layer contact with ice. Thus, the required heat for the melting is mainly provided by the heat and mass transfer mechanisms within the fuel layer. The current work suggests that the flame feedback is absorbed by the fuel and is transferred toward the ice to provide the heat for the melting. In addition it is suggested that the convective flows in the liquid fuel (driven mainly by surface tension and to a lesser degree by buoyancy) to be the contributing mechanisms in melting of the ice. The mechanisms influencing the ice melting and formation of lateral cavities during ISB of oils were analyzed through lab-scale experiments and theoretical analyses in order to develop a tool for predicting the lateral cavity length. The insights provided by laboratory-scale experiments on pure liquid fuels of this work are useful to understand the controlling thermophysical parameters and effect of the geometry for large size (pool size of several meters or larger) and multi-component fuels.

The objective of this study is to improve the forecasting of the suitability of ISB by examining the mechanisms of the ice melting (lateral cavity formation) and developing a tool to predict the length of lateral cavity for an ISB operation.

1.5 Layout of the dissertation

This dissertation is organized in seven chapters and one appendix.

- Chapter 1, introduces the general problem of oil spill remediation in the Arctic, introduces *in situ* burning with a focus on its use in ice infested waters and ends up with details related to the knowledge gap related to the problem of lateral cavity formation during ISB in ice-infested waters.
- Chapter 2 reviews the theoretical background and mechanisms that are relevant to the problem of burning liquid fuels adjacent to ice.
- Chapter 3 presents the first experimental study (burning of n-octane in an ice cavity) that provides detailed results on the geometry change of ice and a discussion on the causes for inducing convection in the n-octane layer.
- Chapter 4 focuses on the results of a flow visualization study (conducted by a PIV system), which showed the convective flows in the n-octane layer adjacent to an ice wall.
- Chapter 5 contains a parametric experimental study on liquids adjacent to an ice wall and exposed to heat flux from above and scaling if the surface flow.
- Chapter 6 presents an order of magnitude analysis for estimating the length of lateral cavity and the assessment of the theory with existing experimental data.
- In Chapter 7 conclusions and future work related to this study are discussed.

The appendices consist of additional material such as photographs, plots, and Matlab codes developed during this study.

2 Theoretical background

The survey of literature presented in this chapter is intended to provide the essential knowledge on pool fires in the vicinity of ice and is divided into two sections. Section 2.1 provides a general understanding of liquid fuel fires contained by ice walls. The most relevant research topics in pool fire research with respect to the current work are heat feedback from the flame, pool geometry and ullage effect, ignition and flame spread. Section 2.2 is focused on liquid-phase convection for liquid layers exposed to a temperature gradient. The role of buoyancy, surface tension, viscous force and their combined influence in liquid-phase convection in addition to the effect of liquid properties on convection flow are reviewed.

2.1 Pool fires in vicinity of or in contact with ice

Diffusion flames are stabilized over a vaporizing combustible material and sustain the fuel gasification by heat transfer to its surface. A pool fire is a diffusion flame burning on a flammable liquid free surface, usually contained with rigid walls. Pool fire in the vicinity of ice or pool fire confined by ice, used herein, refers to a case where the containment is provided by ice walls and the liquid is in contact with ice. Pool fires size (diameter of the liquid surface exposed to air) can vary from few millimeters to more than tens of meters. The liquid fuel's depth may also be from a few millimeters (oil slick) to several meters (storage tanks). In a pool fire, the condensed fuel provides flammable vapors to be mixed and combusted with the incoming oxidizer above the liquid surface. Meanwhile, the combustion process provides the energy for the evaporation of more liquid through heat feedback to the fuel surface. Based on Boyle's law, the temperature of the liquid fuel determines the vapor pressure above the fuel surface. Ignition of a liquid fuel is only

possible when the fuel vapor pressure reaches a limit where the fuel-oxidizer concentration is ignitable, known as the LFL (Lower Flammable Limit). This occurs at flash point temperature which is specific for each flammable liquid. The temperature in which sustained flaming (at least 5 seconds) occurs is known as fire point temperature and is approximately 10 °C higher than flash point. In the right condition, the combustion of liquid fuel can be initiated with a small heat source (ignition) and will continue burning to a point where the flaming stops (extinction). The extinction of the flame in a pool fire, caused by the lack of fuel-vapor production, occurs when the energy loop is no longer able to sustain the required temperature for the vaporization of the fuel. As expected, liquids with higher flash point temperature or in very cold environment are susceptible to faster extinction since their thermal upkeep is more demanding.

The regression rate is often used to characterize pool fire burning. Regression rate is defined as the descended distance of the liquid fuel per unit time (mm/min) or the volumetric loss of liquid per unit surface area of the pool in unit time(mm/min). It can be used to compare burning rates of different size pool fires as it is independent of the pool diameter. In general, regression rate and burning rates give valuable information for practical safety use. The rate in which the fuel is burned determines the released radiation energy which is crucial from a safety point of view. The amount of liquid fuel that is removed by burning is also important for applications in oil spill cleanup practice. However, pool fires confined in ice are prone to geometrical variations due to melting of the ice and thus burning rate per unit area is a more appropriate index to compare them.

2.1.1 Heat transfer mechanisms

There are several heat transfer mechanisms working in favor and against sustained flaming of a liquid fuel. The relevant importance or the mode in which these mechanisms work depends on the fuel geometry (diameter and thickness of the fuel layer) and type of the fuel (flash point, smoke yield, etc.). In general, the sustained flaming of a liquid fuel is determined by the fuel surface temperature which in turn is balanced by the gained energy of liquid fuel (by conduction, convection, and radiation from the flame [95, 96]) and its energy loss to ambient. Many studies have addressed the energy conservation of the fuel layer in pool fires of different sizes [97-101]. A schematic of general heat transfer components of pool fires in ice is shown in Figure 2.1.

The burning of the fuel provides a large source of energy above the liquid fuel which is mainly lost to the ambient and only a small portion is transferred back to the fuel layer, mostly by radiation and convection ($\dot{Q}_{radi} + \dot{Q}_{conv}$). In case of containment by side walls and especially for small size pool fires, in-depth conduction through the rims is a large component that contributes to the burning. These components will contribute to the energy that is stored in the fuel layer ($\dot{Q}_{sens}$).

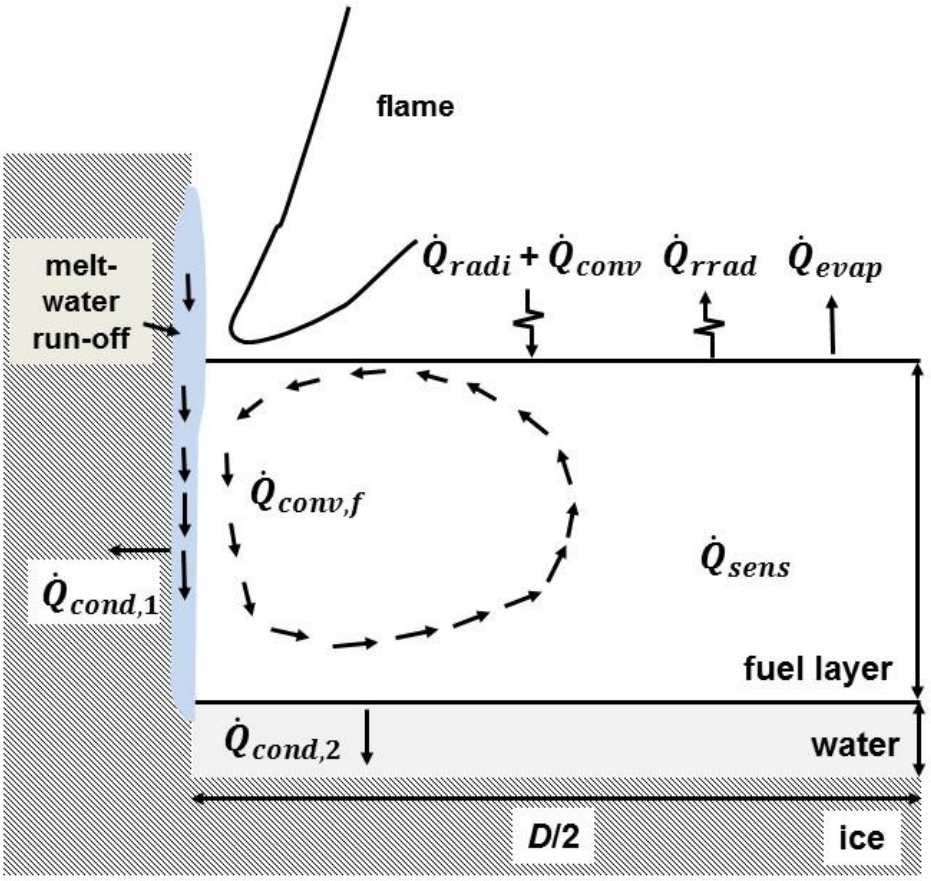

Figure 2.1: Schematic of heat transfer mechanisms in a pool fire confined by ice.

On the other hand, there are a few heat transfer components that deduct energy from the liquid fuel. In case of a water sublayer, conduction loss of the fuel layer to the water is one of the main reasons for energy loss and extinction of the flame ($\dot{Q}_{cond2}$). The heat sink effect of water would be most recognizable when the fuel layer is thin and there is a large water body. When conductive walls of a container are replaced by ice walls, then there is an additional energy loss component due to the ice presence ($\dot{Q}_{cond1}$). This is the opposite effect of what transpires in typical pool fires where heat is conducted through wall material

in depth of the fuel. The presence of ice has adverse effect on burning and can cause early extinction especially for pool fires of small diameter.

The effect of an ice wall on the energy balance of fuel layers is best illustrated in a previous work on pool fires conifned in ice with 5-25 cm diameter [82]. The energy conservation of the fuel layer can be written as follows

$$\dot{Q}_{radi} + \dot{Q}_{conv} - \dot{Q}_{evap} - \dot{Q}_{rrad} - \dot{Q}_{cond,1} - \dot{Q}_{cond,2} - \dot{Q}_{sens} = 0 \qquad (2.1)$$

Pool fires in ice cavities of less than 5 cm are very difficult to ignite, even for volatile liquids, due to the significant lateral heat losses to the ice walls ($\dot{Q}_{cond,1}$). The model presented in the aforementioned study takes the energy losses from sidewalls into the account whereas for typical pool fires energy is gained through conduction from the walls. Nevertheless, the wall effect is circumferential, therefore small diameter pool fires are more affected by the energy losses to the ice. As the pool fire diameter increases, the side wall effects become less significant and radiation prevails as the main mode of heat transfer from the flame to the fuel surface. The effect of pool fire size is discussed in the next section.

2.1.2 Pool geometry and ullage effect

The heat transfer mechanisms that were discussed in the previous section are present in all size of pool fires but the mode and their magnitude may vary depending on the geometrical condition (i.e. diameter of the pool). The buoyancy force above the fuel surface are the controlling mechanism in determining the influence of these mechanisms and especially the flame shape. In the work of Blinov and Khudiakov, published in 1957, burning rates for pool fires of liquid fuels (using vertical cylindrical vessels) at different diameters were measured and their results are shown in Figure 2.2 [61, 97]. Pool fires have been categorized based on the behavior they show at different sizes and different interpretation of those behavior exist in the pool fire literature. For example, pool fires were divided into two main regimes of convective and radiative in the earlier works [102]. In the later interpretations, three modes of conduction, convection, and radiation are used to characterize pool fire behavior [95]. The latter approach is adopted here. For small pool fires of about 5 cm in diameter or less, known as the laminar flow regime due to the steady conical shape of the flame, the regression rate decreases with the increase in diameter. The energy balance in

the laminar flow regime is governed by in-depth conduction through the rims of the container (fuel absorbs most of the energy through convection). Therefore, as the diameter increases, the sidewall effect becomes less and regression rate reaches a minimum. From 5 to 100 cm diameter, known as transitional regime, the laminar flow transitions toward turbulent flow regime first by dominance of convection and then radiation in the heat feedback. In the transitional and turbulent regimes, the fuel layer absorbs energy through the flame heat feedback and as the flame shape gets more disordered more heat is generated. At this stage, the turbulence intensity determines the regression rate and the increase in diameter enhances the regression rate. The regression rate in pool fires of over 100 cm remains the same with the increase in diameter.

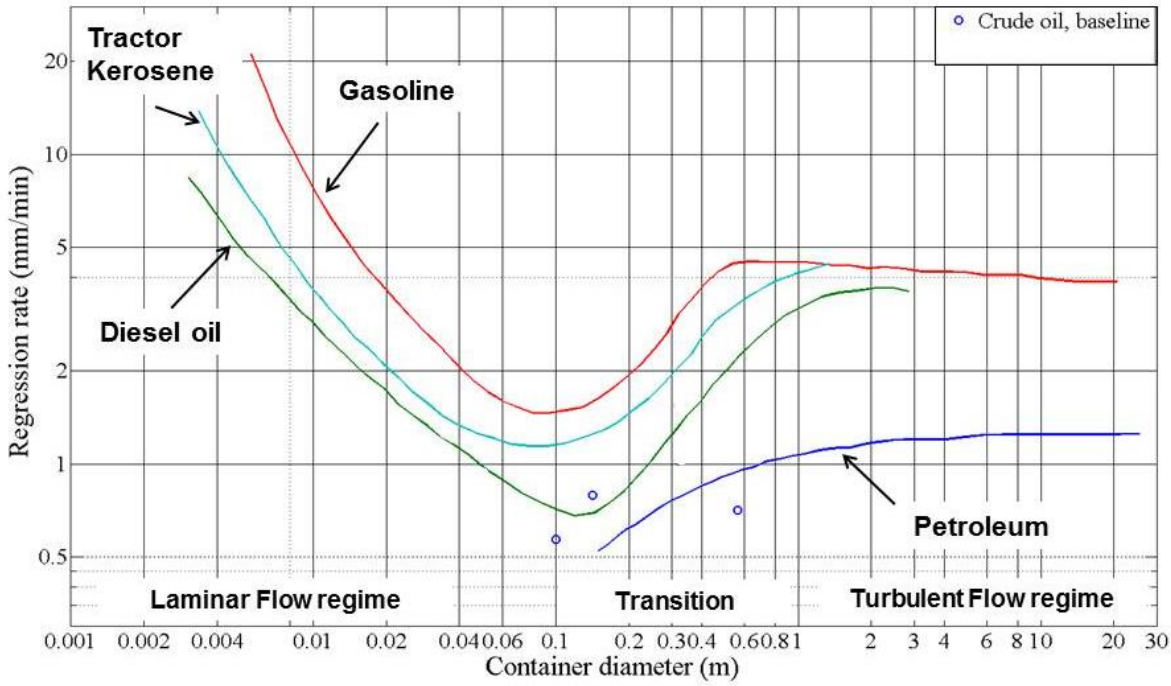

Figure 2.2: Regression rates for liquid pool fires with diameters in the range of 3.7 $\times 10^{-3}$ to 22.9 m. Based on reference [95].

The thickness (depth) of the liquid fuel will not influence the burning rates given the initial thickness is enough for the pool fire to reach a steady state burning. However, very thin layers of oil are prone to significant conduction losses which in turn may result in poor flaming or early extinction. Generally, for pool burning on water the thickness can determine the burning efficiency, intensity of boilover, amount of burn residue, etc. [103-105].

In pool fires (shown in Figure 2.3), the heat that is produced by the combustion of the fuel vapors above the liquid surface melts the ice wall and changes the geometry of the problem by widening of the pool. The widening process provides more burning surface for the liquid and increases the burning rate. In addition, the increase in diameter can contribute to the variation of heat feedback mode by increasing the level of flame turbulence. For example, a 5 cm diameter pool of n-octane in ice can increase to 20 cm in a burning period of 10 minutes. Therefore, the burning rate is enhanced both by the surface area increase and also by transition of flame regime from laminar toward turbulent regime.

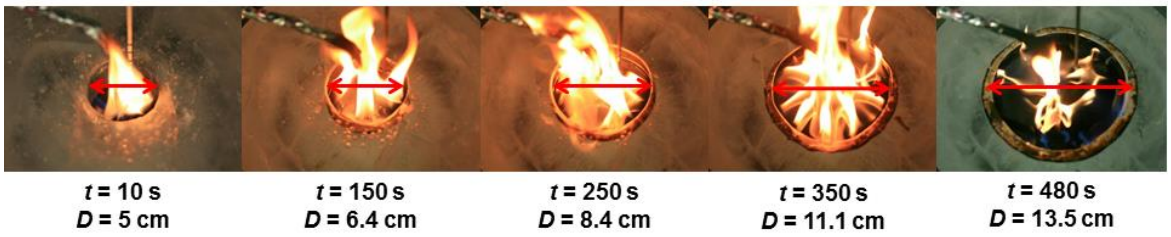

Figure 2.3: Surface area expansion for a 5 cm diameter ANS crude oil burning in ice [82].

The ullage (defined as the vertical distance from fuel surface to the container rim) is another geometrical parameter that affects the pool fires. A pool fire contained by rigid walls has an ullage that is increasing over time due to evaporation of the fuel. Thus, air entrainment becomes difficult and the flame extinct at a certain ullage height which is called the self-quenching ullage height. The ullage height and its effects on burning rate have been reported in the literature [98, 106-108]. The ullage height is especially affective on small size of pool fires. Dlugogorski and Wilson [109], investigated the effect of ullage on properties of small scale pool fires. Their experimental technique was conducted to measure the steady state consumption of ethanol in containers of 4.5 cm in diameter constructed from various materials (Copper and Pyrex). The results of their study indicated that the ullage size and container material profoundly influence the burning behavior. For glass containers of approximately 5 cm diameter, burning at larger ullage resulted in lower fuel consumption rate. For example, the value for burning rate was 0.02 kg/m^{2}s for an ullage of zero and decreased to 0.005 kg/m^{2}s for an ullage of 10 mm. The trend for copper was obtained to be very different. Due to heat conduction from the vessels walls to the fuel layer, burning rate stayed constant for the first 10 mm of ullage and then decreased. Still, the burning rates were higher in copper than in Pyrex containers.

The ullage situation for pool fires in ice cavities is completely different because of ice melting and accumulation of water underneath the fuel layer. For a closed bottom pool, the oil layer elevates if the amount of melt-water is more than the amount of oil that is removed by burning and vice versa. In general, the smaller size pool brings more melting and less burning of the oil level that translates to faster accumulation of the melt-water and more vertical displacement of the fuel layer. A larger pool, however, tends to have higher regression and less melting thus the oil level will not vary significantly during the *in situ* burn. The consequences of such vertical movements in oil pools can vary from extinguishments because of overflow or causing a secondary unwanted fire. Thus, the ullage effect in pool fires in ice has different indications than normal pool fire. In cases where the oil is in open bottom pools, the level of the oil will not be affected by the ice melting or regression of the oil.

2.1.3 Heat feedback from the flame

Understanding the mechanisms of heat transfer and the aerodynamics of the reacting system that forms the flame shape is essential to describe the fire phenomenon. In a pool fire, the burning rate is controlled by the balance of the energy transferred from combusting vapors above a liquid fuel to its surface and the flux of fuel vapors out of the liquid. Consequently, the determination of the heat feedback to the surface is of primary concern for quantifying the surface temperature of the fuel and its burning rate [100]. The ratio of energy that is used to vaporize fuel (heat feedback) to the ideal total energy release of combustion is known as heat feedback fraction. The heat feedback fraction is independent of amount of mass burning rate and is solely related to the fuel properties. However, the total heat feedback can depend on many parameters such as pool diameter, flame shape and luminosity, and spatial distribution of soot and temperature in the fire [110].

In small size pool fires, i.e. in the laminar flow regime, the radiative flux along the pool surface is nearly constant for all luminous and non-luminous flames. The experimental and analytical analysis of Nakakuki et al. [111, 112] have shown the conductive flux through the walls is dominant over radiation. The implication of their work is that the energy balance of the liquid fuel should consider the heat transfer at the liquid surface as well as the burner wall. The surface temperature would be higher near the rims compared to the center of the pool.

For quasi-laminar flow regimes (diameters of around 10 cm), the heat feedback mechanism is a mix of conduction and convection when flame vortex appears above the fuel. Experimental work on measurement of heat feedback of heptane and toluene pool fires of 10 and 30 cm diameter [113-115] show radiation effect becomes a more significant mode of heat feedback. The contribution of the combustion gases emission to total radiation is significant at this diameter range. However, assuming radiation is the only mode of feedback will lead to under prediction of the heat flux.

The radiation hazards of pool fires increase with their size and have been the center of attention for fire safety researchers. Similarly, radiation feedback to the fuel surface increases in the transitional flow regime toward an asymptote for large pool fires in turbulent regime. Hamins et al. [116], investigated the heat feedback from the flame to the surface of burning liquid fuels experimentally. The radial variation of the local radiative and local heat flux incident on the surface of a 30 cm diameter pool fires were measured in their study. The measurement of the radiative heat flux was done with a water cooled, nitrogen purged, narrow view-angle gauge. The fuel level was kept 0.5 cm below the rims of burner. The experimental results showed that the intensity of energy released by the heptane flame to the fuel surface received by the heat flux gauge decreased from 17,000 (W/m^2-sr) to 7000 (W/m^2-sr) when moved from the center to the rim of the container.

In the turbulent flow regime, the radiative flux from the flames to the burning fuel surface is maximum at the center of the fuel bed and it decreases gradually toward the edge of the fire [117, 118]. Measurements and modeling of very large pool fires show significant gradients in the heat flux incident on the fuel surface. The presence of these gradients will result in temporal gradients on the fuel surface and consequently changing the local fuel vaporization and fuel transport within the pool [119].

An empirical correlation for heat release rate of pool fires was used in Ref. [120] to be used in the energy conservation of burning liquid fuels. The net heat feedback per unit area to the fuel has been found to be independent of the pool diameter and observed to be less than 1% of total heat released for small pool fires [120-122].The heat flux reaching the surface can be expressed as

$$\dot{q}_s'' = \frac{4}{\pi}\,\chi_s \rho_\infty C_p \left[T_\infty g\left(T_f - T_\infty\right)\right]^{\frac{1}{2}} D^{1/2}\,, \qquad (2.2)$$

where ρ_∞, C_p, and T_∞ are properties of air at ambient temperature; T_f is the temperature of hot gases above the liquid and can be assumed to be constant around 1200 K. χ_s is a specific fraction of the heat released fed back to the fuel surface and is independent of pool diameter. The value corresponding to χ_s is documented well [120-123]. However, for pool size smaller than 1 m in diameter χ_s can be very small [120]. The fraction (χ_s) for 30 cm diameter pools was found to be 0.010, 0.054, 0.017, and 0.012 for Heptane, Methyl Alcohol, Methyl Methacrylate, and Toluene, respectively [110]. A comprehensive review of studies related to thermal feedback in pool fires is presented in the work of Joulain [118] that address the characteristics of pool fire flame and plume structure, including flame height, the entrainment of air, the pulsation of the flame and the influence of cross-flow, the formation and properties of soot, the heat feedback, and mass burning including radiation transport and radiative energy blockage.

Although there are only a handful of studies conducted in ice with proper measurements, it can be seen that the heat feedback in pool fires in ice follows that of the typical pool fires. The exception is laminar flow regime of pool fires in ice (diameter of less than 5 cm) where ignitibility of the fuel is a problem due to considerable lateral heat losses. For the transitional flow regime, the surface temperature profile has been found to decrease when going away from center and increase near the ice wall near the flame anchoring location [87]. Pool fires in larger diameter ice cavities of about 1 m also show a high surface temperature at the center that decreases to lower values near the ice wall [94]. Nonetheless, the fundamental research on pool fire adjacent to ice walls is very new and more information on heat fluxes and fuel temperature profiles are needed to form coherent conclusions. Especially, temperature profile of the fuel surface in the vicinity of ice would be useful in understanding the ice melting.

2.1.4 Ignition and flame spread

Ignition of a liquid pool by a heat source is a stimulating scientific problem that has practical relevance in fire safety and other applications such as ISB. The increase of fuel vapor concentration above a liquid fuel to its lower flammable limit renders the fuel-air mixture as ignitable. Addition of a heat source (spark or pilot flame) to this mixture will produce flashing. This process is known as ignition and the minimum temperature of the fuel that permits ignition is fire point temperature. Flame spread is the self-sustained flaming of the

liquid fuel and its propagation over the fuel surface. In order for the flames to be self-sustainable and spreading, the released heat from ignition should induce evaporation rates that are equal to or higher than the reaction rate of the fuel with oxidizer [66, 124, 125]. The temperature that corresponds to this evaporation rate is known as fire point and is normally 5-10 °C above the flash point temperature [126].

Ignition and flame spread over liquid fuel pools are characterized based on their initial bulk temperature. If the initial liquid temperature is above the flash point, then ignition will be spontaneous and the flame will spread across the liquid surface as a premixed laminar flame. However, if the bulk temperature of the liquid fuel is lower than its flash point temperature, ignition will be delayed so the fuel temperature reaches the flash point. In addition, flame spreading is also a strong functions of the fuel's temperature [127]. Flame spreading can be divided into two distinct categories: sub-flash spreading and super-flash spreading with an intervening transition zone characterized by pulsating spread. Flame spread is governed by liquid-phase convection, that is preheating the liquid ahead of it to the proximity of the flash point in order to create a combustible mixture ahead of the flame into which it could propagate [128-130].

Imposing a heat source to a liquid fuel at sub-flash temperatures will create a temperature gradient on the surface that drives a Marangoni flow on the surface and viscos shear stress forms a bulk flow. Figure 2.4 shows the liquid flows induced by an ignition source. It is expected to flow toward the ice to be stronger and deeper. Because the heat addition is from above, the pool is stably stratified and buoyancy-driven flow should be non-existent except near the ice wall. However, buoyancy and surface tension forces are coupled inherently. Murad et al. investigated the parameters that control the ignitibility of a liquid pool of fuel at a sub-flash temperature. It was found that for liquid fuels below their flash point temperature, the heat source will induce fluid motion that delay ignition [131, 132]. Addition of surfactant (to suppress the surface tension) and viscosities (to suppress all convection together) resulted in two and ten times faster ignition, respectively.

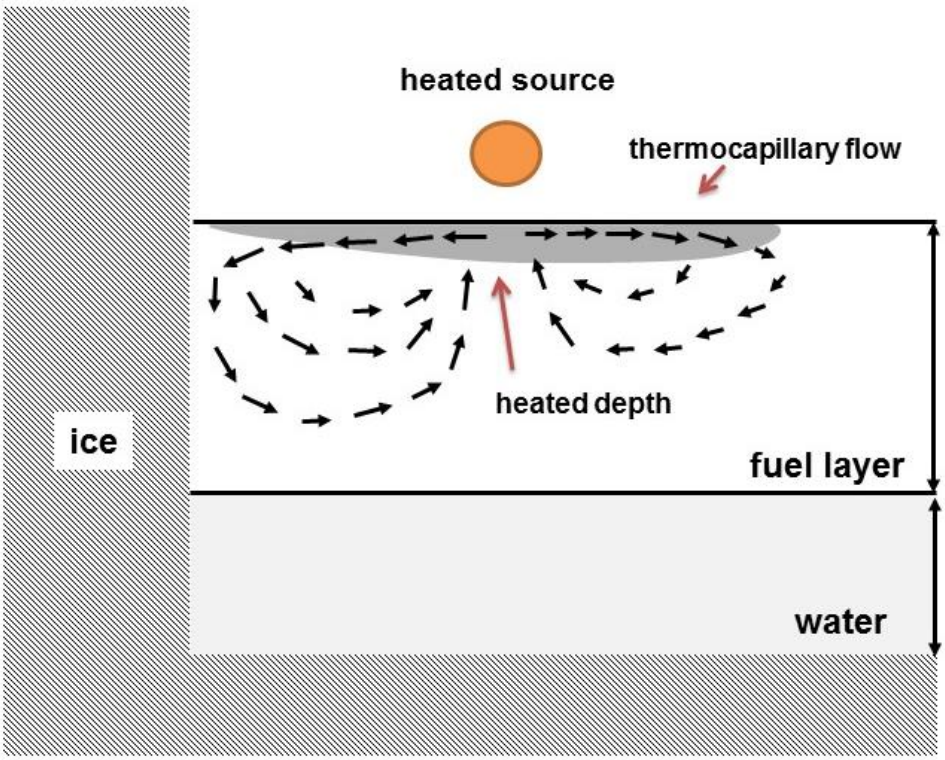

Figure 2.4: Qualitative liquid flow fields prior to ignition.

Unlike ignition, in sub-flash flame spread convective motions generally assist the flame spread [133]. A thin sub-surface layer streams rapidly outward from the ignition area that preheats the liquid in front of the flames. The preheating zone is driven by thermocapillary force but it breaks into several eddies by the viscos shear stress. Liquid flow pattern for less viscos fuels is therefore disordered and turbulent [134, 135]. The initial surface temperature of the liquid fuel results to be a control parameter of flame spread velocity. Flame spread is proportional to a characteristic surface temperature difference and inversely proportional to the distance over which this temperature difference exists [125].

Degroot and Ybarra [136-139], studied the flame propagation over liquid alcohols (methanol, ethanol, propanol and butanol). The initial fuel temperature was kept uniform along the horizontal with a refrigerant circuit. Methanol was ignited at one end of the channel and flame spread was observed. The different spreading regimes above liquid fuels was experimentally described for a wide range of initial surface temperatures. The critical transition temperatures between these regimes was characterized. First was the uniform regime where the flame spread rate had a constant value (for T > 17.3 ℃ the flame velocity was 65 cm/s). The second regime was the pulsating regime which happened at temperatures

below the critical temperature of the system with velocity of the flame 0-15 cm/s and the third regime was named pseudo- uniform regime which had a very low constant flame velocity (1 cm/s). The third regime happened for temperatures below the pulsating regime.

For *in situ* burning in ice-infested waters the fuel temperature would most likely be below its flash point, and thus only sub-flash ignition and flame spread are of interest. The ambient condition, i.e. wind, is also crucial in determining the ignition success [131]. Crude oils are viscos and have high flash point which both increase with the degree of weathering. In cold ambient, ignition and flame spread might be accomplished by the same mechanisms as for solid fuels [140]. This is definitely true when taken to an extreme, since the high viscosity would effectively eliminate liquid convection. Wu et al. [141] studied the ignition of weathered oil on a water sub-layer. Their experimental study was designed to provide a tool to assess the ignitibility and flash point of weathered fuels in an oil spill accident. It was observed that ANS crude oil in its natural state ignited at ambient temperature so there was no external energy needed. When the oil was weathered, the ignition delay time, t_{ig}, decreased with increase in external heat flux and a linear dependency between heat flux and $t_{ig}^{-1/2}$ was attained. Also, the higher levels of weathering required application of greater external heat fluxes. For example 7% (by mass) weathered ANS did not require external heat flux to ignite but when the weathering degree increased to 20%, an external heat flux of 4 kW/m^2 was required to initiate the ignition. For fuel layer thicknesses of 8 mm and above the results were independent of thickness and for thinner layers higher heat flux was required. For instance, the required critical heat fluxes for igniting the 3 mm thick Cook Inlet were recorded to be 2.2 kW/m^2 while for same condition and 8 mm of thickness only 1 kW/m^2 was needed.

2.2 Liquid-phase convection

The phenomenology and understanding the controlling mechanisms of liquid flow in pool fires have aided fire researchers in providing means to lessen the risks associated with use of liquid fuels. Numerous studies on ignition and flame spread over liquid fuels have demonstrated the importance of convective motion in liquid fuels [128]. Liquid-phase convection was a key finding in the research area of ignition and flame spread. Liquid-phase convection in pool fires (during ignition, flame spread, and burning period) is mainly

driven by Marangoni flow and buoyancy forces and also by evaporation and thermal expansion.

Surface tension and buoyancy are more attended to as the main forces in this area of research. Liquid surface temperature near and under the leading edge of the flame is near its flash point but it continues to rise under the trailing convective-diffusion flame to a value near its boiling point. Heating of the liquid fuel at the location of flame anchoring produces surface-tension driven flows on the surface. This leads to motions in the liquid bulk by viscous shear stresses and appearance of complex eddying motions [142]. Because the liquid layer is no longer thermally stratified, buoyancy's role in returning the warmer liquid upward becomes significant too. The diffusion flame in transitional turbulent pool fire regime exerts non-uniform feedback energy that induces fluid motion throughout the burning period. A rather thick layer of constant temperature liquid (3-4 mm) is found beneath the surface of burning liquid fuels that is caused by the convection in the liquid. This layer grows for a system with minimal heat losses, and leads to superheating of the water sublayer and boilover. The notion of disregarding the liquid-phase convection in pool fires (assuming heat transfer within the liquid by conduction only) might have been ideal for simplifying the temperature field of liquids in pool fire problems. But when liquid fuels are bound with walls that are prone to melting, accurate understanding of heat transfer within the liquid is essential. To this end, the following sections are addressing problems concerning liquid-phase convection in liquid layers that are heated from above.

2.2.1 Liquid-phase convection in pool fires

Although extensive work on convective flow in the flame spread process has been undertaken, only a few studies have addressed the transport phenomena throughout the burning of pool fires [143-145]. The study of Yumoto et al. [143] was one of the first studies to consider convection in the liquid fuel and its effect on pool burning rate. In burning of Hexane in a 3 cm diameter glass vessel, convective motion occurred upon ignition and vortices started to develop below the fuel surface. The size of the vortices grew in the first two minutes and then they diminished as the fuel and vessel wall obtained similar and uniform temperature. Two groups of vortices were identified, one in the upper part and the other in the lower part of the pool. The vortices in the upper part had large radii and relative high fluid velocities and were traveling from the side walls toward the center. The flow

direction can be explained by the surface temperature of laminar pool fire regime where the surface temperature increases going from center toward the side walls. Due to the higher temperature near the vessel wall, the surface flow is toward the center (by surface tension gradient) and flow near the walls is upward (by buoyancy effect). The vortices in the lower part had small radii and low fluid velocities and unknown rotation direction. Nonetheless, the magnitude of vertical and horizontal velocities reported in Yumoto's work seem to be incorrect. Velocities of around 12 cm/s are shown for the liquid flow which is at least an order of magnitude higher than the flow velocity observed in sub-flash flame spread studies.

In a more recent study [144], a two dimensional Particle Image Velocimetry system was used to study convective field within a 9 cm diameter methanol pool fire. Their experiments were conducted at steady state burning condition and with bottom wall temperatures varying from -5 °C to 40 °C. Similar to Yumoto's work, the methanol velocity field showed an intense mixing motion in the top layer of the liquid fuel. However, two strong counter-rotating vortices were observed in the upper part and near the wall. The vortex closest to the left wall, rotated clockwise directing fluid away from the wall toward the center of the pool. This was potentially driven by buoyancy force. Surface tension gradient is another potential force in driving the flows away from the wall. The second vortex rotation was counter clockwise and merged with the wall vortex at a stagnation point in about 0.6-1 cm distance from the wall. Since colder free surfaces pull the fluid from hotter regions, it can be assumed that fuel surface in center and near wall regions had higher temperatures. Therefore, the two surface flows were traveling toward the stagnation point. In contrast to the top layer of the liquid, the bottom layer was rather quiescent with low vertical velocity. Nevertheless, the liquid-phase convection mechanisms have strong contributions to the energy transfer in the liquid pool. Specifically, the wall adjacent to the liquid may have temperatures different than that of the liquid, which would intensify the convective heat transfer.

Although there are a limited number of studies analyzing the liquid convection in pool fires, a significant number of studies on the same topic is present for ignition and flame spread problems. However, these studies do not benefit from the big pool of data on classical convection problems. Convection in shallow layers or cavity flows subjected to partial heating have been a subject of experimental and theoretical study for decades and as a result many flow patterns/regimes are characterized. These basic studies are a valuable source for

practical problems such as pool fire. The following sections are provided to create a connection between the basic knowledge and practical studies related to liquid convection.

2.2.2 Thermocapillary-buoyant flow

Since convection in the fuel layer is found to have strong contributions in liquid energy transfer in the pool fires, one can suppose that ice melting in pool fires is largely influenced by liquid-phase convection. A summary of publications that have studied combined thermocapillary-buoyancy flows, as the main effective forces, is considered here. In particular, the studies that mimic the physics of the problem in hand, convection in liquid layers subjected to localized heat flux or horizontal temperature gradients, were of interest.

Study of the buoyant and thermocapillary forces and the flows associated with these two mechanisms, considered independently, are examined extensively [146-150]. However, the dynamics observed in different applications such as crystal growth, micro-scale material processing, welding, etc. are very complex and involve a combination of these mechanisms. Therefore, consideration of the existing knowledge on the buoyant-thermocapillary flow is necessary to comprehend the liquid-phase convection.

The most general form of buoyant-thermocapillary flow problem that is considered for the study is the convection in a cavity with its free surface imposed to a temperature gradient. This simple geometry choice has less parameters and has enabled researchers to study this complicated problem under a more controlled conditions. Nevertheless, there are still parameters that influence liquid convection in a cavity that include Prandtl number (see Section 2.2.3) of the working fluid, the cavity aspect ratio, contact angle of the fluid and the wall, and the imposed temperature difference which defines the Rayleigh ($Ra = \frac{\beta g H^3 \Delta T_v}{\vartheta \alpha}$) and Marangoni ($Ma = \frac{\sigma_T R \Delta T_h}{\mu \alpha}$) number [151, 152] (See section 3.2.3 and 4.2.2). Where, $\sigma_T = -\frac{\partial \sigma}{\partial T}$ is the change of surface tension per °C, R is the radius of the cavity, H is the depth of the cavity, g is the acceleration due to gravity, and β, μ, ϑ, and α are thermal expansion, viscosity, kinematic viscosity and thermal diffusivity of the working liquid, respectively [153]. Consequently, a large number of different types of flow can be found in such systems.

The basic surface tension induced flow draws the surface fluid from the hot region toward the cold. In the combined buoyancy-thermocapillary flow problem, the buoyant force may assist or compete with thermocapillary. Generally, for fluids with surface tension decreasing with increasing temperature, these mechanisms reinforce each other to drive the convection, but their scaling may be different. The relative contribution of each mechanism is determined by the dynamic Bond number, which is the ratio of the Rayleigh number to the Marangoni number [154-157]. The basic flow leads to a large one roll with fluid moving from hot toward cold side on the surface. Here, the basic flow is assumed to have the primary roll and buoyancy is of secondary importance since heating is from above.

The basic surface tension induced flow may destabilize into different stationary and traveling patterns by the increase in temperature difference. When temperature difference is increased above a threshold, around 5 °C, the basic flow changes and depending on the height of the liquid layer different flow conditions are expected. For small cavity heights (<5mm) multi-roll condition consisted of co-rotating rolls that are encircled by the basic flow will appear. Larger liquid heights can lead to the same rolls that are now superimposed on the basic flow [154, 158].

Above a second temperature difference threshold, the flow pattern becomes time-dependent and 3 dimensional. Few studies address this flow pattern as disordered and chaotic regime, while other use terms such as oscillatory regime or traveling waves [159, 160]. The discrepancies in results of these studies could be explained by the differences in the geometry or the boundary conditions. Still, one common conclusion that can be made from the previous works is that the surface tension flows result in the presence of a rapid mixing motion near the surface.

2.2.3 Prandtl number and other fluid properties

The main parameter amongst physical properties of a fluid related to convective transfer is the viscosity. Viscosity (μ) is defined as the resistance of a fluid to flow and has the unit of kg/m.s in SI system. When the dynamic viscosity is divided by the density of the fluid, the kinematic viscosity, which has the units of m^2/s (similar to thermal diffusion coefficient, α.) is obtained. The relative strength of momentum diffusivity over thermal diffusivity in convective flows is characterized by a non-dimensional number known as the Prandtl

number, *Pr*. The Prandtl number is defined as the ratio of the kinematic viscosity ($\vartheta = \mu/\rho$) to the thermal diffusivity ($\alpha = k/\rho c_p$) which is equal to $c_p\mu/k$ where c_p is the specific heat, μ is the dynamic viscosity and k is the thermal conductivity of the liquid. Small values of the Prandtl number ($Pr << 1$) means that the thermal diffusivity dominates the heat transfer, whereas for large values ($Pr >> 1$), the momentum diffusivity dominates the behavior [161]. It is possible to write the Marangoni number based on the Reynolds and Prandtl numbers, *Ma= Re.Pr*. Similarly, the Rayleigh number can also be written as the product of Grashof and Prandtl number, *Ra= Gr.Pr*. Most hydrocarbon liquid fuels have a Prandtl number of 10 to 50 [162] and are expected to be dominated by momentum diffusivity.

Surface tension is the elastic tendency of a liquid at its interface with air and is an important property of fluids in microscale geometries. It arises from the imbalance because the attraction of liquid molecules to each other (cohesion) is larger than to the molecules in the air (due to adhesion). Surface tension induced flow occurs when there is a gradient of the surface tension created by concentration or temperature variation along the interface. A rather strong convective motion may be produced if variation of surface tension is large. The surface tension driven motion creates shear stress at the surface that is similar to what the wind can create [163]. The flow for a surface tension flow created by temperature variation is from hot to cold region. In presence of gravity variation in density give rise to convection known as buoyancy. The change in density of a fluid per unit temperature, known as thermal expansion coefficient, is another fluid property that defines the magnitude of buoyancy convection.

The boiling point is another parameter that is very important in defining the level of flammability of a liquid hydrocarbon. The other importance of the boiling point of a liquid fire is that it defines the upper limit of temperature difference in a burning liquid fuel. And this temperature difference is instrumental in determining the extent of convective flows as it appears in both Rayleigh and Marangoni number.

A literature review on related aspects of pool fires to the pool fires was presented in this chapter. A good understanding of the phenomena involved in the burning of pool fires was established. Some of the pool fire fundamentals were studied and relevant problem parameters were identified. The most important piece of finding that must be emphasized

herein is the lack information on the liquid-phase convection. Hence, a series of experimental and theoretical studies are developed to investigate the effect of liquid-phase convection on melting of ice in pool fires.

3 Burning of n-octane in an ice cavity

In a typical pool fire (contained with sidewalls), a portion of the heat produced by the flame transfers to the body of liquid fuel in deeper areas by conduction through the rim of the pan and then convection in the fuel layer [98]. When the rigid walls of the pan are replaced with walls of ice, the heat transfer mechanisms are significantly altered. The fuel layer losses energy to the ice wall, whereas in typical pool fires energy is added to the fuel by the in-depth conduction through the rims. The lost energy to the ice wall melts the ice into a unique form that is called a lateral cavity. The low temperature of the ice also change heat transfer pathways in the fuel that has important implications for the burning as discussed in Section 2.1.1.

From a practical point of view there are some disadvantages to these ice deformations. For example, such a deformation will allow a portion of the oil to drift underneath the lateral cavity. This is presumed to be a potential factor in reducing the burning efficiencies by preventing the exposure of air to the trapped oil. The other explanation for this is the strong heat losses that occur inside a lateral cavity due to large contact area of liquid with the ice. A decrease in the burning efficiency necessary results in a larger amount of oil residue. In addition, the confined residue in the cavity would be harder to collect and this would increase the cost of the post-burn cleanup during *in situ* burning operations. In particular, if the residue stays untreated, it could be encapsulated due to freezing of the water in colder seasons and potentially remain in the ecosystem for years.

In this chapter the lateral cavity formation during burning of n-octane in a cylindrical ice cavity is investigated. The hypothesis to explain the formation of lateral cavities is that the penetration in ice is caused by flows in the liquid fuel layer. The observations made during experiments of this study corroborate existence of a flow close to the free surface of the

fuel. The driving forces behind the flow in liquid fuel are anticipated to be buoyancy and surface tension, relating to natural and Marangoni convection, respectively. However, the relative contribution of each of these mechanisms needs to be studied. Therefore, it is required to determine the influence of these convective flows within the fuel layer in order to understand the formation of lateral cavities in the ice walls.

The objectives of this study are to systematically observe lateral cavity evolution during burning to understand the role of convective motions in the fuel layer (role of thermocapillary and natural convection). Further, the relation of these flow mechanisms to the lateral cavity formations during *in situ* burning of liquid fuels in ice cavities is investigated.

3.1 Methodology

An experimental approach consisting of observations and measurements was used to conduct this part of the research. Measurements were made of the geometry change of ice during burning, fuel mass loss, and the temperature field of the liquid phase. A detailed description of experimental design and parameters related to this study is provided in the following.

3.1.1 Experimental setup

Figure 3.1 shows the experimental setup with n-octane in a 5.7 cm diameter ice cavity. Each experiment used an ice block with a circular cavity excavated in its center. The depth of the cavity (H) and initial fuel layer thickness (L) were chosen based on the data obtained from preliminary tests to prevent overflow and spillage during the burning of n-octane. The ice block was placed on a drip pan on top of a load cell (precision of 0.01 g) to record mass loss of the fuel. Then, 30±0.1 g n-octane was added to the cavity (with no water base-layer) and a propane torch igniter was used to ignite the fuel layer immediately after the n-octane was poured into the cavity.

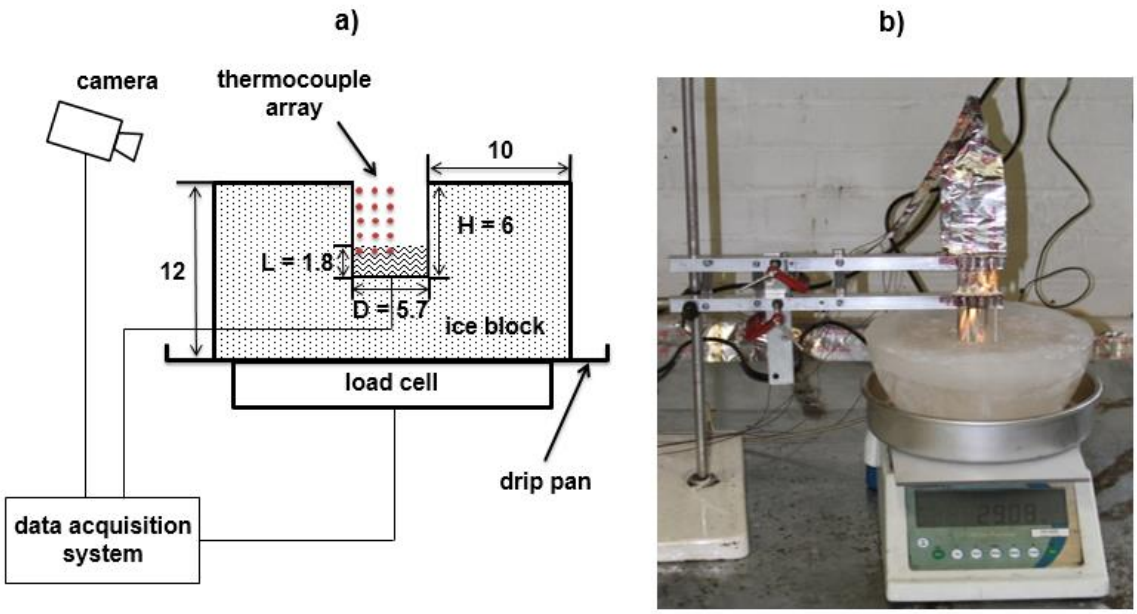

Figure 3.1: a) Schematic of the experimental setup. b) A picture of the experimental setup. The dimensions are in cm with an uncertainty of ±0.05 cm for D and ±0.1 cm for H.

3.1.2 Experiment procedures

Two sets of experiments were performed to collect data for analysis. In the first set, ten identical tests were conducted where the only varying parameter was the burning duration. In the first experiment, n-octane was allowed to burn only for 1 minute and then it was extinguished. The second experiment was extinguished after 2 minutes and so on. After each test the ice blocks were cut in half and a photograph was taken from the cross section. In addition, measurement of the ice cavity geometry was made by processing the images. These tests were intended to give an understanding of the process of geometrical changes of the ice and lateral cavity formation. In addition, the free surface of the fuel was tracked visually by the camera which was positioned on top of the ice block and the interface of the fuel-water was calculated based on the fuel layer thickness at each time stamp. The fuel layer thickness was also calculated based on the diameter of the cavity and the remaining mass of the fuel (Load cell data). In the second set, experiments were conducted with 3 thermocouples (type K, gauge 36, and 0.13 mm diameter protected by ceramic tubes with a 1-2 mm exposed junction) placed inside the cavity as shown with solid circles in Figure 3.1. These tests were repeated 5 times with the thermocouple (TC) array placed at different

elevations in the cavity to create a temperature map of the liquid fuel within the cavity. A more detailed description of the TC implementation is given in Section 3.2.2.

3.2 Results

Measurements of mass loss over time as well as the images taken from the cavity were used to measure and analyze the geometry change of the cavity and thickness of the fuel layer. The results are reported in Section 3.2.1 along with a discussion on lateral cavity formation. The temperature profile of the fuel layer was obtained by using different arrangements of TCs inside the cavity and within the fuel layer. The results of the temperature analyses are reported in Section 3.2.2. A discussion on convective flow within the fuel layer and the effects of the fuel layer on melting of the ice follows in Section 3.2.3.

3.2.1 Geometry change of the ice cavity

The geometry change of the original cavity in ice during combustion of liquid fuels has been reported to be an important reason in affecting the burning rate and efficiency of a liquid fuel [87]. However, the exact changeover of the cavity into its final shape and formation of lateral cavity has not been discussed in earlier studies [86, 87]. In order to provide a detailed observation of the geometry change of the ice cavity, 10 experiments with similar initial condition were performed as explained in Section 3.1.1. Figure 3.2 shows the change in cavity geometry along with some of the corresponding dimensions.

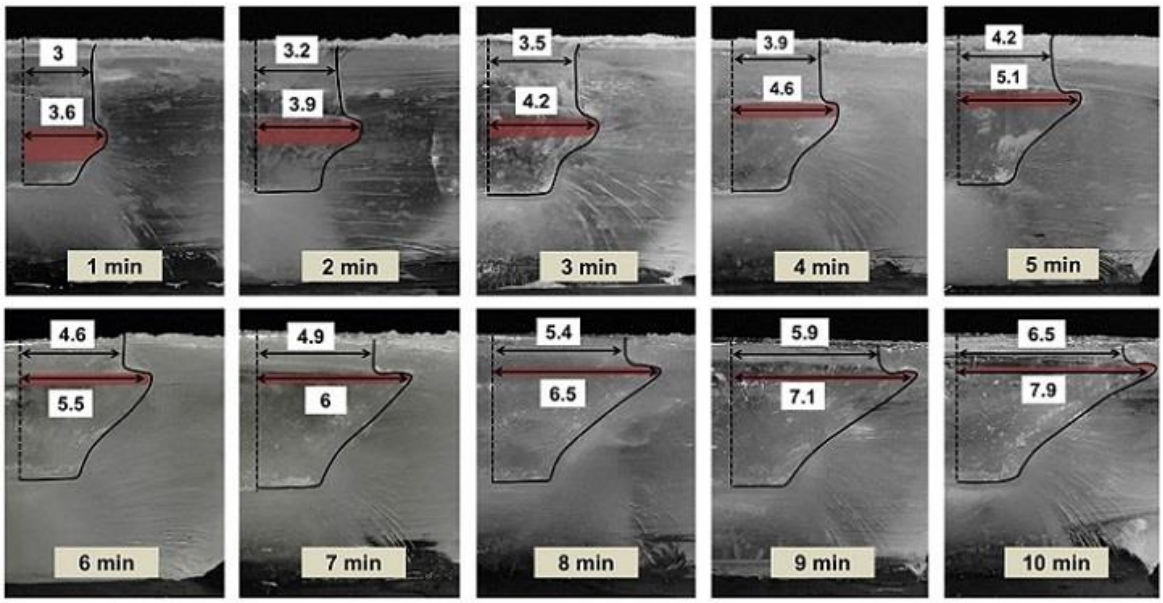

Figure 3.2: Lateral cavity formation in sequential steps from top left in photos of ice blocks cut in half after the experiment. The dashed line represents the centerline of the cavity. The dimensions are in cm.

As shown in Figure 3.2, at any instance during burning of the n-octane pool, the ice walls of the cavity were melting and the diameter of the cavity was constantly increasing. However, it was observed that the rate of melting of the ice walls were higher in areas where the fuel layer was in contact with ice than in places where only the flame was present. The melted ice created a semi-hemisphere void inside and around the circumference of the cavity. Thus, a lateral penetration of the fuel layer was observed around the perimeter of the original cavity. The final diameter of the cavity measured at the location of the fuel layer (D) was 15.8 cm where the diameter at the top surface of ice ($D`$) was 13 cm. This translates into a partial penetration length (defined as $\frac{D-D`}{2}$) of roughly 1.4 cm for a 10 minute burning period. The intrusion length, L, of n-octane to the ice can be calculated by subtracting the original radius of the ice cavity (2.85 cm) from the lower number in each image. Note that the total intrusion length (calculated from original position of the ice wall) of the fuel layer was larger (about 5 cm). With this estimation the area of the fuel layer would be roughly 30 % larger than the cavity opening area which means difficult air entrainment for a portion of the fuel. Thus, the burning rate of the fuel would be lower.

As mentioned, during burning of the n-octane pool, the penetration length into the ice wall was observed to be larger wherever the liquid fuel was in contact with ice. Contrary to the intuitive assumption that the flame's leading edge (temperature range of 1000-1300 °C) can

melt the ice faster, it became evident that the liquid fuel (temperature range of 80-125 °C) is melting the ice at a much faster pace. Melting is an endothermic process and it requires a significant portion of the produced heat by combustion of the fuel to be consumed. This suggests existence of a great heat transfer coefficient in the liquid phase compared with that of the gas phase [164].

In burning of the fuels in an ice cavity, a portion of the released heat by the burning of the fuel is transferred to the walls thus converting the ice to water. Because of the higher density of water (compared with that of the fuel) a layer of water forms at the base of ice cavity forcing the fuel layer to elevate with respect to the bottom of the cavity [86]. For these experiments, the change in the thickness of the fuel layer (because of expansion of the cavity and evaporation of the fuel) and position of the fuel layer at each time stamps are shown in Figure 3.3.

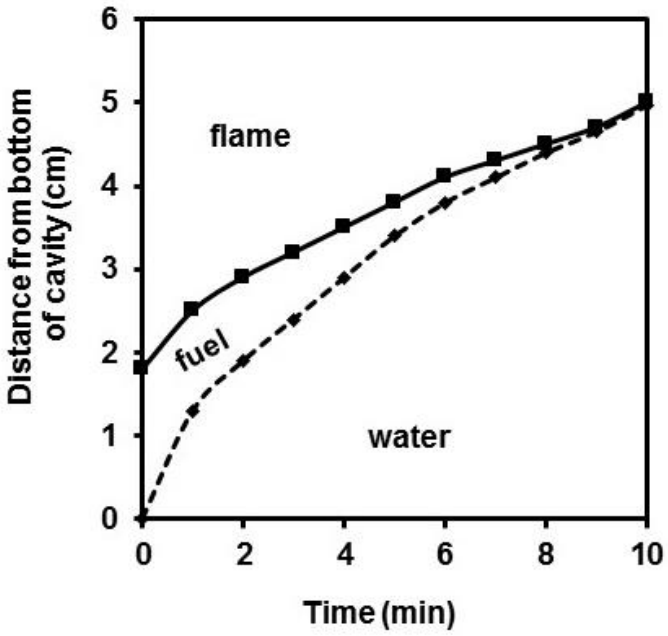

Figure 3.3: Elevation of the fuel layer in cavity (free surface and water-fuel interface shown in solid and dashed line, respectively). The time in the figure is the time after ignition.

As illustrated in Figure 3.3 the thickness of the fuel layer was initially at 1.8 cm (equal to ~30 g of n-octane) and reduced to ~0 cm at the end of the burning. The evaporation of the liquid fuel during burning and the increase in the diameter of cavity are the two main reasons for the fast regression of the fuel layer thickness. It should be noted that in the final stage of burning (last 3 minutes) the fuel layer accumulated in a ring shape around the

perimeter of the cavity. This ring shrunk and became slimmer as more fuel evaporated but maintained a 2 mm thickness, which has been found necessary for continuous burning [56]. Because of accumulation of water at the base of the cavity, the fuel layer elevated relative to the volume of the melt water. In a 5.7 cm diameter ice cavity, combustion of 30 g n-octane resulted in melting of 350 g ice. This amount of melted water makes a significant increase in a fairly small cavity. However, for large cavity diameters the elevation of the fuel layer is expected to be insignificant.

3.2.2 Temperature history

The temperature distribution of the fuel layer was measured by thermocouples (TCs). The initial fuel layer was 1.8 cm as shown in Figure 3.4. But through evaporation and geometry change of the ice cavity it became as thin as about 2 mm during the final stage of burning. As shown in Figure 3.4, the 2 mm fuel layer remained only near the perimeter of the cavity and formed a ring shape slick. The thermocouple array setup is also shown in Figure 3.4. The TC array consisted of 3 parallel ceramic tubes enclosing the TC wires each 1 cm apart horizontally. Insulated thermocouple wires were passed through the ceramic tubes for protection against flame and liquid fuel. The opening of the tube (immersed in liquid) was also blocked by heat resistant cement to prevent fuel from entering into the ceramic tube. Thus, the only exposed parts of the TCs were the 1-2 mm junctions (shown in Figure 3.4). A holder was used to position the 3 TC beads at fixed elevations for each test. A total number of 5 tests were performed with TC array being at different elevations (each 1 cm apart) with respect to the bottom of the cavity for test 1 through test 5. Thermocouple measurements were used to create a temperature map of the liquid fuel as it rose up within the cavity. The corresponding location of TCs for each test is shown in Figure 3.4. The uncertainty for the location of the TC array was 0.1 cm.

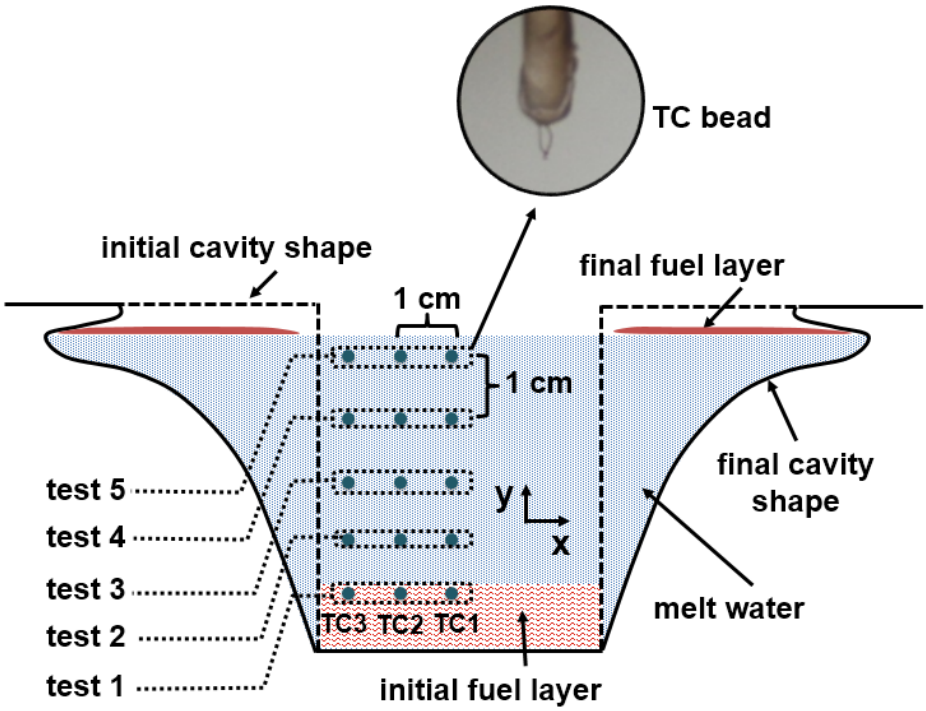

Figure 3.4: Thermocouple array setup used to obtain the temperature history of the liquid fuel.

The three TCs positioned at different locations along the x-direction (TC1 being at the center of cavity and TC3 near the ice wall, as shown in Figure 3.4) recorded the temperature field in the cavity. Figure 3.5 (a) and (b) show a sample temperature measurements of TC groups where the TC array position is 5 mm below and above the initial fuel layer surface (tests 1 and 2). For Figure 3.5(a) the TCs are located below the initial fuel layer surface and record the temperature of the Octane first and then that of melted water. In Figure 3.5 (b) the TCs are located 5 mm above the initial fuel layer surface and record the temperature of gas phase and because melting of ice causes the fuel layer to rise, eventually record the temperature of fuel layer surface and that of water.

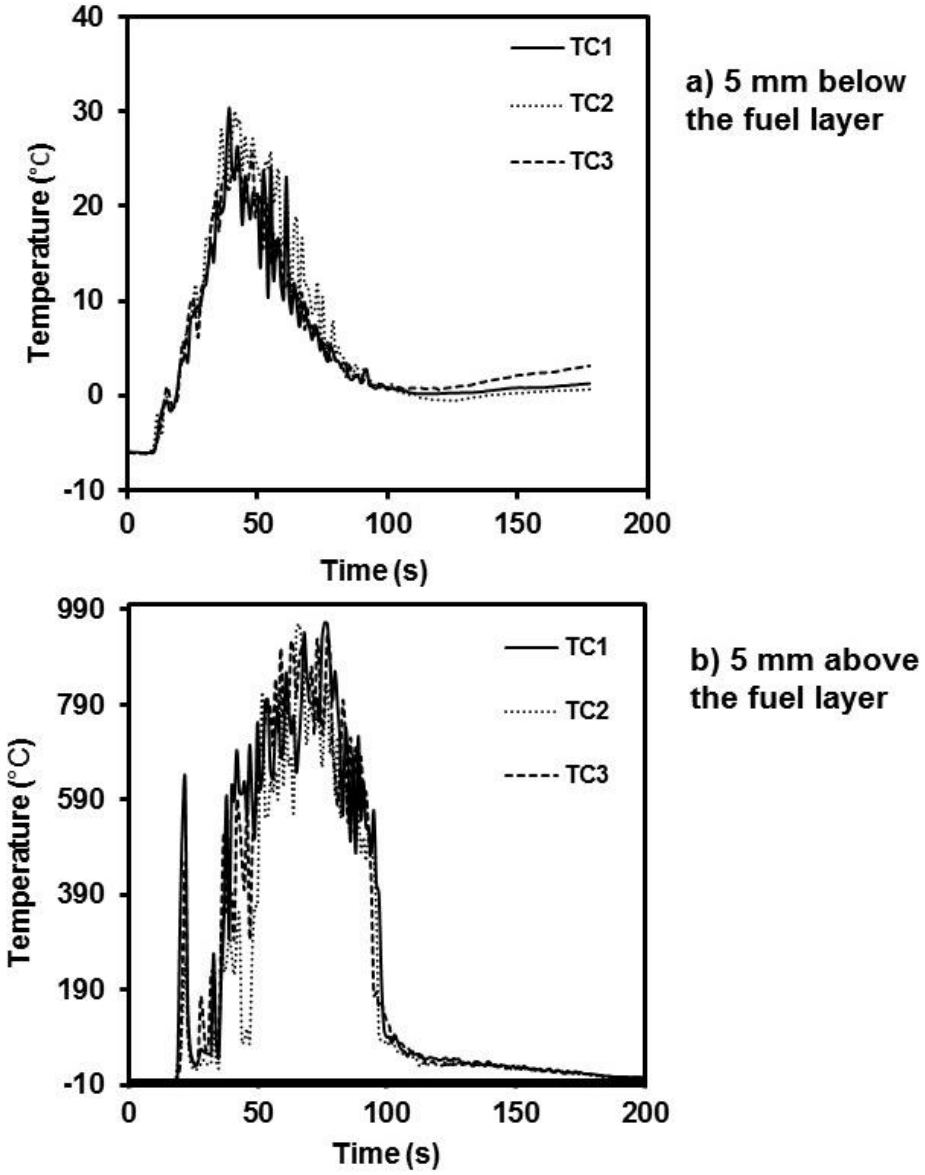

Figure 3.5: Temperature measurements in the cavity of tests 1 and 2. Note the completely different scales on the y-axis in the results from a) 5 mm below the fuel layer and b) 5 mm above the fuel layer.

The elevation of the liquid layer caused a sudden drop in the temperature recorded by these TCs. This moment was defined as the instant that the TCs immerse into the liquid fuel (500-700 °C drop in temperature readings). Considering the boiling point of n-octane is 125℃, the temperature measurements in a 5 seconds period after this moment were averaged. This averaged value was assumed to be the instantaneous surface temperature of the fuel. As expected, the temperature of the fuel layer free surface measured at the center line of the cavity had the greatest value compared with the other locations measured. This is due to the higher input radiation from the flame in the center [95]. Based on the findings of Hamins et al. [110], there should be a constant decrease of local heat feedback outward from the

center and then a rise near the rims because of local heating of the fuel by the heat conducted through the rims to the body of the fuel. In a pool fire in ice the component of heat transfer of the flame through rims to the body of the fuel does not exist. Still, the temperature readings at location TC3 are higher than those of TC2. The explanation for this difference would be the existence of a high local burning rate near the perimeter of the ice cavity [99].

Using the temperature data, the temperature gradient of the fuel layer along vertical and lateral directions were obtained. In Figure 3.6 (a) the horizontal temperature gradient (ΔT_h) on the fuel surface is shown for the distances between the TCs and the ice wall. The assumption was that the temperature of n-octane adjacent to the ice wall is similar to that of ice (0 °C). Except for the first data point (25 s after ignition) the ΔT_h trend shows a monotonic increase. This initial non-linearity may be due to the effect of ignition by the propane torch. The vertical temperature gradient (ΔT_v) was also specified as the temperature difference between the free surface of the fuel and fuel-water interface. Figure 3.6 (b) shows the vertical temperature difference of n-octane. As expected, the ΔT_v of the fuel layer was initially high and plummeted to small values toward the end of the burning. The decline in the fuel layer thickness increased the in-depth heat transfer, and resulted in higher temperature at the fuel-water interface.

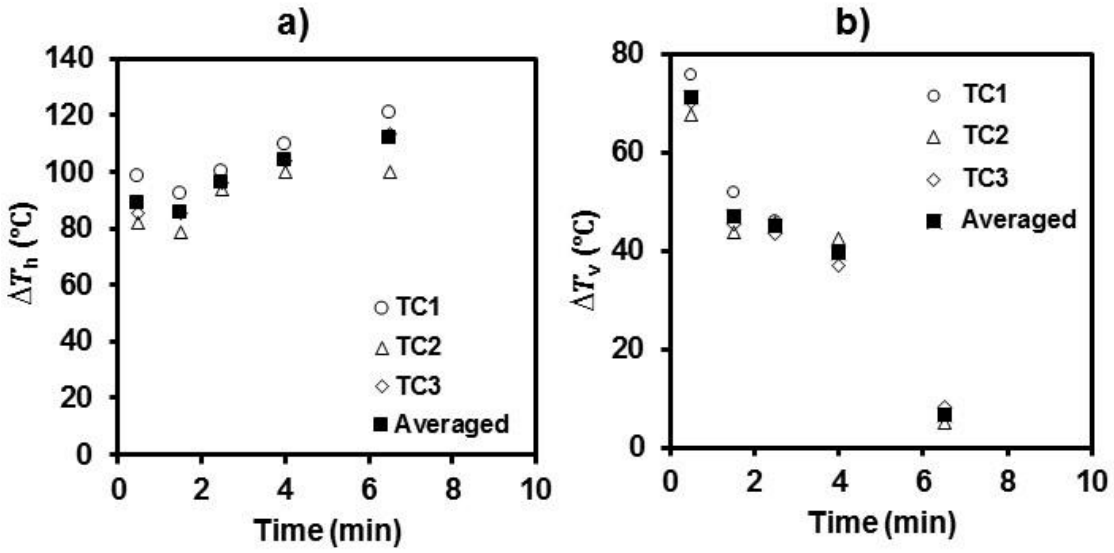

Figure 3.6: Temperature gradients of the fuel layer in a) horizontal and b) vertical directions.

3.2.3 Convective flows in the liquid fuel

The melting of the ice alongside the n-octane pool was assumed to be associated with the dynamic heat and mass transfer in the fuel layer. Thus far, the convective flows in the liquid phase of pool fires in an ice cavity have not been studied. Therefore, it is important to analyze the convective flows in these situations opposed to the convective flows in the classical bounded pool fires problem. In typical pool fires, the convective motion in liquid fuels had been attributed mostly to buoyancy driven flows (occurring near the rims of the pan) and to surface tension driven flows. Normally, the flow in the liquid fuel is retarded by the convective motion related to the Rayleigh number and is enhanced by the convective motion related to the Marangoni number. Though, when the liquid fuel is bounded by ice (instead of rigid walls) the mechanisms inducing the convective motions alter significantly. In areas closer to the ice a downward flow is expected to occur because of the low temperature of the ice. In addition, because of presence of the ice, a horizontal temperature gradient along the fuel surface produces surface tension variation on the surface of the fuel. Surface tension is a decreasing function of temperature for most liquids. Therefore, for a liquid of non-uniform surface temperature, variation of surface tension will lead to flow in the liquid. This phenomenon is known as Marangoni or thermocapillary convection [165].

The temperature of the fuel surface in centerline of the pool is about 125 °C and decreases to 0 °C directly at the side of the ice walls. Therefore, a surface tension driven flow should arise toward the ice wall outward from the center (thermocapillary convection) and downward in the liquid adjacent to the wall (natural convection). The coupling between the buoyancy driven and surface tension driven flows creates a significant transport of mass and heat that provides the necessary heat to melt the ice. The relative contributions of these mechanisms are shown and discussed further in this section.

In addition, the pattern of flow is of an intriguing nature. The pattern of flow and vortices formed in the liquid fuel burning of contained pool fires are reported to include two groups of vortices. A main counter rotating vortex in the center of pool (characterized by a larger radii and higher velocities) and a vortex closed to the rims of vessel formed due to buoyancy [143, 144]. The exact flow pattern of the burning liquid fuel in this study remains unstudied. However, by the observations made during this study it is likely to see vortices with large radii near the free surface of the fuel. Figure 3.7 shows the conceptual paths of the flow for

the two cases. The velocity of the vortices is expected to increase during the second half of burning, as the fuel layer becomes thinner.

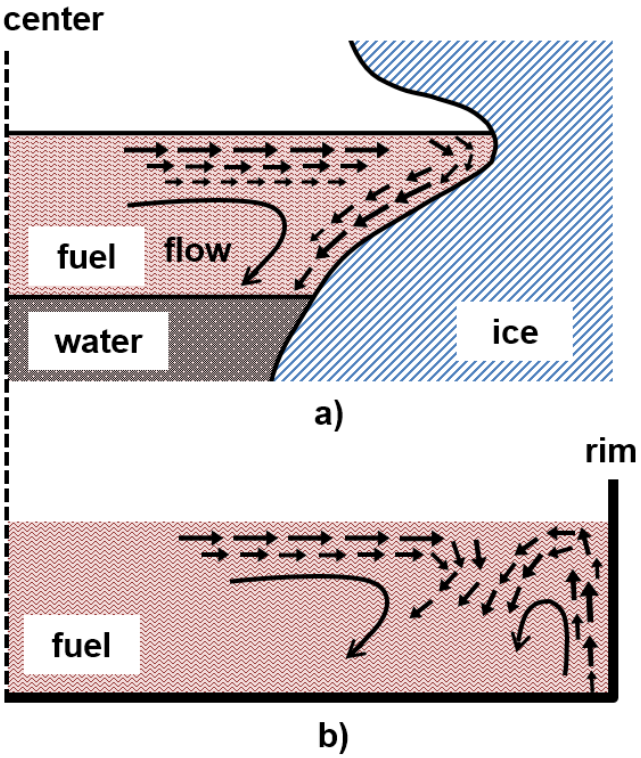

Figure 3.7: Conceptual sketch showing the paths of the flow within the fuel layer for a) contained pool fires, b) pool fires in ice cavity.

The observation made during experiments showed soot particles to be traveling on the fuel surface away from center toward the ice wall. Figure 3.8 displays one rather large particle captured on camera. This particle traveled a length of 1.5 cm in 1.28 seconds, which is equal to traversing the final diameter of cavity (~16 cm) about 50 times in the duration of the burning (10 minutes). This motion should not be mistaken with surface standing waves, which are associated with the gas phase pulsation exerting perturbation on liquid surface [110].

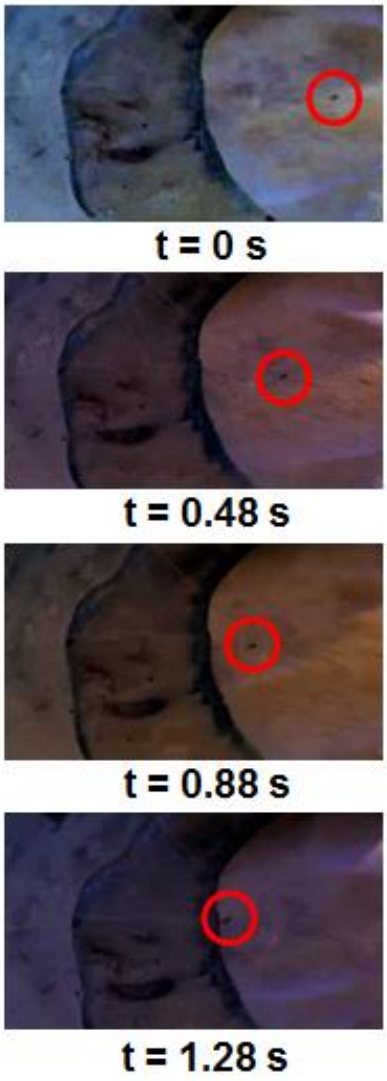

Figure 3.8: Movement of a soot particle on the surface of the fuel. The particle travels a length of 1.5 cm in 1.28 seconds towards the ice wall. Solid ice, ice cavity, and fuel surface from left to right.

To analyze the proportionality of the driving forces in the liquid fuel, Marangoni and Rayleigh numbers were used as the relevant dimensionless groups for thermocapillary and natural convection, respectively [143]. The effect of evaporation on the fluid flow was assumed to be negligible so only surface tension and buoyancy were considered as driving forces for fluid motion [135, 146, 166-168]. These dimensionless numbers can be represented as (similar to explanations in Section 2.3):

$$Ma = \frac{\sigma_T R \Delta T_h}{\mu \alpha} \tag{3.1}$$

$$Ra = \frac{\beta g H^3 \Delta T_v}{\vartheta \alpha} \tag{3.2}$$

Where, $\sigma_T = \frac{\partial \sigma}{\partial T}$ is the change of surface tension per °C, R is the radius of the cavity, H is the thickness of the fuel, g is the acceleration due to gravity, and β, μ, ϑ, and α are thermal expansion, viscosity, kinematic viscosity and thermal diffusivity of the liquid, respectively. The physical properties of the n-octane were acquired by using a commercial software (Aspen HYSYS) and the change of surface tension was calculated for the temperature range of 80-125 °C. The dimensions (R and L) and also the temperature differences (ΔT_h and ΔT_v) were obtained experimentally as explained in section 3.2.1 and 3.2.2.

After collecting all the relevant variables, *Ma* and *Ra* numbers can be calculated. Figure 3.9 shows the ratio of *Ma* to *Ra* calculated for the first 7 minutes of burning. Because of the severe reduction of thickness of the fuel layer and ΔT_v during the course of combustion, the Rayleigh number reduced several orders of magnitude due to its strong dependency to the thickness. On the contrary, the radius of the cavity and ΔT_h are increasing functions of time, hence the Marangoni number increased by a factor of 4. Consequently, the *Ma/Ra* ratio increased from very small values to unity and larger after about 5-6 minutes. Two major convective phases could be assigned to the fuel layer based on this ratio. The first phase would be the first 6 minutes of burning where buoyancy driven forces are dominant and the second phase occurs during the rest of burning time where Marangoni convection is dominant.

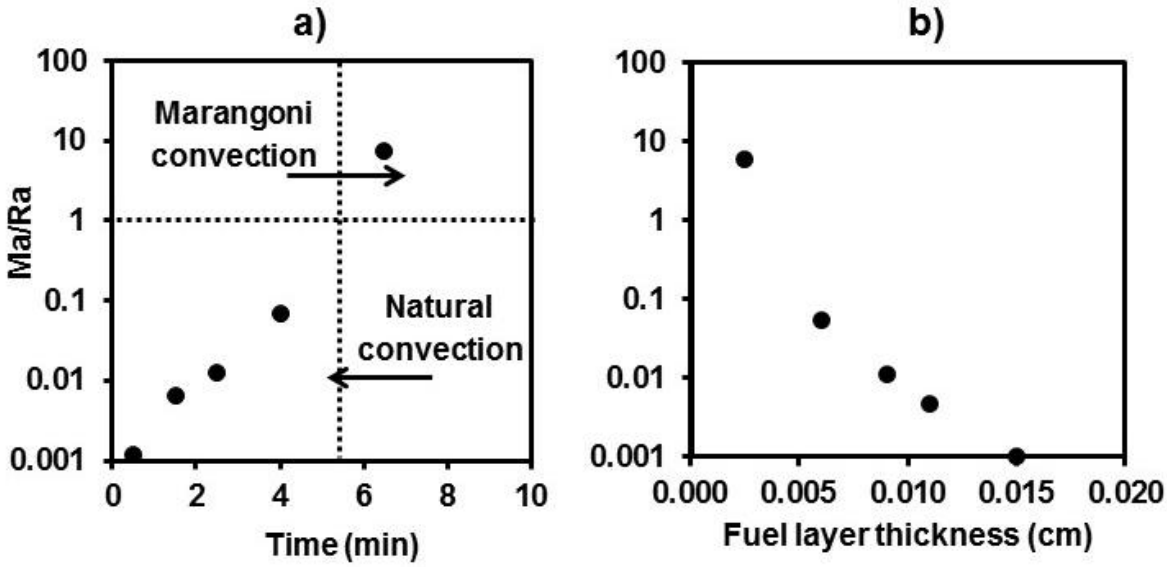

Figure 3.9: The ratio of Marangoni to Rayleigh number a) over the time of burning b) based on the fuel layer thickness. On the abscissa of the left plot, 0 indicates the ignition time and 10 is the time for extinction of the flame.

The results of the analysis showed dominance of natural convection in the first half of the burning period when the fuel layer was relatively thick (1.8-0.5 cm). However, the Marangoni convection became dominant in the final half of the burning. The corresponding total penetration lengths of the fuel layer in ice for the first and second half of the burning were 2.1 and 2.8 cm, respectively. Also, the partial penetration lengths for the first and second half of the burning were 0.9 and 1.4 cm, respectively. It is agreed that a large amount of the produced heat should be transferred to the ice through the fuel layer to melt the ice. In view of that, the heat transfer rate to the ice is obviously higher during the second phase, which means that the Marangoni convection could actually play a bigger role in melting the ice.

The two driving mechanisms (buoyancy and surface tension variation) inducing the convective flow in the liquid were analyzed to understand their contribution to the melting process. Usually, pressure, viscous, inertial and surface tension forces are of secondary importance and buoyancy alone is the dominating force for flow in liquid. Hence, it is uncommon for the Marangoni force, under normal gravitational condition and for a macroscopic scale, to overcome the buoyancy effect [149, 169]. Yet, because of the particular circumstances involved in burning of a liquid fuel adjacent to ice such occurrence was observed.

3.3 Conclusions based on n-octane burning in an ice cavity

A series of experiments were conducted to develop an understanding on the geometry change of an ice cavity during burning of n-octane. Based on the observations made during the experiments it became evident that the fuel layer is capable of melting the ice at a faster pace compared with the flame. Thus, a void is shaped in the circumference of the ice wall which is called lateral cavity. Temperature measurements of the fuel layer obtained during the burning of n-octane show a temperature gradient both in vertical and horizontal axes. This gradient contributed to creating convective motion in the liquid fuel. The driving forces inducing the convective motion were assumed to be surface tension and buoyancy. The Marangoni and the Rayleigh numbers were calculated as the relevant dimensionless numbers for surface tension and buoyancy, respectively. The results of the analysis showed the Rayleigh number was larger in the first half of the burning period, when the fuel layer

was considerably thick (1.8 - 0.5 cm). However, the Marangoni number was dominant in the final half of the burning. The corresponding total intrusion lengths of the fuel layer in ice for the first and second half of the burning were 21 and 28 mm, respectively. This means that the influence of the natural convection on melting is insignificant and is of second order importance when compared to the Marangoni convection. A flow visualization study on this subject is required to comprehend the pattern of flow and shape of vortices in the liquid fuel.

4 Burning of n-octane adjacent to an ice wall

In the previous part of this study a convection-melt phenomenon, which is referred as lateral cavity formation, was studied during burning of n-octane in an ice cavity with a diameter of 5.7 cm. The ice melting process was found to be more significant in the regions of the fuel layer contact with the ice versus regions of flame impingement. The previous findings supported existence of a flow close to the free surface of the fuel. It was hypothesized that the formation of lateral cavities is due to the convective flows in the liquid fuel layer driven by surface tension and buoyancy, relating to Marangoni and natural convection, respectively.

To assess the previously presented hypothesis a series of experiments were designed to investigate the thermal and flow field of n-octane burning adjacent to an ice wall. The mass loss rate, temperature field, and velocity field of n-octane along with the melting shape of the ice wall were measured. Flow visualization was conducted by Particle Image Velocimetry (PIV) technique, which in turn was coupled with the temperature field measurements to analyze the flow characteristics. Exploring the extent of convective flows could explain the causes for melting of the ice and formation of the lateral cavity. The objective of this part of the study was to improve the understanding of the thermal and flow field of n-octane burning adjacent to an ice wall

4.1 Experimental setup

The experimental setup was developed to observe the melting of the ice and investigate convective flows within the liquid phase of an n-octane pool fire. A schematic of the experimental setup is shown in Figure 4.1. The custom-made borosilicate glass tray used

for the burning (2 mm wall thickness) was an open top square with outside dimensions of 100 × 100 mm and a depth of 50 mm. The liquid fuel used herein was n-octane, which has a Prandtl number well above unity (7.8), density of 703 kg/m^3 and a boiling point of 125 °C. as the liquid fuel. Each experiment used a 96 × 60 × 30 mm ice wall placed on one side of the tray as shown with dark color in Figure 4.1 (a) and (b). In order to create an ice wall free of visual imperfections, such as gas bubbles and other impurities, demineralized water was frozen using a directional freezing method. A bracket-shaped holder (shown with dashed line in Figure 4.1) was used to keep the ice wall fixed at the wall of the tray. A base-layer of water with initial temperature of 0-2 °C was poured into the tray to a depth of 20 mm, followed by an n-octane layer that was 15 mm thick and had a temperature of 10-12 °C. The tray was then placed on a load cell (0.01 g precision) to record mass loss. A camera was placed in front of the test setup to capture the flame heights during the burning process. A propane torch igniter was used to ignite the fuel layer after it was poured into the tray.

Preliminary tests with and without the ice wall were repeated three times to ensure the reproducibility of the results for burning duration, mass loss, and flame. The flame height was measured by capturing random frames each four seconds from the videos of the tests. Then, the flame height was measured for each image via ImageJ [170]. The measured flame heights of each test were averaged to obtain an average flame height for the duration of the n-octane burning.

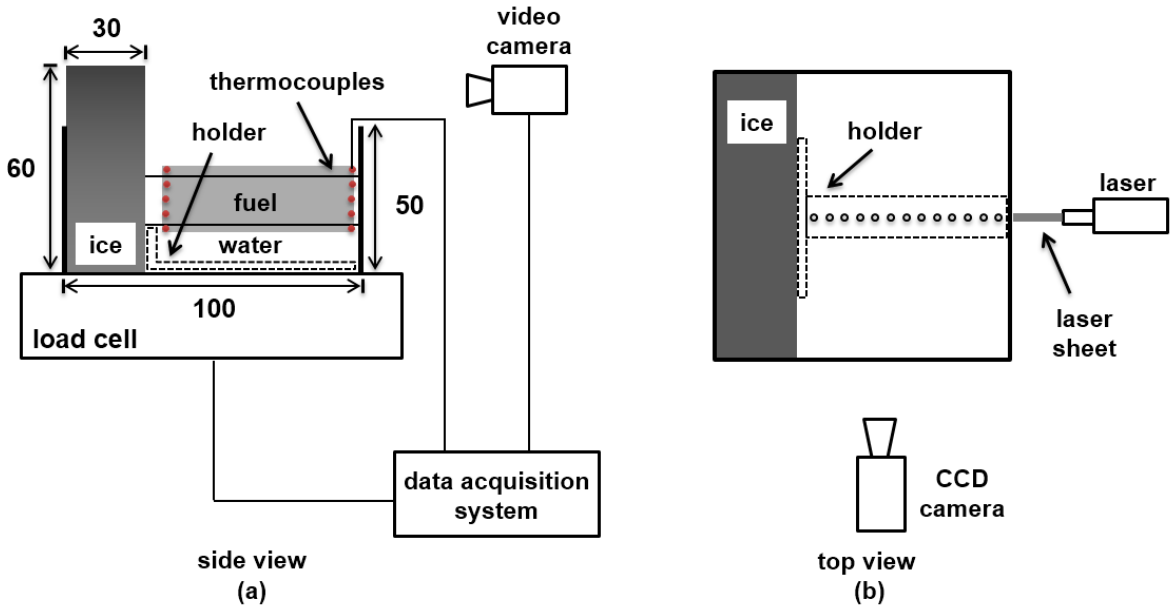

Figure 4.1: Schematic of the experimental setup, a) side view of the tray showing the water and fuel layer bound by ice, shaded area corresponds to field of view, b) top view of the tray with PIV setup. The dimensions are in mm.

The velocity field on the mid-plane of the liquid fuel perpendicular to the ice wall was obtained by PIV measurements. The specifications of the PIV equipment used in this study are provided in Table 4.1. The liquid fuel in the tray was seeded with 10 μm silver coated hollow glass sphere particles. The PIV technique assumes that fluid and particles move identically. However, the time required for a particle to adjust its velocity to a new condition within the fluid, known as "relaxation time", must be evaluated to verify this assumption. The particles relaxation time, can be determined by the following [171] expression:

$$t_p = d_p^2 \rho_p / 18\mu_l \tag{4.1}$$

where d_p (m) and ρ_p (kg/m^3) are the seeding particle diameter and density, respectively. μ_l is the liquid viscosity with units of *Pa.s*. The particles relaxation time was found to be 0.11 μs, which confirms for rapid adjustment to the fluid motion. The particles density was slightly higher than the seeded fuel. The settling velocity, U_g, is expressed as follows:

$$U_g = d_p^2 (\rho_p - \rho_l) g / 18\mu_l \tag{4.2}$$

where ρ_l and μ_l are the liquid density and viscosity, respectively. The effect of gravity, due to density difference of the liquid and seeding particles, on descending of the particles in

the liquid was calculated to be 27 μm/s. This value for settling velocity is reasonably low for an experiment with short duration. The shaded area in Figure 4.1 (a) shows the field of view for the camera. The location of the laser sheet for the velocity measurements is shown in Figure 4.1 (b). The camera was placed perpendicular to the laser that illuminated a thin light sheet in the flow.

Table 4.1: Details of the PIV equipment used in the current study

Laser	Type	Nd:YAG, NewWave Solo (Neodym–Yttrium–Aluminum–Granat)
	Energy/pulses	100 mJ/pulse
	Wavelength	532 nm (frequency doubled)
CCD camera	Type	HiSense 12 bit
	Resolution	1280 × 1024 pixel (32 × 32 pixel interrogation area with 50% overlapping)
Particles		Silver coated hollow glass sphere, 10 μm
Software		Flowmanager, Dantec Dynamics

Five thermocouples (K-type, wire and bead diameter of 0.10 mm and 0.25 mm, respectively) were also used to measure the temperature of the fuel in the vertical mid-plane perpendicular to the ice. These thermocouples were arranged vertically with 5 mm intervals (see Figure 4.1 (a), with detail shown as solid circles). The ends of the thermocouple wires were parallel to the fuel surface to minimize conduction loss. The radiation loss was assumed to be negligible due to the low temperature in the liquid phase. The experimental procedure included moving the thermocouple array for each test in 5 mm increments, thus creating a temperature map of the fuel 20 mm × 60 mm, with a 5 mm resolution over the course of the experiments (see Figure 4.1 (a), shaded area representing the temperature map position). The bracket-shaped holder that was used to fix the ice at the side of the tray was designed to act as a holder for positioning the thermocouple array at designated locations for each test.

4.2 Results and analysis

The geometry change of the ice was monitored with the CCD camera to obtain melting front velocity. In addition, measurements of mass loss over time as well as the video taken from the flame were used to evaluate the burning behavior of the n-octane with and without the ice wall in the tray. The results are reported in Section 4.2.1. Results of the PIV study showing the flow field within the fuel layer is presented in Section 4.2.2. Finally, the results of the temperature analyses are reported in Section 4.2.3.

4.2.1 Geometry change due to melting and burning behavior

As expected based on observations of the previous studies [87, 172], the melting of the ice was more significant in the regions of the fuel layer contact with the ice wall versus regions of flame impingement. Thus, the fuel layer created a void in the ice that eventually cut the ice into two pieces, which caused the top section to fall in to the pool. Figure 4.2 shows the splitting sequence from the beginning to the end of an experiment. The ice, n-octane and water are only labeled in Figure 4.2 (a).

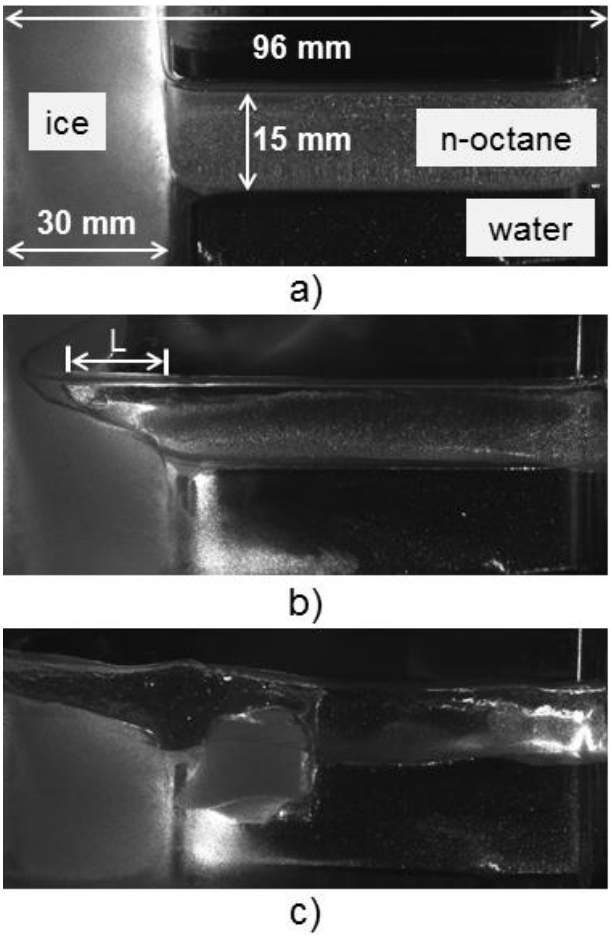

Figure 4.2: Melting process of the ice in the tray with ice on the left and n-octane on top of water layer on right, a) before ignition, b) 130 seconds after ignition, and c) splitting after 195±5 seconds. To improve the visualization, the ice was made with tap water in this experiment.

Figure 4.3 shows the intrusion of the fuel layer into the ice (indicated as intrusion length "L" in Figure 4.2 (b)) with respect to time. The slope of the lines indicate the melting front velocity. Three distinct periods with different values of melting front velocity are identified in Figure 4.3. In the period before ignition, minor melting occurs due to higher ambient and pool temperatures with a melting front velocity of around 0.04 cm/min. This has an important implication for lateral cavity formation in arctic oil spill, as the sunlight can potentially contribute to ice melting due to the high emission absorptivity of crude oils. After igniting the fuel and in the first 50 seconds (Phase 1), the melting front velocity was measured to be around 0.6 cm/min. In the rest of the burning time (Phase 2), the melting front velocity was found to be 1.0 cm/min.

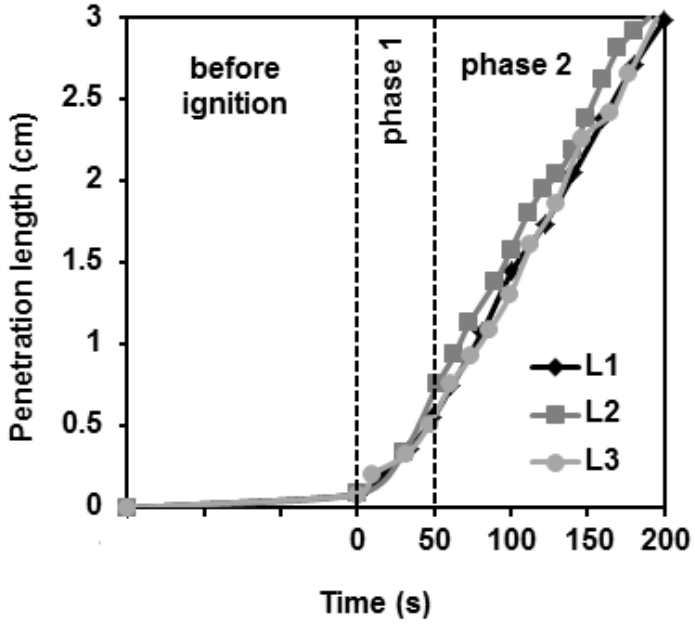

Figure 4.3: Intrusion length of the fuel in the ice versus burning time for three experiments labeled as *L_1, L_2, and L_3*. The melting front velocity (slope of the curve) is roughly 0.04 cm/min for the period before ignition, 0.6 cm/min in the first phase, and 1.0 cm/min in the second phase.

The mass loss rate and flame height from three identical experiments are compared and their average trend is reported in the following. Experiments with similar initial conditions but without the ice wall in the tray were also performed to compare the burning behavior of the fuel with and without the ice in the tray. The thickness of the fuel layer was initially at 15 mm (equal to 73 g of n-octane) and reduced to 11.5 mm (60 g) at the end of the experiment. However, because of the accumulation of melt-water under the fuel layer, the fuel layer was slightly elevated with respect to the bottom of the tray at the end (~3 mm). The measurements were stopped after the ice top detached for the tests with ice wall. The splitting of the ice was used as an end-point to the experiments, and this occurred consistently after 195±5 seconds. During the ~200 seconds burning, 13.1 g of n-octane was consumed in each test with ice present, giving an average burning rate of 0.066 g/s, while tests performed without the ice wall consumed 16.4 g of n-octane giving an average burning rate of 0.082 g/s. The average burning rate per unit area of the tray was 8.6 g/s.m^2 for ice wall tests, compared to 8.9 g/s.m^2 for tests without an ice wall. Because the ice occupied a portion of the tray and gradually melted away, the average burning rate per unit area of the experiments with ice was calculated based on an average area (96×80 mm). The reduction in the overall surface area of the pool in the presence of ice was the main reason for the lower burning rates in the cases with ice. Figure 4.4, shows the averaged mass loss rate

during the 200 seconds burning of n-octane. The experiments with the ice wall present in the tray are shown with dotted line, and the experiments without the ice wall are presented with dashed line.

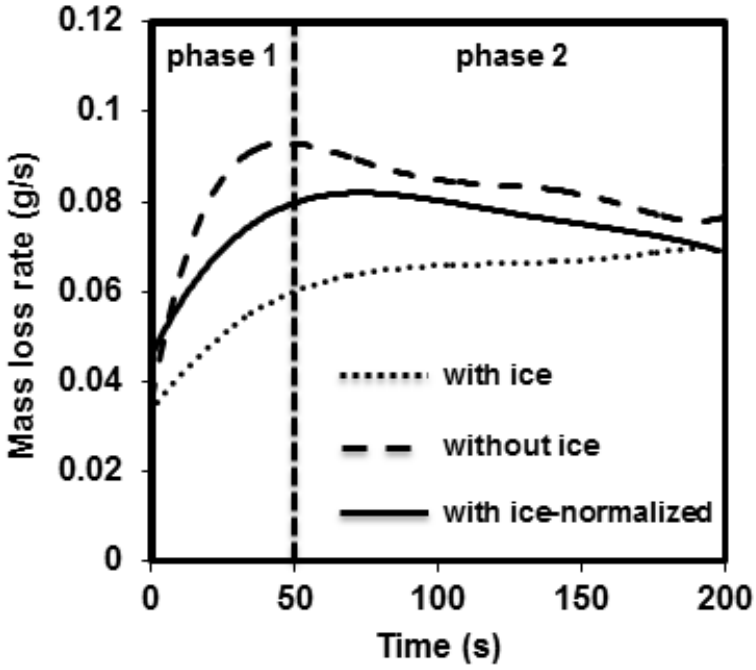

Figure 4.4: Mass loss rate of n-octane over the time for experiments with and without the ice wall. The case with ice is normalized to account for the reduced burning area of the fuel due to the presence of the ice.

Phases 1 and 2, as shown in Figure 4.3, are also identified in the mass loss rate trends in Figure 4.4. In the tests without the ice wall, the mass loss rate increased with time and reached a maximum value at around 50 seconds. During this period the ullage distance also increased due to surface regression. As a result, after a point, the mass loss rate gradually decreased, because an increase in the ullage decreases the transport of oxygen and heat towards the surface. On the other hand, the mass loss rate showed only an increasing trend for the case with ice. This is due to the fact that as the ice melts, the water level beneath the pool surface increases and this reduces the ullage distance. As mentioned, one of the reasons for the lower burning rate for the case with ice is the reduction in the pool surface area. A third curve is added to Figure 4 (solid line) representing the normalized mass loss rate of n-octane with ice. This curve is normalized based on the available surface area of the fuel to burn (the surface area of the tray minus the area occupied by the ice wall). The normalized curve provides a comparison of the mass loss rate of the two cases without the influence of geometry (equal surface area for the fuel to burn). As can be seen, the presence of ice (with

the assumption of similar surface area) has minimal effect on the burning rate. The lower burning rate in the normalized case may be attributed to the fact that n-octane has heat losses to the ice. Thus, for the same heat flux received from the flame, the case with ice burns at a slower rate than the case without ice.

Figure 4.5 shows the results of flame height analysis for the case with and without the ice wall. The tests with ice show slightly smaller flame height compared to the case without the ice. The flame heights results for both experiments showed a period of growth within the first 50 seconds of experiments (Phase 1) before reaching a steady fluctuating phase (Phase 2). The vertical line in Figure 4.5 separates the two phases.

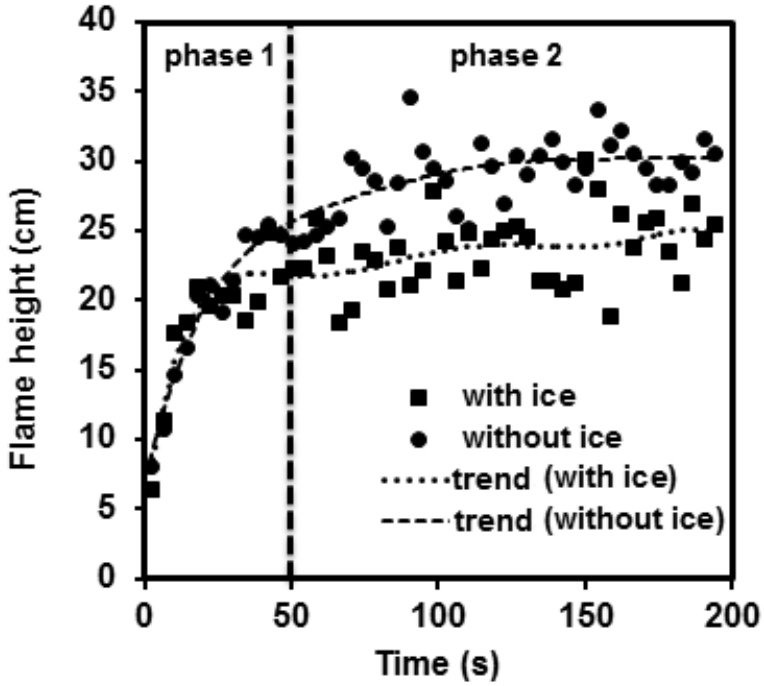

Figure 4.5: Flame height of n-octane over the time for experiments with and without the ice wall.

4.2.2 Flow visualization and velocity field

The flame impingement on the fuel surface and the presence of the ice alongside the n-octane pool created a convective field for the transfer of heat and mass in the fuel layer. The heat received on the fuel surface increased the free surface temperature to sustain the burning and the rest was transferred towards heating the liquid portion below the surface and the ice wall. In an earlier study [172], it was hypothesized that the melting of the ice wall is related to the convective motions in the liquid phase. In this study the hypothesis

was examined through flow visualization and careful analysis of the flow structure. The buoyant and surface tension forces can be considered as the driving forces for convection within the liquid-phase of the pool fire that contributed to the melting of ice and formation of the lateral cavity [135, 166]. The Rayleigh and Marangoni numbers corresponding to the convective flow in the fuel layer [154, 156] can be expressed as

$$Ra = \frac{\partial \rho}{\partial T} \frac{g \Delta T_v H^3}{\mu \alpha}, \tag{4.3}$$

$$Ma = \left|\frac{\partial \sigma}{\partial T}\right| \frac{\Delta T_h R}{\mu \alpha}, \tag{4.4}$$

where R is the half-length of the pool, H is the thickness of the fuel, g is the acceleration due to gravity, and σ, ρ, μ, ϑ, and α are surface tension, density, dynamic viscosity, kinematic viscosity and thermal diffusivity of the liquid, respectively. The vertical temperature difference on the bulk of the liquid can be assumed to be ΔT_v and on the horizontal free surface of the liquid as ΔT_h. The Rayleigh and Marangoni numbers used herein are similar to the described numbers in Section 2.3. The only difference is that the change in density (thermal expansion) and surface tension (surface tension coefficient) are expressed with respect to change in the liquid temperature. Table 4.2 provides the properties of the fuel and the related experimental measurements that are used to estimate the Rayleigh and Marangoni number.

Table 4.2: Properties and dimensions used to calculate Ra and Ma.

n-octane properties at 20 °C (obtained from Aspen HYSYS®)		Regime		Vert. temp. grad. ΔT_v (°C)*	Horiz. temp. grad. ΔT_h(°C)	Fuel height H^3 (m^3)	Half length of tray R (m)	Rayleigh and Marangoni number
$\frac{\partial \rho}{\partial T}$ (kg/m^3.K)	0.82	Combined (before ignition)		4.5	5.2	3×10^{-6}	0.03	$Ra_0 \sim 2.3\times10^6$ $Ma_0 \sim 3.2\times10^5$
$\frac{\partial \sigma}{\partial T}$ (N/m.K)	-9.5×10^{-5}							
μ (kg/m.s)	5.46×10^{-4}	Separated (after ignition)	Phase 1	45.8	65.6	2×10^{-6}	0.04	$Ra_1 \sim 1.5\times10^7$ $Ma_1 \sim 5.3\times10^6$
α (m^2/s)	8.6×10^{-8}							
ϑ (m^2/s)	7.76×10^{-7}		Phase 2	109.1	122.2	1×10^{-6}	0.05	$Ra_2 \sim 1.8\times10^7$ $Ma_2 \sim 1.2\times10^7$
g (m/s^2)	9.81							

* The temperature differences are obtained from the experiments.

After the fuel was poured into the glass tray, when both ΔT_v and ΔT_h were low and the Rayleigh number was larger than the Marangoni number ($Ra_0 \sim 2.3 \times 10^6$ and $Ma_0 \sim 3.2 \times 10^5$), the flow field showed one combined convection roll with two distinctive group of vectors [156]. The first group induced by the Marangoni effect, created a horizontal flow 3-4 mm below the free surface with a weak return flow for -15 < Y < -4 mm. Figure 4.6 shows the horizontal velocity profile of the fuel, obtained from PIV measurements 3 and 8 mm away from the ice wall. The Marangoni induced flow had a velocity of 3-4 mm/s below the surface as shown in Figure. 4.6. The second group of vectors was traveling downward, adjacent to the ice due to the buoyancy effect. The combination of these two flows is representing a combined convection regime due to the coupling of thermocapillary and buoyancy forces.

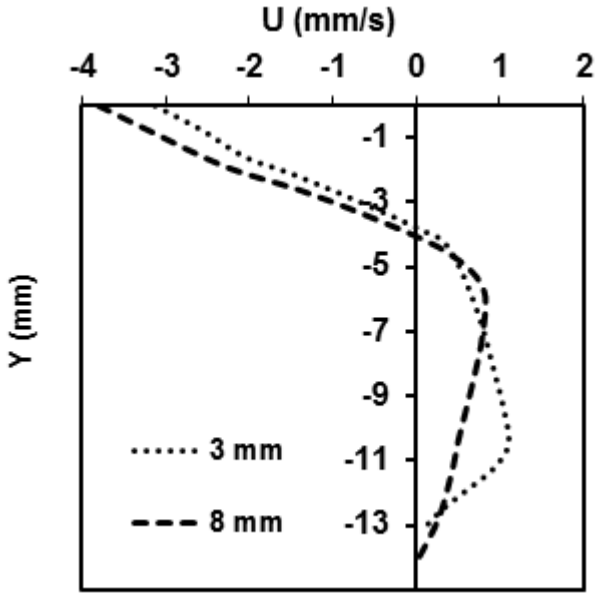

Figure 4.6: Horizontal component of velocity (U) over the fuel depth at 3 mm and 8 mm away from the ice wall obtained from PIV measurements.

The velocity field of the liquid fuel on the vertical mid-plane prependicular to the ice wall was measured by the PIV system described in section 4.1. The coupling of thermocapillary and buoyancy in the combined regime (before ignition), and formation of a large convection roll in the flow field near the ice wall is shown in Figure 4.7. More especifically, Figure 4.7 (a) and (b) show the velocity vector field overlaid on the velocity magnitude map and streamlines of flow with background map of vorticity magnitude, respectively. The return flow is apparent on the lower left side of the domain in Figure 4.7 (a). The maximum velocity magnitude of 4-5 mm/s was found below the free surface and near the ice. The streamlines of flow showed a large convective roll covering the whole domain with vorticity magnitude of less than 2 s^{-1}. The pattern of the flow and the convective roll formed in the liquid fuel before ignition corroborates the hypothesis that was proposed in the previous study by the authors [172] and was presented in Figure 3.7. However, the flow measurement after ignition revealed a more complicated flow field than what was anticipated.

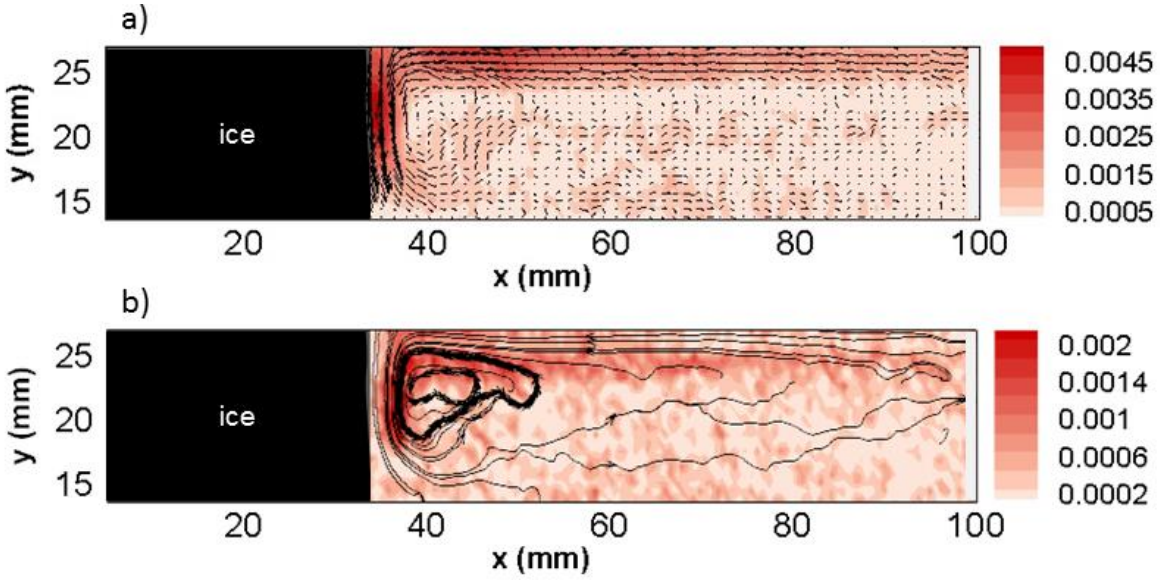

Figure 4.7: Flow field of n-octane before ignition a) The vector field with background color map of velocity magnitude (m/s) b) Streamlines of flow with background color map of vorticity magnitude ($s^{-1} \times 10^{-3}$).

After ignition, impingements of the growing flame on the fuel surface increased the temperature differences (ΔT_v and ΔT_h), and thereby augmenting the Rayleigh number and the Marangoni number ($Ra_1 \sim 1.5 \times 10^7$ and $Ma_1 \sim 5.3 \times 10^6$). An unstable flow regime denoted as a separated regime (Table 2), was formed due to the increase of the Marangoni number. Phase 1 (the first ~40 seconds after ignition) began with individual vortices traveling toward the ice and ended with presence of the multi-roll structure near the fuel surface. During the first phase, a multi-roll structure began to appear due to separation of buoyant and surface tension forces [157]. The flow field 10 seconds after ignition, as seen in Figure 4.8, shows a main counter clockwise vortex. Figures 4.8 (a) and (b) show the velocity vector field overlaid on the velocity magnitude map and streamlines of flow with background map of vorticity magnitude, respectively. As expected, after ignition the velocity magnitudes increased and more regions of the fuel became involved in convective flows. The maximum velocity of 8 mm/s was measured to occur below the fuel surface. As shown in Figure 4.8 (b) the counter clockwise rotating vortex was formed in the upper half and near the fuel surface that moved toward the ice with a vorticity magnitude of 4 s^{-1}. The vorticity color map also shows that most of the rotations occur near the fuel surface.

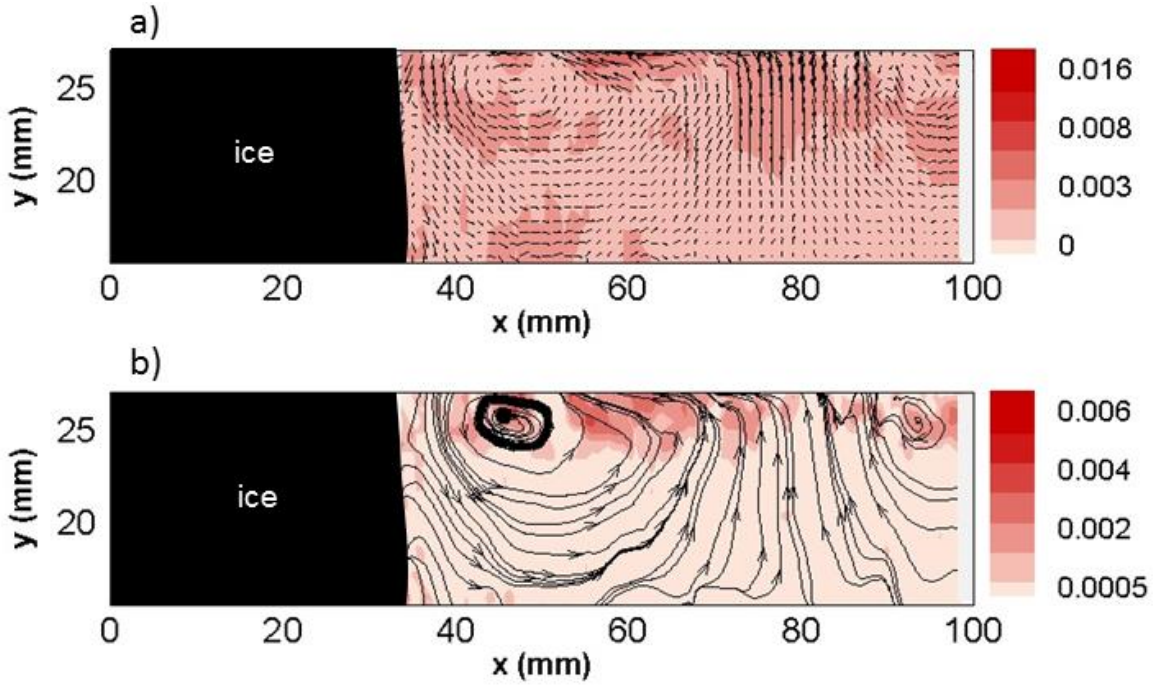

Figure 4.8: Flow field of n-octane 20 seconds after ignition, a) the vector field with background color map of velocity magnitude (m/s), b) streamlines of flow with background color map of vorticity magnitude ($s^{-1} \times 10^{-3}$).

As the flame heights/burning rate increased, complete separation of buoyant and surface tension flows initiated the multi-roll structure layer [154, 173] with axes of the rolls parallel to the ice wall (below the free surface of the fuel and near the ice). The multi-roll layer separated from the main flow, with thickness of 3-4 mm, and consisted of many rotating waves with relatively small radii that were visually observable through the tray walls. In pool fire literature, the multi-roll layer structure is introduced by the name of *inversion layer* and is stated to be driven by the thermal instabilities caused by buoyancy only [105, 174, 175].

Figures 4.9 (a) and (b) show the velocity vector field overlaid on the velocity magnitude map and streamlines of flow with background map of vorticity magnitude, respectively. The flow field became more complex and showed a significant change in the magnitudes and pattern as the pool surface was extended into the ice cavity. Still, the downward movement of the liquid near the ice surface remained intact. The maximum velocity magnitude was expected to be seen below the surface and near the ice, but the multi-roll structure repelled the seeding particles and made the measurments to be partially insufficient. Thus, the maximum velocity magnitude was recorded around 16 mm/s in the middle of the pool.

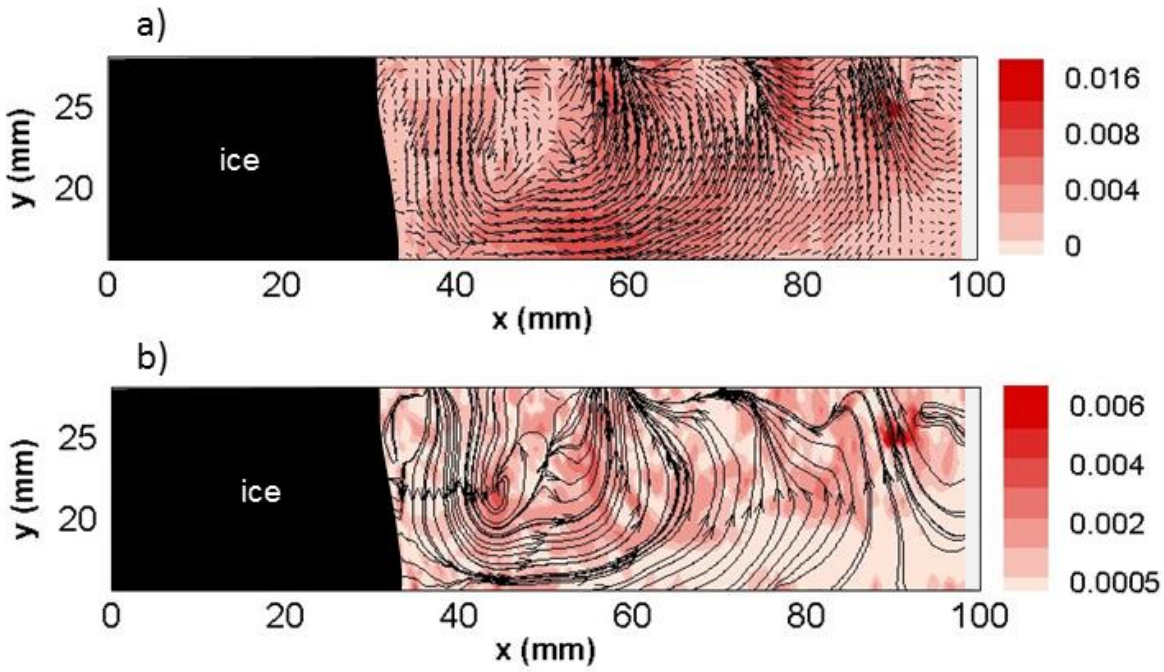

Figure 4.9: Flow field of n-octane 40 seconds after ignition, a) the vector field with background color map of velocity magnitude (m/s), b) streamlines of flow with background color map of vorticity magnitude ($s^{-1} \times 10^{-3}$).

The separation of buoyant and surface tension forces in Phase 1 resulted in the appearance of the single traveling vortex initially, which then took turn to the creation of the multi-roll structure. The multi-roll structure remained intact for the rest of the burning period. When the flame height and the burning rate reached their maximum in the second phase, both ΔT_v and ΔT_h increased significantly, resulting in $Ra_2 \sim 1.8 \times 10^7$ and $Ma_2 \sim 1.2 \times 10^7$. Note that the value of Ma_2 has increased significantly. The term spatiotemporal chaos is used herein to describe a constantly varying instantaneous velocity field with high velocity magnitudes mainly because of an increase in the Marangoni number to around 1.2×10^7 in the second phase. The exact value of the Marangoni number that initiates the mentioned behavior is dependent on geometry of the liquid, its contact angle to solid, and etc. Thus, generic interpretation of the Marangoni number without considering its context is insufficient.

The PIV measurements were rather difficult in the liquid after the onset of the 3-dimensional unsteady flow during the second phase of the burning. Presence of the ice in the liquid pool intensified the temperature differences and consequently complicated the experimental measurmnets further. The quality of images that were taken after ignition slowly started to deteriorate. Two major issues made the PIV measurements less useful after about 40 seconds. Figure 4.10 (a) shows these issues from an image that was taken

after 50 seconds from the ignition. Labeled areas in Figure 4.10 (a) show the dark, blurry, and stretched region numbered 1 and 2, respectively. The first issue (label 1) was a dark region without tracer particles that corresponds to the location of the multi-roll structure. This dark region started to appear near the ice during Phase 1 and was stretched to the entire pool length by the end of experiments. The centrifugal force acting on the particles in the multi-roll layer repelled the particles thus a black region was seen in the images [176]. As shown in Figure 4.10, the thickness of this region was greater near the ice which clearly shows a higher intensity of the rolls near the ice wall. Region 2 depicts the formation of a blurry area in the vicinity of the ice wall, which may be caused by mixing of hot fuel heated by the flame and cold fuel cooled by the ice. Region 3 originates because of the high temperature variation and subsequent variation in the refractive index of the fuel. The scattered light from tracer particles was stretched and distorted arbitrarily causing high measurement uncertainty. The vector field shown in Figure 4.10 (b) is produced by an image pair of which one is depicted in Figure 4.10 (a). While the vector field near the ice is not representing the actual displacement of the liquid due to the absence of tracer particles, an instantaneous downward flow in the middle of the pool and below the surface with high velocity magnitudes is observed. A maximum velocity of around 20 mm/s was observed for this region, but greater velocities are expected to have occurred closer to the ice.

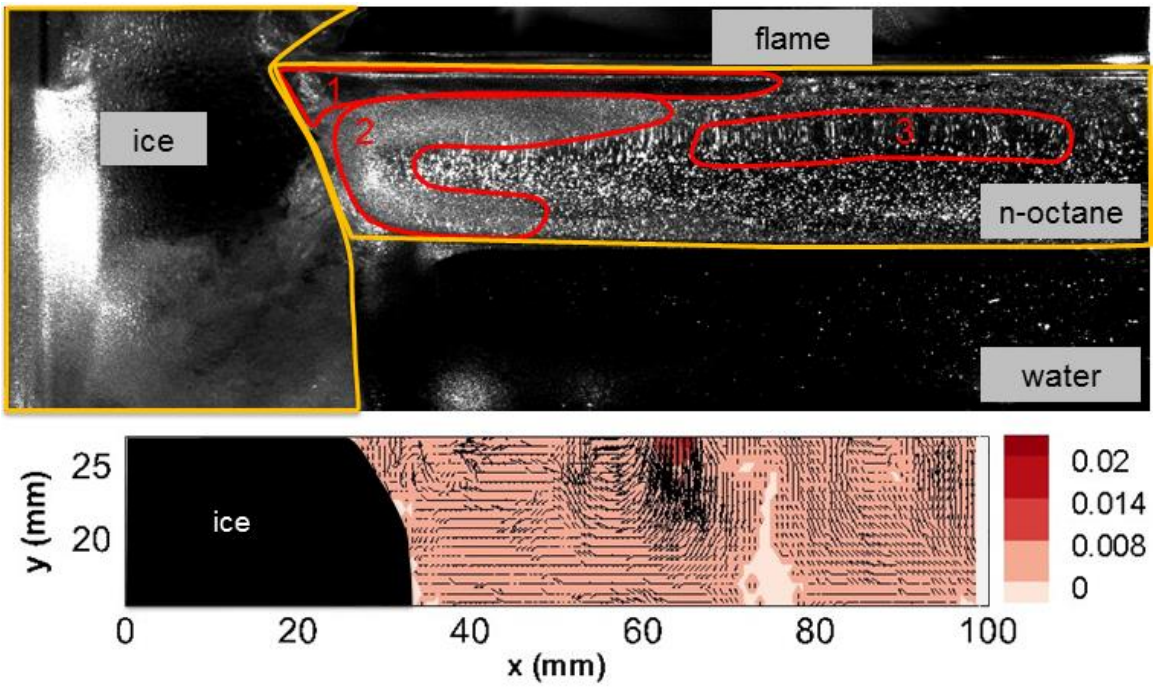

Figure 4.10: Deterioration of PIV image qualities after 50 seconds from ignition on top. The different types of issues are labled by numbers in the top image (9.5 cm length by 4.0 cm height). The vector field of n-octane layer obtained from the same image with background color map of velocity magnitude (m/s) on the bottom.

An earlier part of this overall study (Chapter 3, [24]) introduced two major convective flows (natural and Marangoni convection) as the driving forces for convection in a burning fuel layer adjacent to ice. The two convection mechanisms were also used to demarcate different melting rates that occur in a lab-scale pool fires in an ice cavity. Herein, the convective flows were examined by observations with a PIV system and also through Ra and Ma numbers. Also, the convective regimes (characterized by magnitude of Ra and Ma numbers) that relate to two distinct melting rates were evaluated herein. The extensions of these results to a larger scale or fuels that are multi-component require additional information and validation experiments at larger scales (1 to 30 m), as discussed by Emori and Saito [177], and is thus beyond the scope of the current study.

4.2.3 Temperature field

As part of this study, the temperature field of the fuel layer was measured by a thermocouple array as described in Section 2. Contours of temperature within the liquid phase are shown in Figure 4.11 (a-e) (with the ice on the left side). The temperature contours are plotted with linear interpolation in x and y direction. The thermocouple positioned at the top of the array

recorded the temperature of the gas phase and because melting of the ice caused the fuel layer to rise, it eventually recorded the temperature of n-octane surface. The elevation of the top surface and interface of the fuel-water were tracked via the images obtained from the PIV experiments and are presented in Figure 4.11 to detail the fuel layer displacement. Note that the top layer elevates during time. The red solid line in Figure 4.11 shows the interface of the fuel-water. The thermocouple at the bottom of the array remained in the water layer and recorded the temperature of the water layer only. The boiling point temperature of n-octane (125 ℃) was assigned to the top layer.

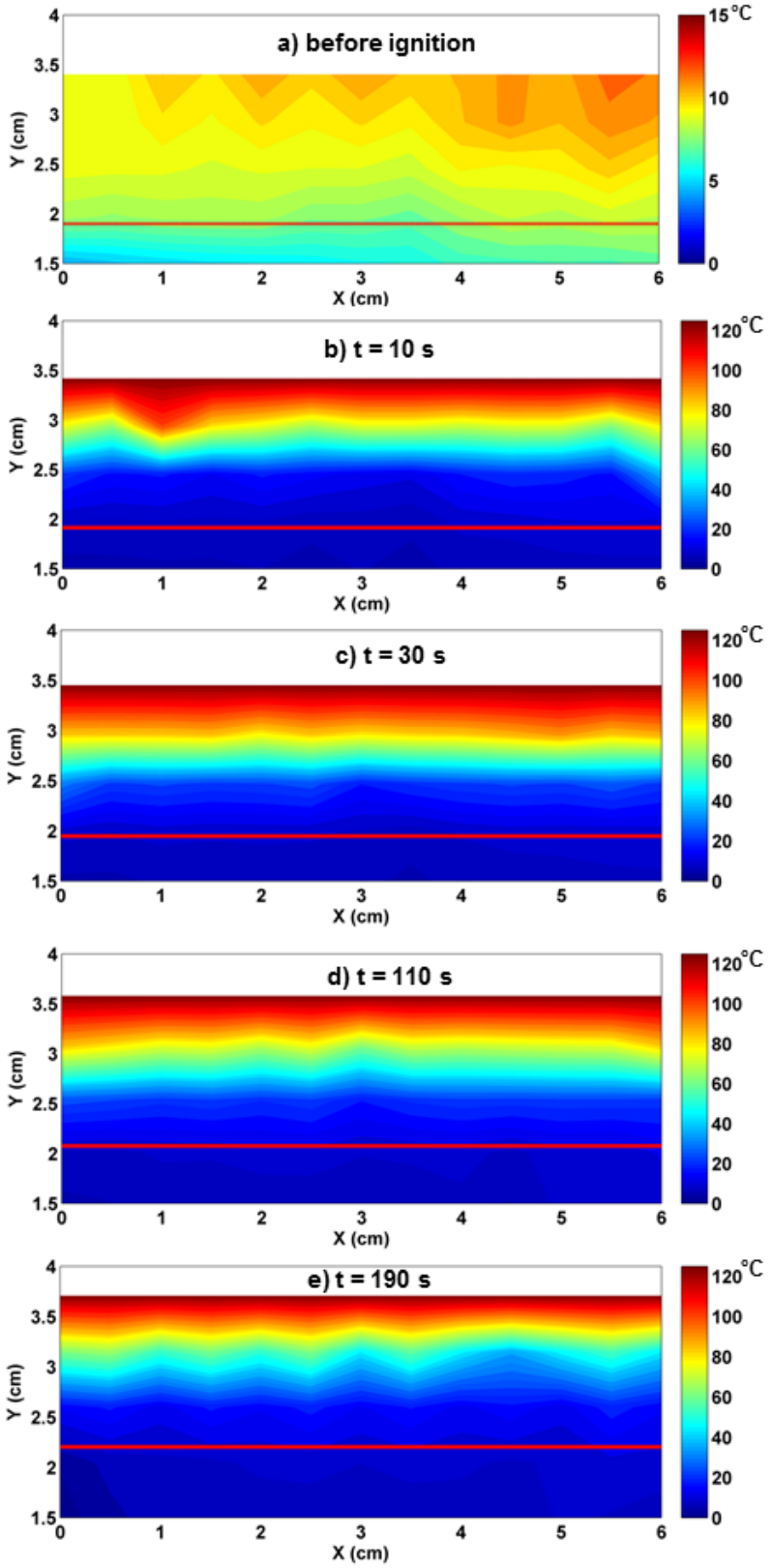

Figure 4.11: Temperature (℃) distribution within the liquid phase of n-octane pool fire with ice wall located on the left side of the fuel (t = 0 s is the moment of ignition), a) before ignition, b) t = 10 s, c) t = 30 s, d) t = 130 s, e) t = 190 s. The red line shows the fuel-water interface.

Figure 4.11 (a) shows the temperature distributions before ignition along the vertical direction of the fuel layer. Due to the proximity of the ice wall on the left side of the contours, lower temperatures were recorded in this area. After ignition (Figure 4.11 (b-e)), the temperature distributions showed a two-layer thermal structure within the liquid fuel. The upper layer with a temperature range of 60 – 125 ℃ had a steep temperature gradient in the vertical direction. This layer maintained a thickness of approximately 8 mm as the fuel burned. The top section of the upper layer (hot zone), with temperature range of above 100 ℃ and thickness of about 3 mm, corresponding to the location of the multi-roll layer greatly contributed in the ice melting process. In contrast, the lower layer remained relatively cold for the entire length of the experiments. Also, a gradual decrease of temperature in horizontal direction and toward the ice, top left side of the Figure 4.5 (b), was observed which is due to the presence of the ice in the early stage of burning.

Figure 4.12 shows the ice shape and the fuel layer location around 160 seconds after ignition of the fuel. The unstable flow regime and the multi-roll structure in the upper layer of the fuel is clearly visible in Figure 4.12. The structure was experimentally observed to originate near the ice wall and expand horizontally with the progress in burning. The wavy line in Figure 4.12 shows the lower boundary of the multi-roll layer that was stablished during Phase 2. This implies the presence of a strong transport mechanism in the upper fuel layer that is responsible for the transfer of heat (flame feedback) towards the ice wall. In addition, the fuel layer had horizontal parallel isotherms at the beginning of the burning period (t = *10* and *30 s*) indicating a uniform temperature distribution in Phase 1. Later in the experiments (Phase 2), the isotherms became wavy, which is most obvious in Figure 4.11 (e). The waviness of the isotherms may be attributed to the presence of the multi-roll and the chaotic state of the flow in the latter stage of the burning.

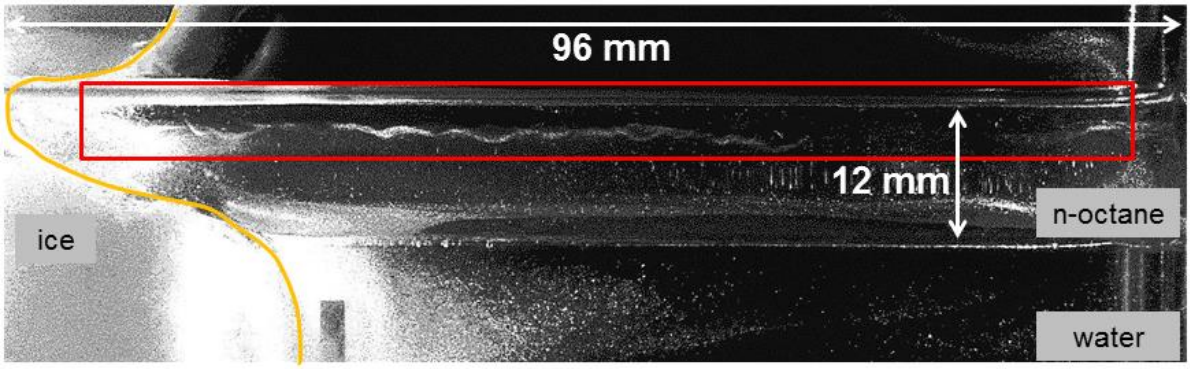

Figure 4.12: The ice wall (yellow line) and location of the fuel layer shown by an image taken about 160 seconds after ignition. The wavy line below the free surface (enclosed by the red rectangle) shows the lower boundary of the multi-roll structure.

4.3 Conclusions on burning of n-octane adjacent to an ice wall

In the previous chapter of this study the melting of ice near a pool fire was associated to the convective motions within the liquid-phase of the pool fires. In order to examine this hypothesis, a series of experiments were conducted to understand the thermal and flow field of n-octane burning adjacent to an ice wall.

Experiment showed that the melting front velocity increase after ignition in two different steps (phases 1 and 2). Before ignition, a combined flow in the fuel layer was established toward the ice (with maximum velocity of 4 mm/s) due to coupling of Marangoni convection and buoyancy. However, after ignition both magnitude and shape of the flow field changed significantly. Transition from combined one roll structure to multi-roll structure followed by spatiotemporal chaos occurred due to the increase in the temperature differences caused by flame impingement. The velocity magnitude increased and reached 16 mm/s in the transition period. At the same time, the vorticity magnitude increased and most of the fuel layer became involved with convective currents. The increased velocity in the separated regime (multi-roll structure) could be the main cause of the melting of the ice. Based on the thermocouple measurements, a two layer thermal structure; 1) a top layer with steep temperature gradient in the vertical direction and 2) a low temperature zone was observed in the fuel layer. The ice melting was much more significant in the upper layer regions of contact where the multi-roll structure was present.

An in-depth analysis of the flow characteristics requires an understanding of the influence of thermo-physical properties of the liquid during the complex process of convection-driven melting. Therefore, a parametric study on the convection-melt phenomenon using liquids with different thermal properties and controlled temperatures could potentially clarify the dominant parameters on melting.

5 Cavity formation in ice by externally heated liquids

The cleanup of oil spills in the Arctic offshore is a more complicated practice compared to cleanup in open waters. The technical difficulties brought upon by the presence of ice in the Arctic impede the conventional methods of cleanup. However, controlled *in situ* burning has proved effective for oil spills in ice conditions and has been used successfully to remove oil from spills in ice-affected waters [39]. Although, numerous studies have addressed the effectiveness of *in situ* burning, the interaction of oil and ice before and during burning is mostly neglected. When oil is spilled in icy waters, the imbalance of forces on the surface vs. bulk of the oil, due to an imposed temperature gradient, leads to the contraction of the oil in the oil-air interface, i.e. surface tension effect. On the oil-ice interface, the attraction between the dissimilar molecules of oil and ice, known as adhesion, leads to inclination of the oil slicks to stick and accumulate in the areas near ice. The combination of these two forces (surface tension and adhesion) leads to a thicker oil slick in the immediate zones near ice that can be further thickened with the use of herder agents [178]. Therefore, the chance of ignition near ice bodies is higher since the oil will stick to the ice and will maintain an ignitable minimum thickness of 1-2 mm [65]. After a successful ignition (sustained flaming of the oil), there are an imposed temperature gradients on the oil layer by the ice and flame, and thereby the interfacial interaction of the oil-water-ice system alters.

Liquids with an imposed temperature gradient on their upper free surface show a mechanical instability, giving rise to subsurface flows, known as Marangoni (thermocapillary) convection. When the surface-tension coefficient of a liquid is negative, a flow drives from hot regions to colder ones. Surface tension of hydrocarbon liquids decrease with increasing temperature, as such hydrocarbon liquid fuels have negative

surface tension coefficient. This type of flow been has been studied due to its practical applications in crystal growth, welding, and ignition and flame spread of liquid fuels at their sub-flash temperatures [128, 179, 180]. Special attention has been devoted to characterization of the surface flows driven by Marangoni convection as it relates to technologies in microgravity and other applications where Marangoni effect is dominant [149, 169]. The surface tension driven flows are also found to be the dominant mechanism in the liquid-phase convection of burning fuels adjacent to ice walls [172, 181, 182]. It was proposed earlier in this overall study that melting of the ice in pool fires in vicinity of ice, known as lateral cavity formation, is a result of convection in the liquid phase. In view of this, the melting rate of the ice should be a function of the magnitude of the convective flows in the liquid fuel. To evaluate whether such a relationship exists, a parametric study with different liquids exposed to heat flux from above was conducted. The experiments provided the melting front velocity of the ice adjacent to different liquids. These melting front velocities were then compared to surface velocities of liquids obtained through a scaling analysis.

The objectives of this part of the study are to experimentally evaluate the extent in which liquids with different thermophysical properties (the properties of a material that vary with temperature and do not alter the material's chemical identity) influence the melting of the ice when exposed to a heat flux from above. Also, a scaling analysis was performed to examine the possible correlation between the surface flow velocity in the liquid layer and the melting front velocity of the ice.

5.1 Experimental setup

The experimental setup was developed to systematically study the cavity formation phenomenon that was observed and studied previously in experiments involving flaming combustion of a liquid fuel bounded by an ice wall [85, 87, 172, 181] that were presented earlier in this dissertation. To provide a controlled environment, experiments on liquids with different thermophysical properties were conducted where they were exposed to different radiative heat fluxes to investigate the influential parameters on melting of the ice. A schematic of the experimental setup used in this study is shown in Figure 5.1 (a). The tray used to contain ice and liquids (2 mm wall thickness) was made of borosilicate glass

with outside dimensions of 70 × 70 mm and a depth of 45 mm. Each experiment used a 66 × 50 × 20 mm ice wall placed on one side of the vessel as shown in Fig. 1 (a) and (b). Figure 1 (b) shows an image of the ice wall and liquid inside the tray. The ice wall was covered with an insulation shield during the experiments to protect the top section of the ice (the part above the liquid surface) from melting directly by the radiation of the cone heater. Demineralized water was frozen using a directional freezing method to minimize the visual imperfections and reduce the inclusions of gas bubbles. A DSLR (100 mm focal length lens) was placed at an approximately 50 cm distance from the tray and directly facing the ice wall. Images were captured with intervals of ten seconds to track the ice-liquid interface movement due to the melting.

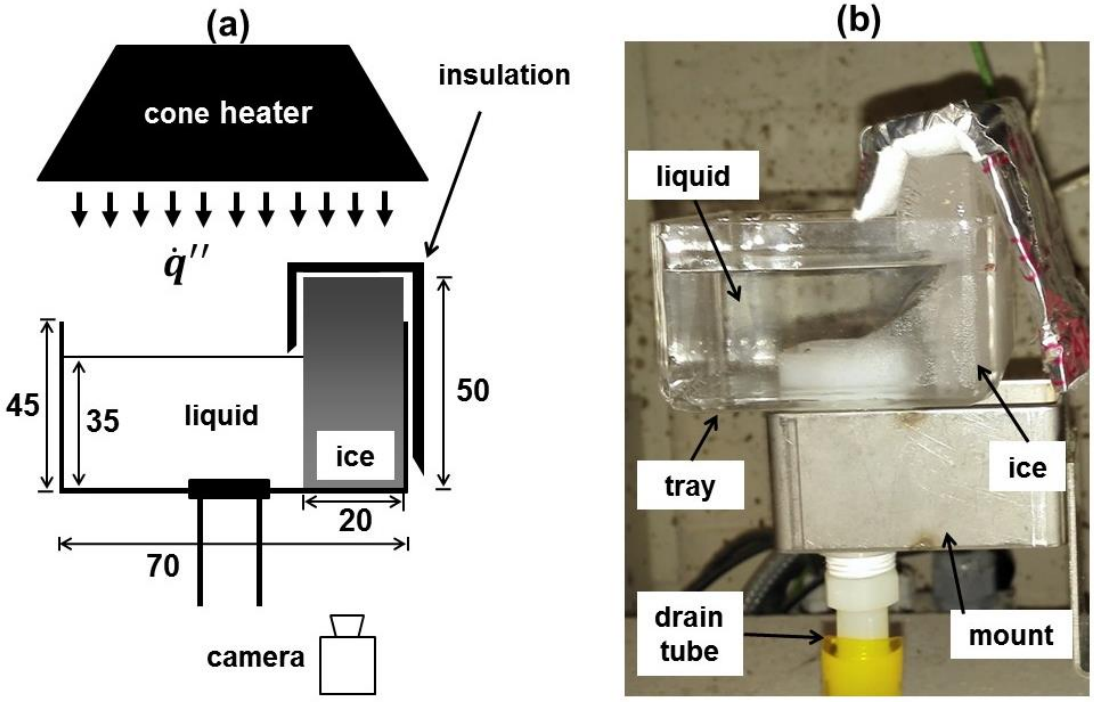

Figure 5.1: a) Schematic of the experimental apparatus (not to scale), b) a photograph of the tray with details labeled. Dimensions are reported in mm.

Water, n-pentane, n-dodecane, n-octane, m-xylene, and 1-butanol, all were carefully chosen based on their thermophysical properties for a number of reasons; 1) transparency of liquids to observe the melt front movement, 2) a relatively wide range of thermophysical properties to examine the influence of the various thermophysical properties on melting front velocity. Liquid thermo-physical properties were obtained by commercial software (Aspen HYSYS™) and are reported in Table 5.1 in their SI units.

Table 5.1: Thermophysical properties of the liquids used herein (values given at 20 °C and 101.3 kPa), obtained by Aspen HYSYS™.

	Surface tension coefficient (N/m.K) $\times 10^{-4}$	Density (kg/m^3)	Thermal conductivity (W/m.K)	Dynamic viscosity (kg/m.s)	Boiling point (℃)	Specific heat (kJ/kg.K)
Butanol, C_4H_9OH	-1.08	828	0.147	2.99×10^{-3}	118	2.76
Dodecane, $C_{12}H_{26}$	-0.78	749	0.137	1.43×10^{-3}	216	2.03
n-Octane, C_8H_{18}	-0.93	704	0.127	5.47×10^{-4}	125	2.09
Pentane, C_5H_{12}	-1.11	626	0.107	2.30×10^{-4}	36	2.24
m-Xylene, C_8H_{10}	-1.08	866	0.141	6.19×10^{-4}	139	1.61
Water, H_2O	-1.75	998	0.603	1.00×10^{-3}	99	4.20

* Surface tension coefficient is obtained by assumption of linear functionality with temperature.

Table 5.2 presents the experimental matrix of the tests indicating the liquids and heat fluxes used in the experiments. The use of high heat fluxes was not possible due to low auto-ignition temperature of some of the liquids. Thus, only water was tested at 12 and 15 kW/m^2. All experiments were repeated three times to ensure the reproducibility of the results.

Table 5.2: Experimental Matrix- note that the use of high heat fluxes was not possible due to low auto-ignition temperature of some of the liquids.

Liquids	Heat flux (kW/m^2)
Water	2, 5, 8, 12, 15
m-xylene, n-octane, 1-butanol, Dodacane	2, 5, 8
n-pentane	2, 5

The experiments initiated with heating of the cone to a desired temperature, which corresponded to a certain heat flux. The cone heater was calibrated to an accuracy of 5 % with a water-cooled heat flux gauge (Schmidt-Boelter type). Then, the ice wall was placed in the tray and the liquid was added into the tray to a depth of 35 mm (with initial temperature of 0-2 °C). The ice walls were carefully sized to uniform thickness of 20 mm by a ruler with accuracy of 1 mm. To start the experiments the radiation shield of the cone heater was removed to expose the liquid to the incident heat flux. The fuel layer melted the ice and created a void in the ice wall that eventually led to the splitting of the ice wall. The splitting was defined to be the end point of the experiments which was recorded with accuracy of 3 seconds. All images taken from the experiments were processed via ImageJ [170] to track the ice-liquid interface and create the melting profile of the ice wall. To convert pixels to the length unit a ruler with 1 mm accuracy was placed at the focal point of the camera as the calibration target before each test. The melting profiles were used to obtain the changes in length and width of the lateral cavity during each test. This is further explained in Section 3.1. In addition, the ice wall mass was measured before and after each experiment to obtain the amount of melted ice and the melting rate. The largest possible error for melting front velocity based on uncertainty of length and time measurements yields an error of 7 %.

5.2 Results and discussion

The geometry change of the ice was tracked with the camera to obtain melting front velocities of different liquids at varying heat fluxes. In addition, the shape of the lateral cavities were characterized with a length and width which are reported in Section 5.2.1. Results of the scaling analysis of the surface flow and comparison with experimental results are presented in Section 5.2.2.

5.2.1 Cavity profiles

The creation of the void in ice referred to *lateral cavity* earlier in this study (Chapters 3 and 4, [85-87, 172, 181]) but *cavity* is used herein to refer to the geometry change of ice caused by melting. Figure 5.2 (a) shows the intrusion of the liquid layer into the ice, forming the

cavity, with relevant dimensions labled. The cavity formed two faces as it developed, one horizontal face on top paralel to the liquid surface (except for the experiments with n-pentane) and one oblique lower face. Also, the intrusion length of the liquid in ice is introduced as L (cavity length) and δ_c is defined to be the vertical distance of ice melting below the liquid surface, introduced as cavity width. The postprocessed images taken during the experiments were used to obtain cavity evolution as shown in Figure 5.2 (b). The melting time is defined to be the duration of heat exposure that results in splitting of the ice wall.

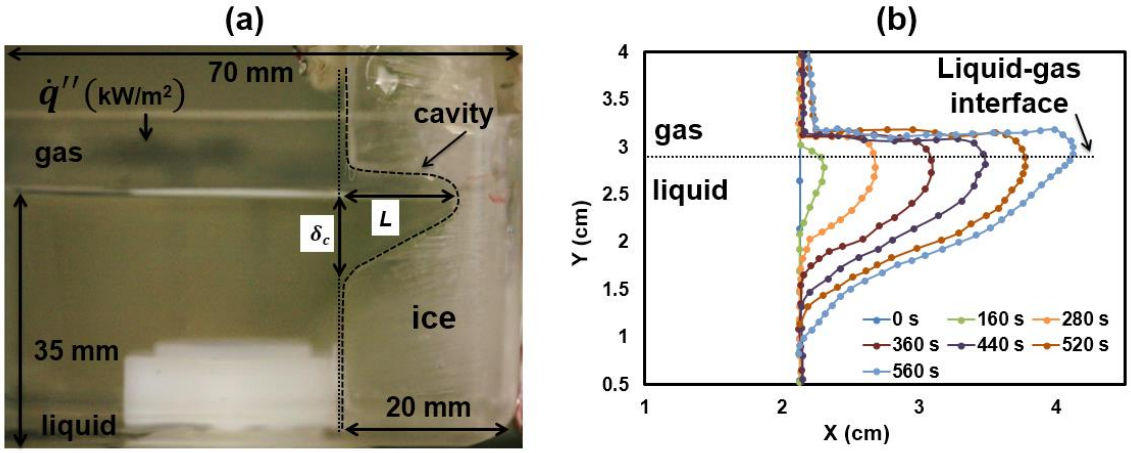

Figure 5.2: a) An image showing a cavity formed in ice with important parameters labeled and b) cavity profile obtained from post-processing the images of a test. Trendlines show the ice surface at different instants during the experiment.

The results of each tests were characterized with the mentioned parameters. The intrusion length, L, was divided by the melting time to give an average melting front velocity, U_m. Figure 5.3 shows the intrusion distance with respect to time for all of the fuels under the varried heat fluxes of the experiments. The duration (melting time) in which the liquids penetrate into the ice decreased as the heat flux increased. As expected, the longest melting time occurs at 2 kW/m^2. The increase of the heat flux to 5 kW/m^2 decreased the melting time of all the experiments significantly whereas the increase to 8 kW/m^2 and more did not decrease the melting time in a similar fashion. In particular, the experiments with water at 12 and 15 kW/m^2 show a similar melting time. There can be multiple reasons for this to happen, one of which is the limitation of the liquid temperature to its boiling point.

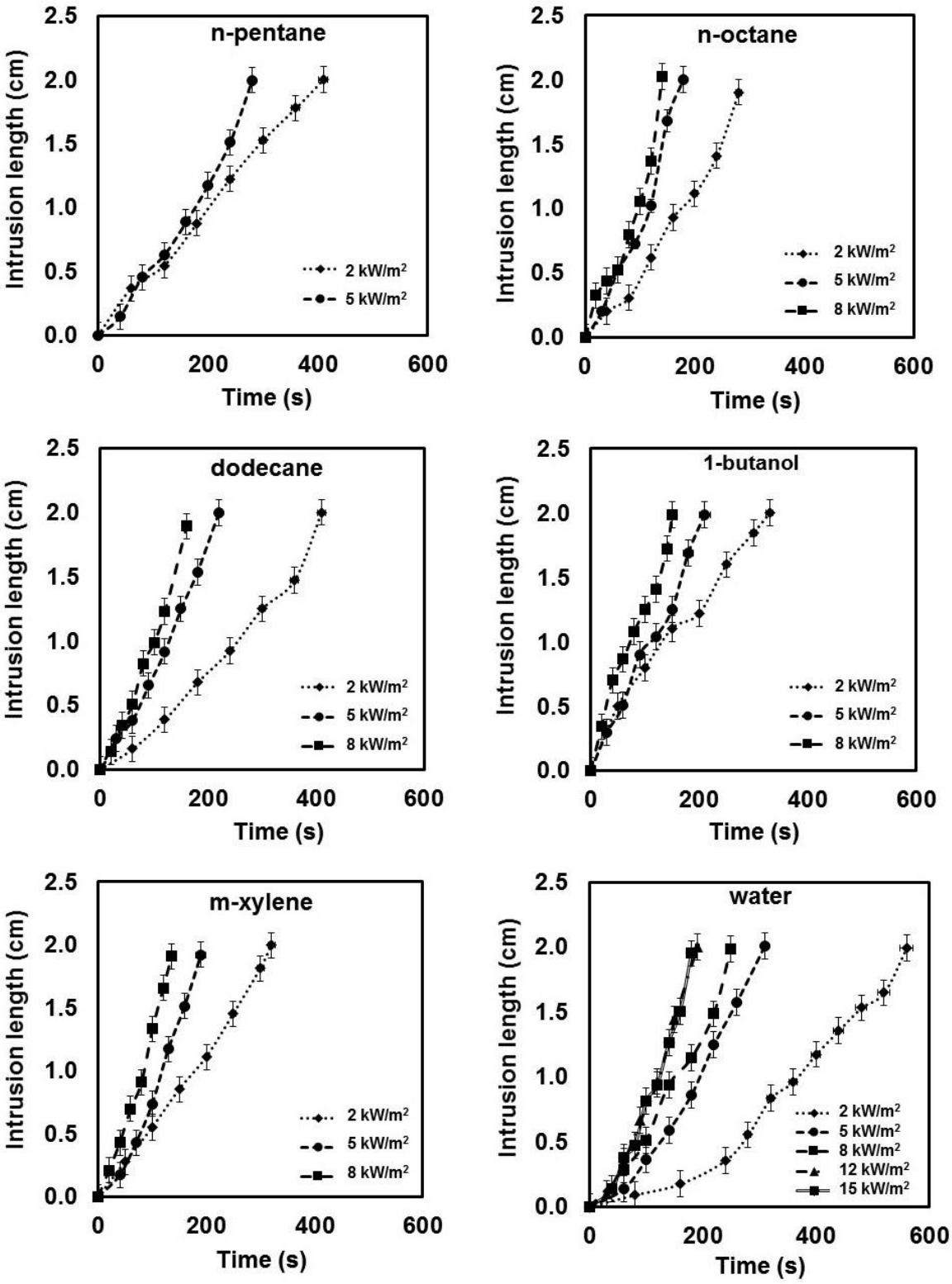

Figure 5.3: Intrusion length with respect to time for all the tested liquids.

Table 5.3 shows the summary of the experimental results for the tests of different liquids exposed different heat fluxes. In the experiments with n-pentane, the high evaporation rate of the liquid (because of its low boiling point) led to some partial melting on the top section

of the ice by the hot gases ascending from the tray. Therefore, the melting rate of ice for cases with n-pentane are not reflecting the amount melted by the liquid. Similarly, other measurments in experiments with n-pentane have rather high uncertainty because of strong evaporation that will be explained further in Section 5.2.2.

Table 5.3: Experimental results summary in terms of average melting front velocity (U_m) and cavity width (δ_c).

Parameter	U_m (mm/min)					δ_c (mm)				
Heat flux (kW/m^2)	2	5	8	12	15	2	5	8	12	15
1-Butanol	3.7	5.7	7.9	-	-	20	18	15	-	-
Dodecane	2.9	5.5	7.0	-	-	21	15	13	-	-
n-octane	4.1	6.7	8.6	-	-	15	15	11	-	-
n-pentane	2.9	4.3	-	-	-	23	20	-	-	-
m-xylene	3.8	6.1	8.4	-	-	16	12	12	-	-
Water	2.1	3.9	4.8	6.3	6.6	20	16	14	14	13

The two general trends that can be seen in the above table are the increase in U_m and decrease of δ_c with an increase in the heat flux. Evidently, the melting rate of ice also increased with the increase in heat flux. To provide an example for the data presented in Table 3, the images of the experiments with water are illustrated in Figure 5.4 and 5.5. Figure 5.4 shows the intrusion length after 120 seconds from exposure of different heat fluxes to the liquid surface. While the intrusion length in the 2 kW/m^2 case was hardly visible around 1-2 mm, the intrusion length for the case with 15 kW/m^2 was nearly equal to the half thickness of the ice wall. The cavity widths created by water at the end of experiments with different heat flux inputs are presented in Figure 5.5. It is observed that the cavity assumes a more longer and elongated shape with an increasing heat flux.

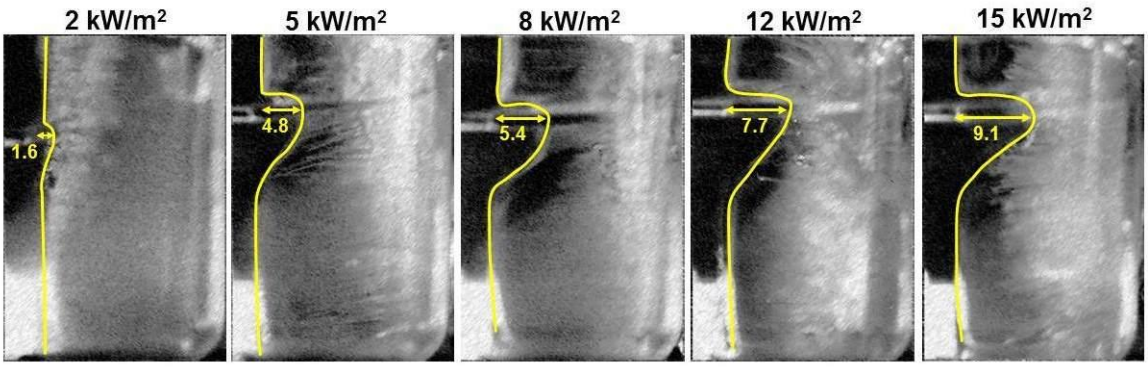

Figure 5.4: Intrusion length (L) of water in ice after 120 seconds exposure to different heat fluxes as shown above each image. The measurements are in mm.

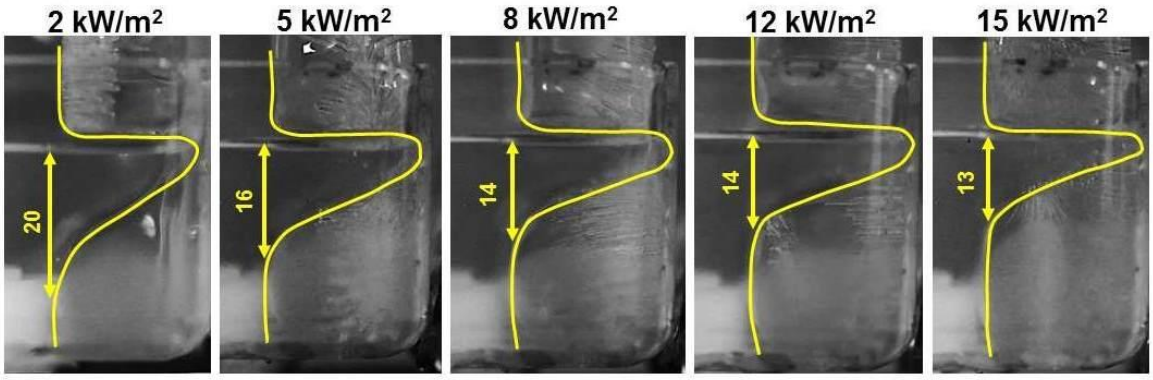

Figure 5.5: Cavity width (δ_c) at the end of the experiments with water at different heat fluxes as shown above each image. The measurements are in mm.

The Properties of the liquids (see Table 5.1) were individually compared with the melting front velocities values obtained from experiments to find potential properties that enhanced melting. n-octane and m-xylene show the highest melting front velocity and it can be seen from Table 5.1 that they posses relatively low viscosity and high surface tension coefficients. But, a single property cannot be picked as the sole parameter inlfuencing the melting process. In addition, the relative contribution of these parameters is unknown. Therefore, it is most useful to find/define a proper grouping of properties through a systematic analytical approach.

5.2.2 Scaling analysis

The following scaling analysis is inspired by previous studies in transport of melt in laser surface melting processes and specifically the outstanding work of Chakraborty [183, 184]. Also, the work of Takahashi et al. [185] on flame spread over liquid fuels has provided some useful insights to address the current melting problem. It was previously hypothesized that the melting front velocity could be correlated with the velocity of liquid surface flow [172, 181]. This hypothesis is examined by comparing the melting front velocities obtained from the experiments to the surface flow velocity correlation. In addition, an appropriate grouping of liquid properties that are influential in the ice melting process is introduced in the surface velocity correlation.

To analyze the convective flows in the liquid pool, scaling analysis of the governing equations was carried out with the proper boundary conditions. A two-dimensional rectangular coordinate system (*x, y*) with cold/ice wall located on the positive *x* direction was considered. Assumptions/simplifications were made to address the specific features of the current problem. A schematic diagram of related physical mechanisms and parameters are shown in Figure 5.6. The heat flux ($\dot{q}$") is supplied to the liquid free surface that creates a significant horizontal temperature difference along the surface due to the presence of the cold/ice wall. All properties used in the following scaling are considered to be constant. This assumption is reasonable since steady state intrusion distance trends were observed as was shown in Figure 5.5. The steady-state equations for incompressible Newtonian fluid are described by the following equations:

Continuity equation,

$$\frac{\partial u}{\partial x} + \frac{\partial v}{\partial y} = 0 \,, \tag{5.1}$$

Navier-Stokes equations,

$$\rho\left(u\frac{\partial u}{\partial x} + v\frac{\partial u}{\partial y}\right) = -\frac{\partial p}{\partial x} + \mu\nabla^2 u \,, \tag{5.2}$$

$$\rho\left(u\frac{\partial v}{\partial x} + v\frac{\partial v}{\partial y}\right) = -\rho g\beta\Delta T - \frac{\partial p}{\partial y} + \mu\nabla^2 v \,, \tag{5.3}$$

and energy equation,

$$\rho C_p(u\frac{\partial T}{\partial x} + v\frac{\partial T}{\partial y}) = k\nabla^2 T \ . \qquad (5.4)$$

Here ρ, μ, β, C_p, and k are density, dynamic viscosity, thermal expansion, specific heat, and thermal conductivity of the liquid. Although thermophysical properties and especially viscosity change with temperature, all thermophysical properties used in the following scaling are considered to be constant for simplicity. Boussinesq approximation is assumed in Navier-Stokes equations. Thus, thermal expansion, β, has appeared in the source term of *y*-momentum equation. The standard value of 9.8 m/s^2 is used for acceleration due to the gravity.

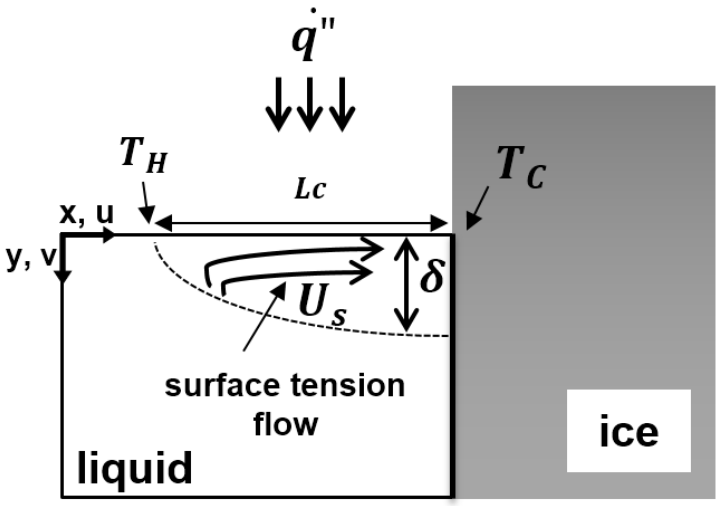

Figure 5.6: Schematic considered for the analysis. Reference point is assumed stationary and horizontal velocity towards ice is positive.

In convective boundary layer of liquids with Prandtl number of larger than unity, viscous and inertia forces should be in balance. In the x-momentum equations, the balance of inertia and viscous forces at the top layer leads to

$$\rho\frac{U_s^2}{L_c} \sim \mu\frac{U_s}{\delta^2}\,, \qquad (5.5)$$

where U_s is the surface velocity scale, L is the reference length scale in *x* direction, and δ is the convective layer thickness. The reference length scale, may be determined from flame spread literature [186] to an average value of L_c= 50 mm for all the liquids that were used. Equation (5.5) may be rearranged to give

$$\delta \sim \sqrt{\frac{\mu\, L_c}{\rho\, U_s}}\,. \tag{5.6}$$

The top surface is assumed to remain flat with no wave, i.e. $v = 0$, also from the balance of shear force and surface tension at the surface one gets

$$\tau_{xy} = \frac{\partial \sigma_{sur}}{\partial T}\,\frac{\partial T}{\partial x}\ . \tag{5.7}$$

where $-\frac{\partial \sigma_{sur}}{\partial T}$ is the variation of surface tension with respect to temperature. The boundary condition at the surface imposes the balance of surface tension variations and viscous shear stress. Resistance of viscous shear stress surface tension flow at the surface leads to flow in the bulk of the liquid. Thus, a momentum balance for the surface flow can be written as

$$\mu\,\frac{U_s}{\delta} \sim \left|\frac{\partial \sigma_{sur}}{\partial T}\right|\,\frac{\Delta T}{L_c},, \tag{5.8}$$

where ΔT is the characteristic temperature difference, $T_H - T_C$. Note that the negative sign is removed from the surface tension coefficient and its value is assumed positive. Re-arranging Eq. 5.8 with Eq. 5.6 gives an expression for U_s

$$U_s \sim \left(\frac{\mu L_c}{\rho}\right)^{\frac{1}{3}} \left(\frac{\partial \sigma_{sur}}{\partial T}\right)^{\frac{2}{3}} \left(\frac{\Delta T}{\mu\, L_c}\right)^{\frac{2}{3}}. \tag{5.9}$$

An assumption is made that the temperature difference in depth (vertical) and on surface of the liquid (horizontal) are of same order. In addition, it is assumed that the incident heat flux on top of the liquid is transferred to the depth of liquid only by conduction. This is obviously contrary to the previous statements where dominance of convective flows were described. Nevertheless, for long exposures and narrow boundary layer depth assumption of heat transfer by conduction is reasonable. Using the top surface boundary condition and assuming an overall energy balance one can write

$$k\left(\frac{\Delta T}{d}\right) = \eta \dot{q}'' \ \text{ or } \ \Delta T = \frac{d\eta \dot{q}''}{k}, \tag{5.10}$$

where η is assumed to be the heat absorption efficiency and constant for all the liquids used herein [187]. k is the thermal conductivity of the liquid. The thermal boundary layer

thickness is assumed to have a constant value for every liquid used in this study [188]. Replacing ΔT in Eq. 5.9 gives the following correlation for the surface velocity

$$U_s \sim \left(\left(\frac{\left(\frac{\partial \sigma_{sur}}{\partial T} \right)^2}{\rho \mu k^2} \right) . \left(\eta \dot{q}" \right)^2 . \left(d^2 / L_c \right) \right)^{\frac{1}{3}} . \quad (5.11)$$

This correlation is based on two convective terms on the RHS. The first term represents the Marangoni component while the second term is due to the effect of buoyancy. Here, the first group of parameters on the RHS of Eq. 5.11 ($\frac{\left(\frac{\partial \sigma_{sur}}{\partial T} \right)^2}{\rho \mu k^2}$) are thermophysical properties of the liquids. Second group ($\eta \dot{q}"$) is the power output of heater received by the liquid. And third group is made of characteristic length scales that are assumed constant for every case to remove their effect.

To assess the scaling analysis presented herein, the equation for surface velocity (Eq. 5.11) was calculated using the liquid properties presented in Table 2. The length scale parameters in Equation 5.11 (d and L_c) were assumed to be similar for every liquid. The obtained values of U_s were then compared with the experimental results of the melting front velocity to check for a possible relationship. As explained, the surface velocity is assumed to be the main component of heat and mass transfer toward the ice. Therefore, it is expected that the melting front velocity (U_m) to associate with the liquid surface velocity, U_s. Furthermore, the grouping of the thermophysical properties in Eq. 5.11 may also reveal the important liquid properties that influence the melting. The increase in the heat flux was found to enhance the melting front velocity and reduce the cavity width in the experiments. The surface velocity correlation obtained herein indicates a relationship of $U_s \sim \dot{q}"^{2/3}$. This interpretation is discussed further in the remaining of this section. The cavity widths obtained from the experiments were found to generally decrease with the increase in heat flux. Additionally, the convective layer thickness, δ in Eq. 5.6, was presented as a reverse function of U_s ($U_s \sim \delta^{-1/2}$) which specifies a reverse functionality to heat flux as well. This might indicate a link between the cavity width and the convective layer thickness, but no further deduction is made here.

The comparison of U_s and U_m for all the experiments with the exception of n-pentane is shown in Figure 5.7, which also includes a line that is fitted to all the data points (with R-

squared value of 0.90). It can be seen that the surface velocity scale and melting front velocity correlate well. It should be noted that the temperature difference scale in Eq. 5.9 that is replaced according to Eq. 5.10 is physically limited to the boiling points of the liquid. This means increase in heat flux after some certain value will only contribute to evaporation and does not affect the temperature on the hot side (T_H). For liquids with low boiling point, a considerable portion of the imposed heat flux is consumed by the latent heat of evaporation. Therefore, in the condition of high heat flux input and for low boiling point liquid, the heat release factor α, will decrease considerably. Therefore, an assumption made herein is that the evaporation is negligible for every liquid and all the liquids receive the heat flux in a similar fashion (i.e. $\eta = 1$) except for the n-pentane cases (boiling point of 36.1 ℃).

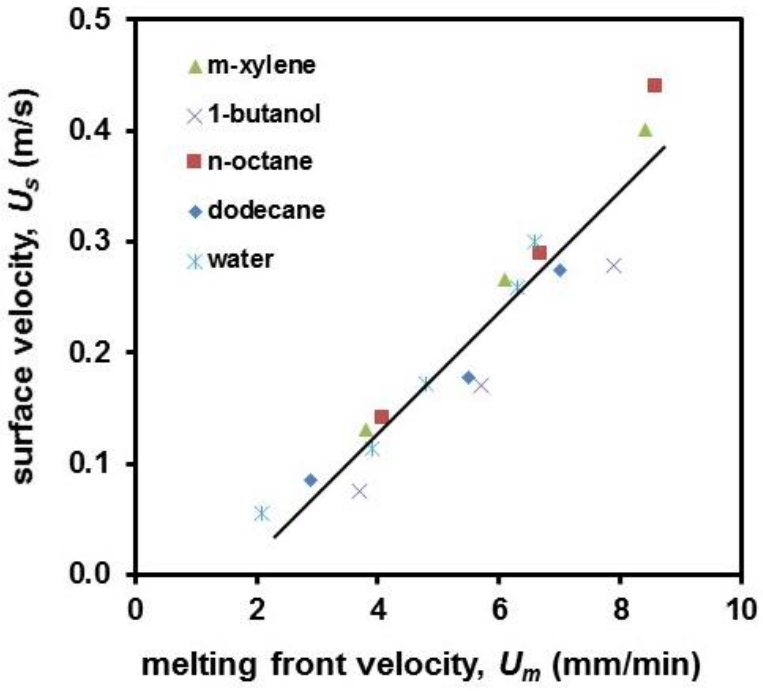

Figure 5.7: Relationship of U_s and U_m for all the experiments. The fitted line R-squared value is 0.90.

The most important outcome of the results presented by Figure 5.7 is that there is a strong correlation between the surface velocity scale and the melting front velocity exists. In addition, it is implied that the thermophysical properties grouping used in the RHS of Eq. 5.11 were an appropriate choice for assessing the ability of a liquid in transferring heat and mass towards the ice.

In addition to the thermal properties that affect the heat transfer, flow field in the liquid-phase is also influential in determining the melting rate and is not addressed by the scaling analysis conducted in this study. For a liquid that is exposed to heat from above and is contained with a cold boundary (ice), two main flow types are assumed; thermocapillary toward the ice on the free surface of the liquid and buoyancy in depth of liquid along the ice wall. When temperature differences in the liquid are low, the combined effect of these two force leads to a primary one roll cell structure. This primary flow structure could develop to a complex flow condition because of the increase in the temperature differences in the system.

It has been shown previously [135, 150, 166] and earlier in this study that that in the presence of large temperature differences on the surface of the liquids, the surface tension driven convection is enhanced and the primary flow structure is altered. The increase in the Marangoni force may exceed a limit in which the surface flow becomes disturbed by resistance of viscous shear stress. This state is described as an unsteady wavy flow field with many small cells appearing below the surface [154, 173, 181, 189]. The visual observations made during the experiments showed a phenomenon that appeared to be related to the multi-roll/unsteady regime. Figure 5.8 depicts three images that are taken toward the end of the m-xylene experiments. As can be seen in Figure 5.8 (a-c), the liquid appeared at rest/normal under 2 kW/m^2, but in the cases with higher energy input the fluid was disturbed which was mostly observable just below the surface. The schematics in Figure 5.8 (d) and (e) illustrate the steady flow vs. the multi-roll flow regime.

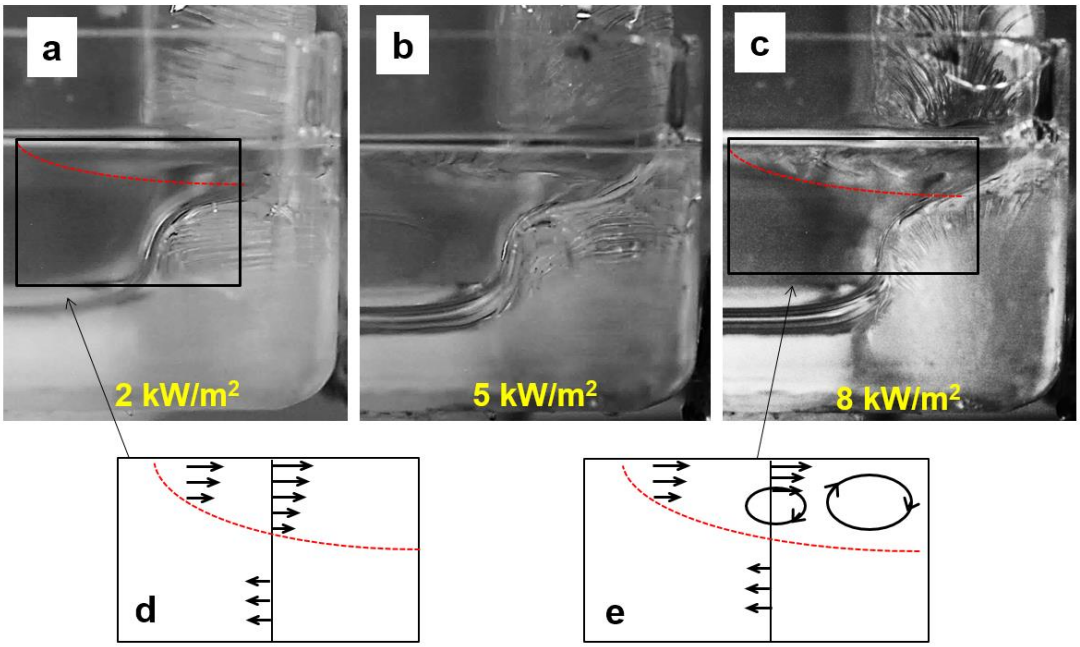

Figure 5.8. Visual comparison of m-xylene under different heat fluxes. Images on top row (a-c) show the ice (on right) with the liquid (on left) of each image. Schematics on the bottom row show the laminar steady flow and unsteady multi-roll condition, from left to right.

Similar types of wavy flow below a liquid layer as those shown in Figure 5.8 have been investigated under the name of propagating waves and were found to be the dominant mechanism in determining the flame spread rate over liquid fuels [128, 190, 191]. For the case of a pool fire confined with ice, or a simulated one as the current experimental setup, these waves are observed to be permanently present in the areas adjacent to the ice wall due to the temperature gradient that is imposed by the ice and the heater/flame. This flow pattern is assumed to contribute significantly to the enhanced melting of the ice that is in contact with the liquid.

The results of the comparison of the surface velocity and melting front velocity may also be grouped by the heat flux inputs to the liquid surface and are shown in Figure 5.9. Three lines are fitted to the data points of the tests with 2, 5, 8 kW/m^2 showing the slope and R-squared value of each fitted line. The slope of the lines determine the factor in which U_s and U_m correlate at a certain heat flux based on the liquids properties. It can be seen in Figure 5.9 that the slope for experiments with 2 kW/m^2 heat flux exposure are noticeably smaller, while the slope of the fitted lines to 5 and 8 kW/m^2 cases are nearly identical.

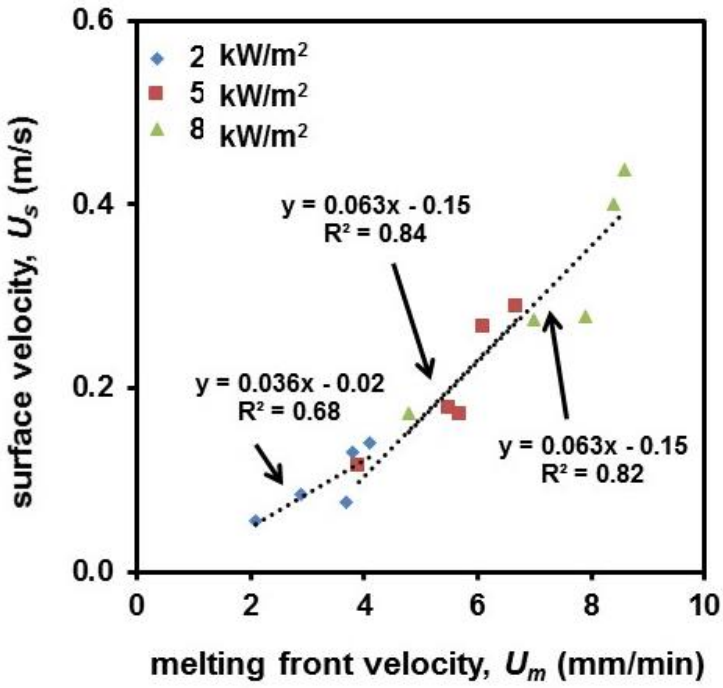

Figure 5.9: Relationship of U_s and U_m shown for all the liquids tested at 2, 5 and 8 kW/m^2 heat flux, grouped by heat flux intensity.

In the cases with 2 kW/m^2, the melting front velocity changed more with the increase in surface velocity (i.e. smaller slope) while for the cases with higher heat flux the slopes were found to be larger. In other words, when the heat flux was low, the surface velocity of liquids had more influence over the melting front velocity and vice versa. The difference in the slopes of the lines associated with different heat fluxes in Figure 5.9 is likely associated with the flow patterns of the liquids that were described in the discussion of Figure 5.8. This difference may also be explained through the variation in the thermophysical properties of the liquids at elevated temperatures.

In addition to the cavity formation problem, ignition and flame spread over liquid fuels (at sub-flash temperatures) are also controlled by the surface convective currents. The addition of a heat source (for the purpose of ignition or in the process of flame spread) induces a surface flow in the fuel layer. Appropriate grouping of the thermophysical properties that are influencing the ignition and flame spread are discussed in the literature [131]. In particular, viscosity and coefficient of surface tension [192, 193] of liquids are thought to be the liquid properties with most influence on the convection induced by an external sources. The correlation obtained in the current study confirms the importance of Marangoni stress (the first term in the RHS of Eq. 5.11) that accounts for the bigger share

in the U_s. For the ignition or flame spread of liquid fuels near the ice therefore, surface tension force is enhanced.

5.3 Conclusions on cavity formation in ice by externally heated liquids

A series of experiments were conducted to obtain the melting front velocity of the ice adjacent to different liquids exposed to various heat fluxes from above. From the experimental results, it can be seen that an increase in the heat flux decreased the melting time (increased the melting front velocity) and decreased the cavity width. Comparison of the experimental results and the liquid properties showed that liquids with higher melting front velocities had relatively lower viscosity and higher surface tension coefficient. But, a single property cannot be picked as the sole parameter influencing the melting process. Therefore, a scaling analysis of the surface flow was undertaken to examine a previously presented theory that showed the melting of ice is governed by the convective flows in the fuel layer. The melting front velocities were then compared to surface velocities of liquids obtained through the scaling analysis. The surface velocity of the liquids (U_s) correlated well to the melting front velocities (U_m) of the ice. Hence, a grouping of the liquid properties, consisting of surface tension coefficient and the viscosity of the liquids, were recognized to be the most influential parameters in determining the magnitude of the surface velocity and consequently the melting front velocity. In addition, the thickness of the convective layer appeared to relate to the cavity width (*D*).

As a result of the cavity formation, the burning efficiency, which is a key success criterion for *in situ* burning of oil, will decrease. Therefore, the knowledge on cavity formation phenomenon is essential so as to enhance the chances for successful implantation of *in situ* burning. The knowledge obtained by the current study may also be used to improve guidelines on ignition and flame spread of an oil spill adjacent to ice bodies. Ignition of and flame spread over a liquid fuel are governed by the same flows that were investigated herein. In particular, presence of ice will significantly increase the Marangoni stress and thereby affecting ignition and flame spread in areas of the fuel layer that is thermally affected by the ice.

6 Order of magnitude analysis

Burning of liquid fuels in ice-infested waters (such as melt pools or adjacent to ice walls) creates a lateral cavity around the spill perimeter and expands the burning area. The formations of lateral cavities could be contributing to reduction of removal efficiency and potential failure of the cleanup operation. By examining the lateral cavity through experimental studies, as discussed in the previous chapters, the primary dynamics involved in the formation of the lateral cavity were evaluated. Also, the few existing article on icy pool fires were reviewed and their reported measurements of lateral cavity size were collected.

Here, an order of magnitude correlation for estimating lateral cavity size of an pool fire confined in ice is introduced. The important physical mechanisms that are found to be influential in lateral cavity formation are included in the current analysis. The order of magnitude analysis includes the heat feedback from the flame to fuel surface, convective transfer toward the ice, and the melting energy continuity of ice. The experimental data on the size of lateral cavities that were formed during burning of varying sizes of icy pool fires are collected and the reliability of the scale analysis is evaluated by these experimental results.

The objective of this part of the study is to scale-up the lateral cavity formation in order to make a predictive tool for the estimation of lateral cavity and provide practical solutions for oil spill cleanup purposes. In the following sections the mechanisms that lead to lateral cavity along with their mathematical expressions are presented. An order of magnitude scaling analysis of these expressions is conducted to obtain a relation for the length of the lateral cavity. Finally, the obtained correlation from scaling is fitted with the available

experimental data to develop a tool to predict the extent of lateral cavity formation in real-life spill accidents.

6.1 Mathematical formulation

A general arrangement that can be found in different oil-in-ice situations is the adjoining of the oil layer to an ice body. Burning of the oil layer in these situations melts the ice in the immediate vicinity of oil and enlarges the oil surface. Melting of the ice in the vicinity of flame is slower compared to that of oil layer and therefore an overhang is created in ice. This turnover of the ice is referred as *lateral cavity formation* and is depicted in Figure 6.1. Additionally, Figure 3.2 and Figure 4.2 show such deformation. Figure 6.1 (a) illustrates an example of pool fire in vicinity of ice. Figure 6.1 (b) and (c) show the lateral cavity that is formed as a result of a 10 and 100 cm square pool fire respectively. Note that for relatively large ullage distance an overhang will form in the ice and for small ullage distance the liquid pool would simply widen on its ends with no overhang.

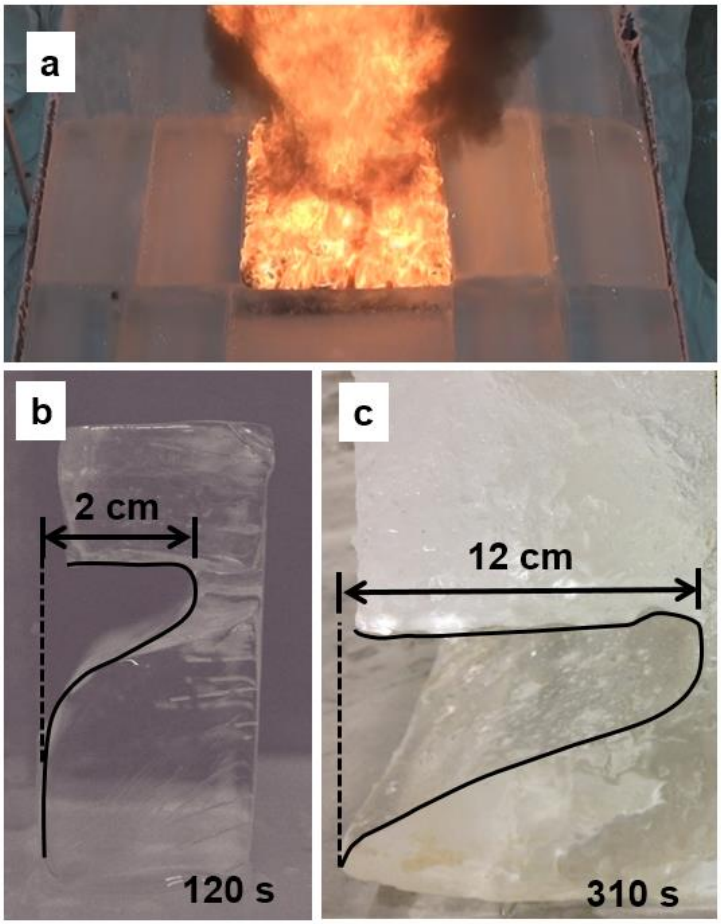

Figure 6.1: Lateral cavity formation in ice as a result of liquid fuels burning in vicinity of an ice wall. a) ANS crude oil burning in a 100 cm square ice opening [85], b) lateral cavity formed by n-octane burning in a 10 cm square tray with an ice wall on the side (120 s after ignition) [181], c) lateral cavity formed by ANS crude oil burning in a 100 cm square ice opening (310 s after ignition) [85].

The important physical phenomena can be expressed mathematically by the following. Consider a layer of liquid fuel bounded by an ice wall as depicted in Figure 6.2. The free surface of the fuel is subject to a heat flux by the flame feedback. The flame impingement and presence of ice near flame anchoring location impose a temperature gradient at the surface. The temperature gradient on the liquid surface give rise to surface-tension driven flows toward the ice. The ice is assumed to be isothermal and near its melting point temperature. Thus, the arriving liquid at the boundary of ice conducts the energy that is required to melt the ice. As this process continues a slender intrusion layer with length of $L(t)$ forms. A schematic of the heat transfer pathways that enable the lateral cavity formation are included in Figure 6.2.

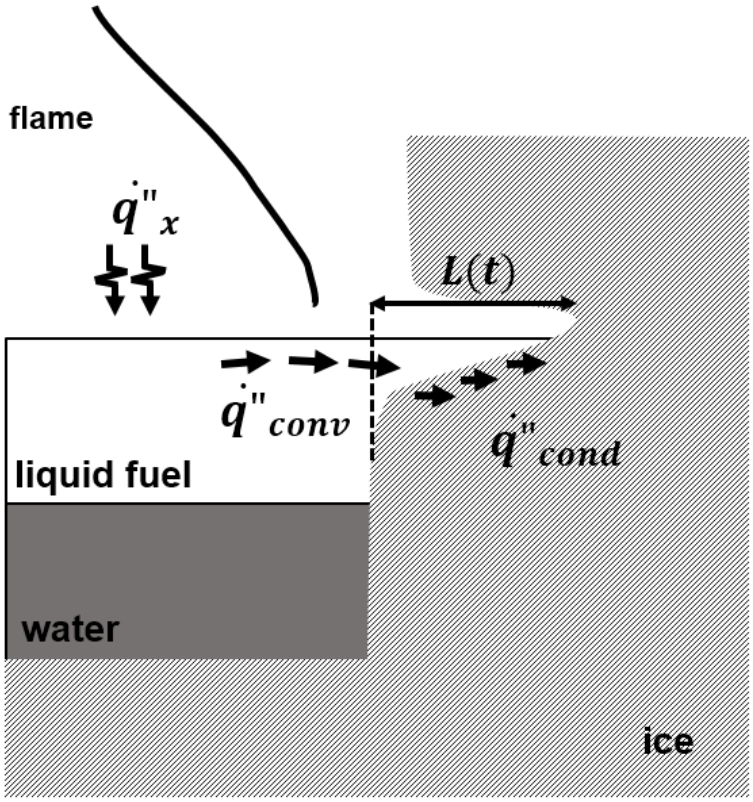

Figure 6.2: Schematic of the heat transfer pathways causing the ice melting. Heat flux from the flame ($\dot{q}''_x$) is absorbed by the fuel and transferred to the ice wall by convection ($\dot{q}''_{conv}$) to provide the energy for melting by conduction ($\dot{q}''_{cond}$).

A two-dimensional rectangular coordinate system (*x*, *y*) for a horizontal liquid layer bound by solid ice and exposed to a heat flux from above is considered. The coordinate system *x*-*y* is attached to the tip of the liquid layer which advances to the right as the lateral cavity expands. A schematic diagram of related geometry and other parameters are shown in Figure 6.3. The liquid is considered Newtonian with constant properties (ϑ, β, α), where ϑ, β , and α are kinematic viscosity, thermal expansion, and thermal diffusivity of the liquid fuel, respectively. Acceleration due to gravity, *g*, is 9.8 m/s^2. The steady-state boundary layer equations of mass, momentum, and energy for this horizontal liquid layer are described by the followings

$$\frac{\partial u}{\partial x} + \frac{\partial v}{\partial y} = 0 \,, \tag{6.1}$$

$$\vartheta \frac{\partial^3 u}{\partial y^3} - g\beta \frac{\partial T}{\partial x} = 0 \,, \tag{6.2}$$

$$u\frac{\partial T}{\partial x} + v\frac{\partial T}{\partial y} = \alpha \nabla^2 T. \tag{6.3}$$

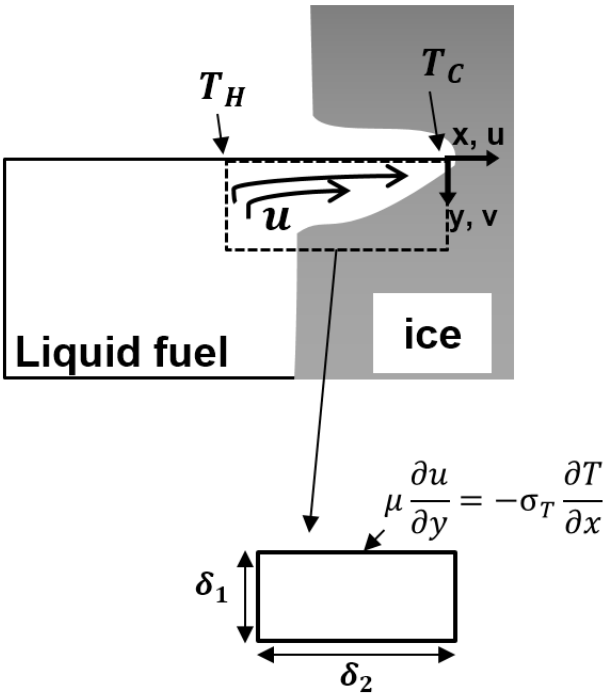

Figure 6.3: Schematics of liquid fuel flow toward the ice driven by temperature difference on the liquid surface (ΔT). Characteristic length and important parameters are labeled.

The form of the Navier-Stokes equation presented in Eq. (6.2) is obtained by cross differentiation of *x* and *y* momentum to remove pressure terms and is explained in details in *Convection Heat Transfer* book by Adrian Bejan [194]. The inertia terms are also removed since Prandtl numbers of considerably greater than unity [195] are assumed for hydrocarbon fuels. This equation contains two basic group of terms; viscous diffusion term and the buoyancy term, respectively [147, 148]. Boussinesq approximation is also used in the buoyancy term of Eq. (6.2) i.e. density is assumed constant everywhere except in the buoyancy source term of the momentum equation. In boundary layer theory the magnitude of the Prandtl number determines whether the thermal boundary layer is larger (Pr << 1) or smaller (Pr >> 1) than the momentum boundary layer. In laminar convection flows, Pr << 1 means the frictional and buoyancy forces are in balance in the thin viscous boundary layer while in the outer flow (large thermal boundary layer) inertial and buoyancy forces are in balance. On the other hand, when Pr >> 1 viscous and buoyancy forces are in balance in the thermal boundary layer and viscous and inertia are in balance in the larger viscous boundary layer. For example water has a Pr number of around 7 and mercury's Pr value is 0.015. The assumption that Prandtl number is greater than unity is therefore justified.

At the top boundary condition, the incident heat flux ($\dot{q}''_x$) imposes a horizontal temperature difference along the surface due to presence of the cold/ice wall, ($\Delta T = T_H - T_C$). The temperature gradient changes the surface tension coefficient of the fuel along its surface. The variation of surface tension coefficient at the interface of liquid fuel and air generates thermocapillary shear stress ($\tau_{xy} = -\sigma_T \frac{\partial T}{\partial x}$) where σ_T is the gradient of surface tension coefficient and is negative since surface tension coefficient is an inverse function of temperature for liquids considered here. The interfacial thermocapillary flow creates a boundary layer flow in the liquid by the resistance of viscous shear stress. So, a momentum balance for the top surface flow can be written as

$$\mu \frac{\partial u}{\partial y} = -\sigma_T \frac{\partial T}{\partial x} \ . \tag{6.4}$$

The temperature difference on top surface of the fuel also can be expressed with the incident heat flux on the surface by assuming a linear approximation of in-depth conduction through the thermal boundary layer,

$$\Delta T = \frac{d\dot{q}''_x}{k}, \tag{6.5}$$

where k is the thermal conductivity of the liquid and d is the thermal boundary layer thickness. The incident heat flux, $\dot{q}''_x$, can be expressed by a correlation of the heat feedback to the fuel surface of pool fires [120]. The validity of this correlation in the energy balance of pool fires in ice is previously confirmed [87]. The following expression can be used for the heat receiving the surface

$$\dot{q}''_x = \frac{4}{\pi} \chi \, \rho_\infty C_{p\infty} \left[T_\infty g \left(T_f - T_\infty\right)\right]^{\frac{1}{2}} D^{1/2}, \tag{6.6}$$

where χ is a specific fraction of the heat released fed back to the fuel surface and is in the range between 0.003 to 0.008 depending on the pool diameter. Here a value of 0.003 is assumed for every case. Further, ρ_∞, $C_{p\infty}$, and T_∞ are the air properties at ambient temperature; T_f is the temperature of the hot gases above the liquid which is assumed to be constant (1200 K). Note that the ambient temperature of 293 K is used in Equation 6.6.

As explained, the coordinate system advances to the right as the lateral cavity expands at velocity $U = \frac{dL}{dt}$. Here, L is the instantaneous intrusion length and it is assumed that the melting front velocity is much slower than surface flow velocity, $U << u$. This means that ice enters the domain from the right hand side and the arriving fluid at the ice wall conducts the energy for the ice to melt. This exchange occurs in the bottom side of the control volume at $y = -\delta_1$, where δ_1 is the height of the domain as shown in Figure 6.3. The flow comes to stop near the ice wall at a stagnation point. Therefore, an energy balance for the control volume of zero thickness that encloses the two-phase interface (melting front) can be written as

$$\dot{m}''_{ice} L_{m,ice} = \dot{q}''_{cond} - \dot{q}''_{ice} \quad . \tag{6.7}$$

The left hand side of Equation (6.6) defines the required heat for phase change where $\dot{m}''_{ice}$ is the mass flux of the ice that enters the domain with velocity U and $L_{m,ice}$ is the latent heat of fusion of ice. The right hand side of Equation (6.6) expresses the difference between the heat flux delivered by the arriving fluid and the heat absorbed by the solid. $\dot{q}''_{cond}$ is the heat conducted to ice by the arriving fluid that can be expressed as $k(\frac{\partial T}{\partial y})_{y=-\delta_1}$ and $\dot{q}''_{ice}$ is conduction within the ice which is negligible since the ice is assumed to be isothermal and near its melting point. Therefore, Equation (6.7) may be written as

$$\rho_{ice} L_{m,ice} U \frac{\partial y}{\partial x} = k_{ice}(\frac{\partial T}{\partial y})_{y=-\delta} \, , \tag{6.8}$$

where ρ_{ice} and $L'_{m,ice}$ is the density of the ice. Equation (6.8) provides the melting front energy continuity that balances the conduction heat flux arriving from the liquid to the ice that enters the domain.

6.2 Scaling by order of magnitude analysis

The system selected for scaling analysis is the intrusive liquid layer of length δ_2 and depth δ_1 that are replaced with *x* and *y*, respectively. The scale of temperature is $\Delta T = T_H - T_C$ where T_H the temperature on the warm side of the cavity is and T_C is the cold side (i.e. ice

temperature). Equations (6.1-6.3) can be written in the following order of magnitude statements,

$$\frac{u}{\delta_2} \sim \frac{v}{\delta_1} \ , \tag{6.9}$$

$$\frac{u}{{\delta_1}^3} \sim g\beta \frac{\Delta T}{\delta_2} \ , \tag{6.10}$$

$$u \ \frac{\Delta T}{\delta_2}, v \ \frac{\Delta T}{\delta_1} \sim \alpha \ \frac{\Delta T}{{\delta_1}^2} \ . \tag{6.11}$$

The mass conservation equation (Equation (6.9)) indicates that the two terms on the left hand side of Equation (6.11) are of same order. The source term in Equation (6.10) states that the flow is governed by buoyancy, however for a thermally stratified liquid, this effect is minimal and it is shown previously that buoyancy effect is negligible [172, 184]. Therefore, fluid boundary condition on its top surface (Equation (6.4)) is considered here that in the order of magnitude sense can be written as

$$\frac{u}{\delta_1} \sim \frac{-\sigma_T}{\mu} \frac{\Delta T}{\delta_2} . \tag{6.12}$$

Also, the melting front conservation of energy equation (Equation (6.8)) may be expressed as the following

$$k_{ice} \frac{\Delta T}{\delta_1} \sim \rho_{ice} L_{m,ice} U \ \frac{\delta_1}{\delta_2} \ . \tag{6.13}$$

Rearranging Equation (6.13) yields the following (note that $U=L/t$ is replaced, too),

$${\delta_1}^2 \sim \frac{kt\Delta T}{\rho_{ice} L_{m,ice}} \frac{\delta_2}{L} . \tag{6.14}$$

Combining the boundary condition with energy conservation equation (Equation (6.12) and (6.11)) and solving for δ_2 yields,

$${\delta_2}^2 \sim \frac{-\sigma_T \Delta T {\delta_1}^3}{\mu\alpha} . \tag{6.15}$$

Equations (6.14) and (6.15) may be combined and solving for the L gives the final equation for the intrusion length of the lateral cavity (Note that Equation 6.6 is replaced for ΔT here),

$$L \sim \left(\frac{-\sigma_T}{\mu\alpha}\right)^{2/3}\left(\frac{\dot{q}''_x d}{k}\right)^{5/3}\left(\frac{k_{ice}t}{\rho_{ice}L_{m,ice}}\right)\left(\frac{1}{\delta_2}\right)^{1/3}. \quad (6.16)$$

The correlation that is obtained here represents the physics that are involved in the problem. A dimensionless intrusion length is also obtained by dividing Equation (6.16) by δ_2,

$$\frac{L}{\delta_2} \sim (Ma)^{\frac{2}{3}}(Ste.Fo), \quad (6.17)$$

where $= \frac{-\sigma_T \Delta T \delta_2}{\mu\alpha}$, $Ste = \frac{C_p \Delta T}{L_{m,ice}}$, and $Fo = \frac{\alpha_{ice} t}{{\delta_2}^2}$ are the dimensionless numbers (Marangoni number, Stefan number, and Froude number) associated with the ice melting problem. The dimensionless melting length presented in Equation 6.17 is developed for the first time and can be used in problems such as welding and other applications that involve melting.

6.3 Assessment of the Scaling with Experiments

The intrusion length of liquid fuels in ice varies with the fire size, oil properties, burning duration. A literature search on pool fires in the vicinity of ice presented a limited number of experimental studies. The summary of these studies are reported in Table 6.1. Initial diameter, fuel layer thickness, burning duration, fuel type, and ice geometry of these experiments were collected. The diameter for the experiments of square and channel geometries were assumed to be equal to that of a circular geometry with similar surface area (i.e. D = $2\sqrt{Area/\pi}$).

Table 6.1: Overview of lateral cavity length reported in pool fire experiments in vicinity of ice.

No.	Initial diameter (cm)	Fuel layer thickness (cm)	Burn duration (s)	Intrusion length (cm)	Fuel type	Geometry / ref.
1	5	2.4	480	5.0	ANS crude	circular [87]
2	5.7	1.8	600	5.1	n-octane	circular [172]
3	5.7	2.0	590	4.8	m-xylene	circular [82]
4	7	1.4	180	3.0	n-octane	square [181]
5	9.5	1.0	350	3.8	ANS crude	circular [196]
6	9.5	2.0	475	6.5	ANS crude	circular [196]
7	10	1.6	450	4.5	ANS crude	circular [87]
8	14.2	4.0	700	6.0	Oil mixture	channel [86]
9	15	1.6	440	6.0	ANS crude	circular [87]
10	25	1.0	220	4.5	ANS crude	circular [196]
11	25	1.5	340	6.0	ANS crude	circular [87]
12	37	0.5	180	5.5	ANS crude	channel [85]
13	37	1.0	260	7.0	ANS crude	channel [85]
14	37	1.5	320	8.8	ANS crude	channel [85]
15	112	1.0	310	12.0	ANS crude	square [85]
16	105	1.0	200	7.0	ANS crude	square [94]
17	103	1.3	250	10.0	ANS crude	square [94]
18	100*	1.5	305	20.0	ANS crude	square [94]
19	100*	1.7	370	28.0	ANS crude	square [94]
20	150*	1.3	230	20.0	ANS crude	square [94]

* Outdoor test with saltwater ice and in the ambient winds.

The information presented in Table 6.1 shows different pool fires burning in vicinity of ice walls that comprise of variable initial conditions. For example, the tests that were conducted in ~100 cm square ice cavity had different initial oil volume which resulted in varying burning duration. Few of the tests at or above 100 cm were performed in outdoor environment with saltwater ice that has lower thermal conductivity and heat of fusion than freshwater ice. Thus, different intrusion lengths for similar size experiments are obtained.

The correlation obtained from scaling analysis (Equation (6.16)) was evaluated with the experimental data reported in Table 6.1. The properties of ANS crude oil [196] and ice

[197] were assumed constant and were taken at 20 ℃ for simplicity. Thermal depth (d) and horizontal characteristic length (δ_2) were also assumed to be constant and equal to 4 and 8 mm, respectively. To adjust the scaling analysis with experiments, Equation (6.16) was fitted to the experimental data on intrusion lengths using a least square regression method. It was shown that the minimum deviation from experimental data could be obtained from parameters a, b_1, b_2, and b_3 in Equation (6.18) when they are equal to 0.48, 0.14, 1.16, and 0.86, respectively. The R-squared value obtained from the least square method and the mentioned set of parameters is 0.92.

$$L \sim a \left(\frac{-\sigma_T}{\mu\alpha}\right)^{b_1} \left(\frac{d\dot{q}''_x}{k}\right)^{b_2} \left(\frac{k_{ice}t}{\rho_{ice}L_{m,ice}}\right)^{b_3} \left(\frac{1}{\delta_2}\right)^{1/3} \tag{6.18}$$

Here, a is a coefficient that correlates the overall output of the model to the experimental results. b_1 represents the effect of thermophysical properties of the oil on intrusion length and is found to be smaller than the power that was initially obtained in Eq. 6.17. The reason for this could be the small overall variation of thermophysical properties compared to the other parameters of the problem. b_2 represents the influence of the heat feedback on ice melting and for scenarios without burning it should be accordingly modified. b_3 is the power representing the effect of ice properties and exposure duration. In order to provide a direct comparison between experiments and the model presented in this study, the values of intrusion lengths obtained from Equation (6.18) were plotted against the experimental data for each test and are shown in Figure 6.4. The sloped lines in Figure 6.4 show the percentage deviation from theoretical model.

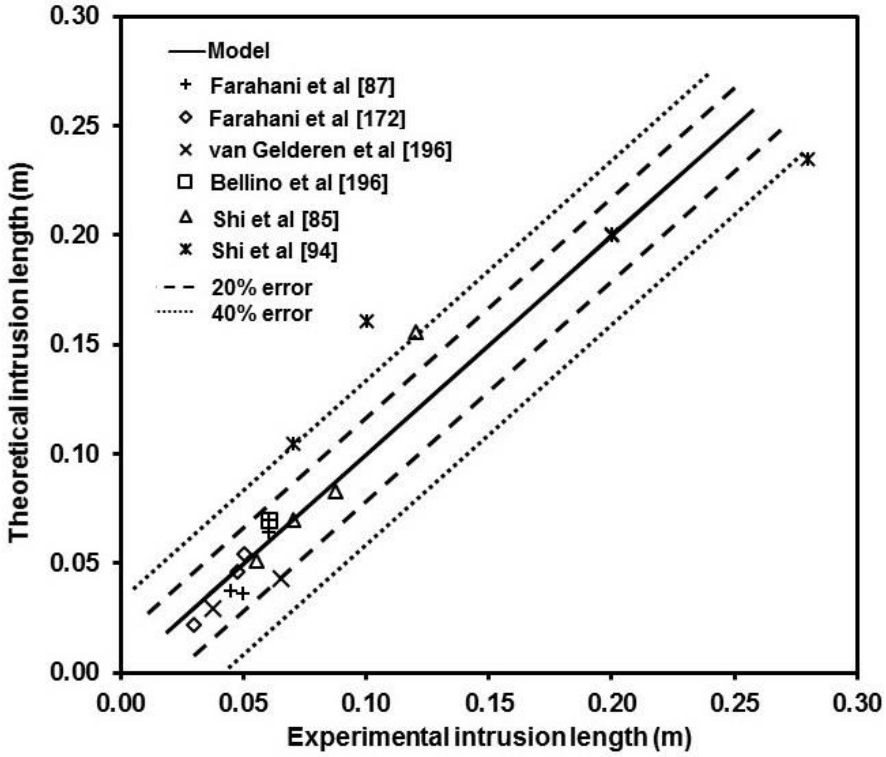

Figure 6.4: Validation plots of the theoretical intrusion lengths vs. experimental intrusion lengths. The sloped lines represent the percentage deviation of experiments from the theoretical intrusion length. The two data points with more than 40% deviation represent those experiments that were conducted outdoors with presence of wind and saltwater ice.

As can be seen from Figure 6.4, the results obtained from Equation (6.18) are in good agreement with the existing experimental data in literature. Nonetheless, the discrepancies between experiments and theoretical model could be associated with the different setting of these experiments. Few of the experiments were conducted with saltwater ice and in presence of ambient wind. The influence of seawater ice on the intrusion length of lateral cavity can be addressed by changing the latent heat of fusion and thermal conductivity of ice in Equation (6.18). Though, the effect of wind is twofold and is more significant [198]. The first effect of wind is toward changing the heat feedback mechanism by deforming and tilting the shape of the flame. In addition, flow of air on the liquid surface can induce convective flows and complicate the problem further. Therefore, more experimental data, especially of larger fires with longer duration similar to real-life scenarios [199], is needed to modify Equation (6.18) and increase its predictability.

Another consideration of the model that should be noted here is the limitation of the heat feedback equation that has replaced the temperature difference (ΔT) in Eq. 16. The fire size

defines the overall energy released by a pool fire and is an important aspect of the lateral cavity formation. However, the temperature difference (ΔT) is the relevant parameter here that governs the ice melting and will not indefinitely change proportional to the fire size as it is limited to the liquid fuel boiling point [200]. Therefore, the weight of the pool diameter in the final correlation, $\dot{q}''_x$, should be limited to an asymptote. Consequently, experiments in larger size are required to determine the value of the asymptote.

Another advantage of the current analysis is its ability to assess the melting that occurs naturally as the results of absorption of sunlight by the spilled oil. As arrival of first responders is delayed due to remoteness of the Arctic, the spilled oil may remain in the environment for several days before cleanup operation is initiated. Because of the higher absorption coefficient of crude oils [201] a temperature difference of 3-8 °C [74] between oil and water is expected in temperate waters. The temperature difference in ice condition could conservatively be assumed to be around 1 °C [202]. It is imperative for first responders to know what length of time the ice will contain the oil and also how the natural melting changes the oil thickness. The melting of ice will change surface area of the oil slick and its thickness that are both important in determining the oil slick burning behavior and its susceptibility to ignition.

A hypothetical experiment for a melt-pool containing an unknown type of oil with initial diameter of 50 cm and thickness of 5 mm is considered. If the oil pool stays untreated it can expand by absorbing the sunlight energy. Figure 5 shows the intrusion length of crude oil, varying viscosity from 0.5 to 50 centi-Poise (cP) is considered, into the ice with respect to the time. Temperature significantly changes viscosity dependency and also liquid fuels viscosity that changes depending on their composition. For the respective change in the slick thickness is also plotted on the second y-axis with gray markers. The evaporation of the oil can contribute to the reduction of slick thickness however only the melting and the consequent geometry change is considered herein. The trend line in Figure 6.5 shows how the delay in response, particularly for seasons with longer days, could change the surface area and thickness of the oil because of natural melting.

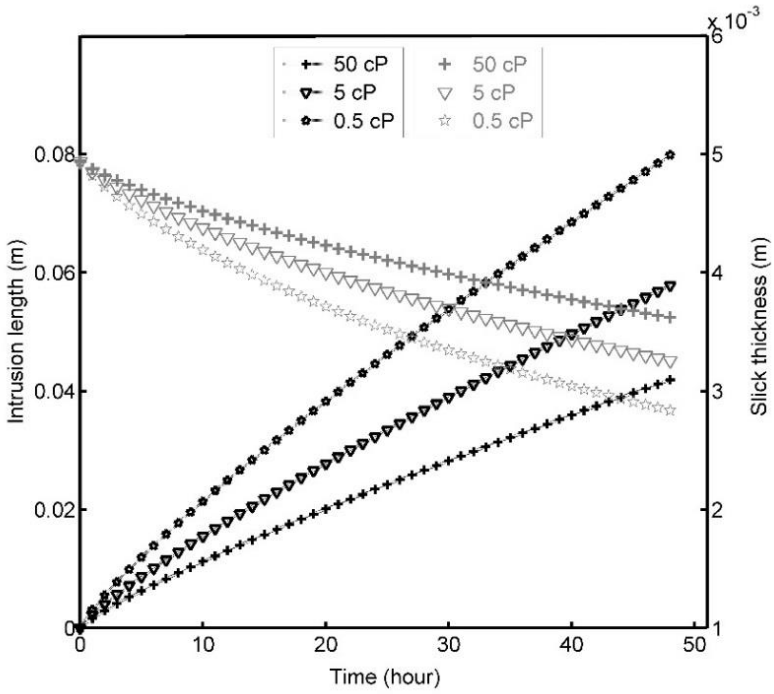

Figure 6.5: Natural melting of ice adjacent to a 0.5 m diameter crude oils with varying viscosity exposed to 48 hours of sunlight. Intrusion length of the oil in ice is shown on the right y-axis. Change in slick thickness caused by intrusion length are shown on the left y-axis with gray markers.

It can be seen from Figure 6.5 that for a 48 hours exposure of the lowest viscosity crude oil, intrusion length of around 8 cm are expected which in turn results in 2 mm thickness reduction. Such a thickness reduction can substantially affect the ignition probability of the oil. Although the uncertainty associated with this calculation should be reduced with more experimental studies, the current analysis is of great value in deciding the time-frame of a cleanup operation.

6.4 Conclusions based on the scaling analysis

Burning of spilled oils in ice-infested waters for the purpose of cleanup results in a unique geometry change of the ice referred as lateral cavity. The ice melting and formation of the lateral cavity is influential in determining the outcome of spill cleanup as it changes the burning behavior of the oil slick. An order of magnitude scaling analysis was conducted to obtain a correlation for intrusion length of the lateral cavity. The analysis considered the different physical aspects of the lateral cavity problem including the heat feedback from the

flame to the fuel surface, the convective transfer toward the ice by surface tension driven flow, and the melting energy continuity of the ice wall. The existing experimental data on the intrusion length of lateral cavity for pool fires of 5 cm to 150 cm were collected. Finally, the experimental data was correlated to the results of the scaling analysis using a least square regression method. The scaling of this problem has provided a predictive tool to estimate the intrusion length of lateral cavity problem. The scaling correlation was validated for pool fires confined in ice of up to 150 cm diameter. However, actual pools of oil found in the Arctic may be larger and burn for a much longer duration depending on the location of spill. In addition, the properties of the spilled oil can vary significantly depending on the source of the spill. Thus, more experiments with different oils and in larger diameters are required to extend the validity domain of the newly developed correlation.

7 Conclusions

The ice melting and lateral cavity formation caused by *in situ* burning of liquid fuels on ice infested waters was studied in order to improve the forecasting of the suitability of ISB by examining the mechanisms of the ice melting (lateral cavity formation) and developing a tool to predict the length of lateral cavity for an ISB operation. The aim of this study was to help understand the mechanisms leading to ice melting of pool fires confined in ice. A quantitative assessment of melting requires the knowledge of the energy transfer to the fuel and its distribution within the liquid fuel.

Since melting of ice during burning of pool fires in ice confinements has significant influence on oil spill cleanup in ice-infested waters, the findings of this work are very important for successful implementation of *in situ* burning in Arctic regions. The survey of literature related to practical aspects of *in situ* burning in ice-infested waters showed a severe lack of information regarding the melting of ice and lateral cavity formation. Furthermore, the fundamental mechanisms that lead to lateral cavity formation during the *in situ* burning operation have also not been studied before.

The lack of practical and theoretical knowledge on the ice melting during *in situ* burning has led to weak estimations and unsuccessful burn operations. Therefore, several experimental setups were designed to study the lateral cavity evolution and the mechanisms leading to this formation. The liquid fuel properties that influence the melting were studied in a parametric study. Finally, a scaling analysis was performed to estimate the size (intrusion length) of a lateral cavity for a given spill scenario. A detailed description of the conclusions of this study and future works are given in Sections 7.1 and 7.22, respectively.

7.1 Outcome of the current work

In the first experimental study n-octane was burned in an ice cavity to study the influence of ice geometry changes. The experiments included a full course of burning, i.e. ignition to natural extinction, where the initial fuel thickness of 18 mm reduced to around 2 mm at the time of extinction. Similar to the observations of earlier studies, the fuel layer was capable of melting the ice at a faster pace than the flame. Hence, a void was formed in the circumference of the ice wall that contributed to growth of the liquid fuel surface area.

A hypothesis was proposed to explain the heat transfer mechanisms that caused the melting. Based on this hypothesis, the temperature difference in the fuel induced convective motion in the liquid fuel that provided the energy to melt the ice. The convective flow was near the surface from center toward the ice wall (surface tension) and downward near the ice wall (buoyancy). The results of the analysis on the Marangoni number ($Ma = \frac{\sigma_T R \Delta T_h}{\mu \alpha}$) and natural convection showed that when the fuel layer was sufficiently thick (first half of the test), natural convection was dominant and for smaller thicknesses (second half of the test) Marangoni flow was dominant. Overall, for the duration of the experiments the value of the Rayleigh number ($Ra = \frac{\beta g H^3 \Delta T_v}{\vartheta \alpha}$) decreased with several orders of magnitude (from ignition to extinction) while Marangoni number increased slightly. The corresponding total melting lengths of the fuel layer in ice for the first and second half of the burning tests however were 21 and 28 mm, respectively. This suggests that surface tension could be the driving force, while the buoyancy had a second order effect.

In the second set of experiments, the fuel layer thickness was kept constant to see the effect of burning rate on melting of ice. The experiment showed that for the period when the burning rate was increasing to reach a maximum (first 50 seconds after ignition), the melting front velocity had an average value of 6 mm/min. After the burning rate reached its maximum and became steady (50 to 200 seconds), the melting velocity had an average value of 10 mm/min. The average burning rate for these two phases were 0.04 and 0.07 g/s, respectively.

Flow visualization of the liquid fuel with PIV showed very distinguished flow behaviors. Before ignition, a one roll flow structure in the fuel layer was observed (with maximum velocity of 4 mm/s), due to coupling of Marangoni convection and buoyancy. However,

after ignition the one roll structure transitioned to multi-roll structure in the first 50 seconds of experiment. The velocity magnitude increased and reached 16 mm/s in the transition period. At the same time, the vorticity magnitude increased and most of the fuel layer became involved with convective currents. The increased velocity of multi-roll structure regime could be the main cause for the enhanced melting of the ice. Based on the thermocouple measurements, a two-layer thermal structure was observed in the fuel layer; 1) a top layer with steep temperature gradient in the vertical direction and 2) a low temperature zone. The ice melting was much more significant in the upper layer regions of contact where the multi-roll structure was present.

In the third study, the focus was on understanding the liquid properties that change the extent of melting. A series of experiments were conducted to obtain the melting front velocity of the ice adjacent to different liquids exposed to various heat fluxes from above. Comparison of the experimental results and the liquid properties showed that viscosity, boiling point, and surface tension coefficient of liquids affects the melting front velocities. However, a single property could not be picked as the sole parameter influencing the melting process. In the previous part of the overall study, it was shown that the melting of ice is governed by the convective flows in the fuel layer. The melting front velocities obtained from experiments were then compared to surface velocities of liquids obtained through a scaling analysis. The surface velocity of the liquids (U_s) correlated well with the melting front velocities (U_m) of the ice. Hence, a grouping of the liquid properties, consisting of surface tension coefficient and the viscosity of the liquids, were recognized to be the most influential parameters in determining the magnitude of the surface velocity and consequently the melting front velocity.

In the last step of this study, scaling of the ice melting was performed with an order of magnitude analysis. This was made possible through valuable knowledge that were obtained in the previous steps of the overall study. The scaling considered important physical mechanisms in the lateral cavity process such as the heat feedback from the flame to fuel surface, the convective transfer toward the ice, and the melting energy continuity of ice. The existing experimental data on the size of lateral cavity were also collected and were correlated to the results of the scaling analysis using a nonlinear regression fitting technique. The scaling of this problem provided a predictive tool to estimate the lateral cavity intrusion length. The model is validated for pool fires of up to 150 cm diameter in

size through laboratory scale experiments. However, the pool fires confined in ice in the Arctic environment may show a rather different behavior. For example, the effect of ambient condition such as wind that is not included in the model may lead to errors in prediction of lateral cavity intrusion length.

Considering a more practical aspect, the results obtained from this comprehensive study could assist the first responders and policy makers to react efficiently to spill incidents in the Arctic. In general, it is valuable to know what length of time the ice would be able to contain the oil when it is burning. In addition, melting of ice and reduction of the oil slick thickness can cause faster extinction of fires and reduce the removal efficiency.

The ability to predict the outcome of *in situ* burning in ice condition in a more accurate fashion is one of the achievement of the current study. Specifically, the correlation developed in Chapter 6 is a powerful tool that is able to determine the ice melting and expansion of the fire area.

Melting is not entirely a negative aspect of the ISB in ice-infested waters. For cases with melt pools formed by brine channels, this study can be used to determine if by ignition of one pool the fire will spread the fire other melt pools nearby. For a situation such as high concentration pack ice where spilled oil is only exposed to air through small cracks and channels, the expansion caused by melting can significantly increase the burning area and removal efficiency.

The practical knowledge generated from this study in predicting the suitability of ISB as oil spill response method can thus be valuable in decision making and responding. The findings of this study can also be extended to the issues related to the global warming where retreat of ice sheets in the poles are of concern.

7.2 Suggestions for future work

Based on the conclusions of this study, some recommendations for future research on pool fires in vicinity of ice are proposed. Ignition and flame spread in cold regions can benefit from this work as they are governed by the same flows that were investigated herein. Although, much consideration must be given to interrelated effect of flash point and

convection to provide a better understanding of the flow field in presence of ice. The Marangoni stress is enhanced in areas of the fuel layer that is thermally affected by the ice and consequently ignition and flame spread are effected. The knowledge obtained by the current study may also be used to improve guidelines on ignition and flame spread of an oil spill adjacent to ice bodies.

The PIV measurement in the liquid-phase of a burning fuel adjacent to ice was found to be very challenging and provided relatively low quality images. A similar flow visualization study with more control over the experimental parameters such as controlled external heating could be very helpful in understanding the flow field of a liquid that is adjacent to ice. Studying the convection induced by external heating of liquid adjacent to a cold vertical boundary would be very informative in terms of understanding the exact flow regimes and heat transfer pathways that lead to melting.

The effect of ambient conditions, and especially wind, should be incorporated to the findings of this study. Wind has a large influence in creating the surface flow that is capable of melting the ice. Also, it can change the flame feedback mechanism by tilting the flame. Therefore, inclusion of wind effects on melting can significantly improve the estimations.

Although the dynamics of melting and pool fire burning are on their own complicated, but a more simple representation of the dynamics can potentially be studied numerically. The experimental setup introduced in Chapter 5 along with the results of those experiments provides a good opportunity for a numerical study. A numerical study of ice melting by a liquid layer exposed to heat flux from the top will be very useful.

Bibliography

[1] J. Frynas, "Corporate social responsibility or government regulation? Evidence on oil spill prevention," *Ecology and Society,* vol. 17, no. 4, 2012.

[2] M. Fingas, *The basics of oil spill cleanup*. CRC Press, 2012.

[3] E. R. Gundlach and M. O. Hayes, "Vulnerability of coastal environments to oil spill impacts," *Marine technology society Journal,* vol. 12, no. 4, pp. 18-27, 1978.

[4] H. N. Psaraftis, G. G. Tharakan, and A. Ceder, "Optimal response to oil spills: the strategic decision case," *Operations Research,* vol. 34, no. 2, pp. 203-217, 1986.

[5] M. S. Foster, J. A. Tarpley, and S. L. Dearn, "To clean or not to clean: the rationale, methods, and consequences of removing oil from temperate shores," *Northwest Environ. J.,* vol. 6, no. 1, pp. 105-120, 1990.

[6] J. V. Mullin and M. A. Champ, "Introduction/Overview to In Situ Burning of Oil Spills," *Spill Science & Technology Bulletin,* vol. 8, no. 4, pp. 323-330, 2003.

[7] A. B. Nordvik, "The technology windows-of-opportunity for marine oil spill response as related to oil weathering and operations," *Spill Science & Technology Bulletin,* vol. 2, no. 1, pp. 17-46, 1995.

[8] P. J. Brandvik, K. R. Sorheim, I. Singaas, and M. Reed, "Short state-of-the-art Report on Oil Spills in Ice-Infested Waters.," in "Oil in Ice," SINTEF Materials and Chemistry2006.

[9] B. O. Johannessen, H. Jensen, L. Solsberg, and T. Lorenzo, "Mechanical Oil Recovery in Ice Infested Waters (MORICE)–Phase 1," *SINTEF Report no.: STF22 F,* , 1996.

[10] J. L. Ramseur, "Deepwater Horizon oil spill: the fate of the oil," 2010: Congressional Research Service, Library of Congress Washington, DC.

[11] J. R. Clayton, J. R. Payne, J. S. Farlow, and C. Sarwar, "Oil spill dispersants: mechanisms of action and laboratory tests," Science Applications International Corp., San Diego, CA (United States)1993.

[12] E. B. Kujawinski, M. C. Kido Soule, D. L. Valentine, A. K. Boysen, K. Longnecker, and M. C. Redmond, "Fate of dispersants associated with the Deepwater Horizon oil spill," *Environmental science & technology,* vol. 45, no. 4, pp. 1298-1306, 2011.

[13] R. R. Lessard and G. DeMarco, "The significance of oil spill dispersants," *Spill Science & Technology Bulletin*, vol. 6, no. 1, pp. 59-68, 2000.

[14] T. Moller, H. Parker, and J. Nichols, "Comparative Costs of Oil Spill Cleanup Techniques 1," in *International Oil Spill Conference*, 1987, no. 1, pp. 123-127: American Petroleum Institute.

[15] A. A. Al-Majed, A. R. Adebayo, and M. E. Hossain, "A sustainable approach to controlling oil spills," *Journal of environmental management*, vol. 113, pp. 213-227, 2012.

[16] W. McLeod and D. McLeod, "Measures to Combat Offshore Artie Oil Spills," in *Offshore Technology Conference*, 1972: Offshore Technology Conference.

[17] A. A. Allen, "Controlled Burning of Crude Oil on Water Following the Grounding of the Exxon Valdez.," in *Proceedings of the 1991 Oil Spill Conference* San Diego, CA, 1991, pp. 213-216: American Petroleum Institute, Washington, D.C.

[18] J. W. Griggs, "BP Gulf of Mexico oil spill," *Energy LJ*, vol. 32, p. 57, 2011.

[19] A. A. Allen, D. Jaeger, N. J. Mabile, and D. Costanzo, "The use of controlled burning during the Gulf of Mexico Deepwater Horizon MC-252 oil spill response," in *International Oil Spill Conference Proceedings (IOSC)*, 2011, vol. 2011, no. 1, p. abs194: American Petroleum Institute.

[20] I. Buist, J. McCourt, S. Potter, s. Ross, and K. Trudel, "In situ Burning," *Pure Appl. Chem.*, vol. 71, no. 1, pp. 43-65, 1999.

[21] D. L. Gautier, K. J. Bird, R. R. Charpentier, A. Grantz, D. W. Houseknecht, T. R. Klett, T. E. Moore, J. K. Pitman, C. J. Schenk, and J. H. Schuenemeyer, "Assessment of undiscovered oil and gas in the Arctic," *Science*, vol. 324, no. 5931, pp. 1175-1179, 2009.

[22] D. L. Gautier, K. J. Bird, R. R. Charpentier, A. Grantz, D. W. Houseknecht, T. R. Klett, T. E. Moore, J. K. Pitman, C. J. Schenk, and J. H. Schuenemeyer, "Oil and gas resource potential north of the Arctic Circle," *Geological Society, London, Memoirs*, vol. 35, no. 1, pp. 151-161, 2011.

[23] AMAP, "Oil and Gas Activities in the Arctic, Effects and Potential Effects,," *Arctic Monitoring and Assessment Programme (AMAP), Oslo, Norway*, vol. 1, pp. 2_212-2_214, 2007.

[24] EPPR, "Guide to Oil Spill Response in Snow and Ice Conditions. Emergency Prevention, Preparedness and Response " 2015.

[25] D. Kramer. (2017) Climate Change in the Arctic Accelerates. *Physics Today*. 24-27.

[26] NIST, "Oil and Gas Technologies for the Arctic and Deepwater," Washington, DC: U.S. Congress, Office of Technology Assessment, OTA-O-270, 1985.

[27] N. W. Glover and D. F. Dickins, "Response plans for Arctic oil and ice encounters," in *International Oil Spill Conference*, 1999, vol. 1999, no. 1, pp. 639-646: American Petroleum Institute.

[28] K. U. Evers, H. V. Jensen, J. M. Resby, S. Ramstad, and I. Singsaas, "State of the art report on oil weathering and on the effectiveness of response alternatives," *Report of ARCOP Work package,* vol. 4, 2004.

[29] D. Dickins and I. Buist, "Countermeasures for ice covered waters," *Pure and applied chemistry,* vol. 71, no. 1, pp. 173-191, 1999.

[30] B. F. Scott, "Investigation of the Weathering of a Selected Crude Oil in a Cold Environment," *American Society for Testing and Materials* pp. 514-525., 1975.

[31] Arctic-Council, "Agreement on Cooperation on Marine Oil Pollution Preparedness and Response in the Arctic," p. 230, 2013.

[32] H. V. Jensen and J.V. Mullin, "MORICE-new technology for mechanical oil recovery in ice infested waters," *Marine pollution bulletin,* vol. 47, no. 9, pp. 453-469, 2003.

[33] D. F. Dickins, "Advancing Oil Spill Response in Ice-Covered Waters," United States Arctic Research Commission & Prince William Sound Oil Spill Recovery Institute2004.

[34] P. Daling, I. Singsaas, and J. Nerbø Hokstad, "Testing of the efficiency of dispersants during arctic conditions," IKU Report1991.

[35] B. Ian, "In Situ Burning of Oil Spills in Ice and Snow," 2000. Alaskan Clean Seas

[36] J. Fritt-Rasmussen, "Marine Oil Pollution: Response Methods," in *Encyclopedia of Environmental Management*: Taylor & Francis, 2014.

[37] S. L. Ross, "Tests to Determine the Limits to In Situ Burning of Thin Oil Slicks in Broken Ice," Report to Minerals Management Service and ExxonMobil Upstream Research. Herndon, VA, U.S.2003.

[38] E. DeCola, T. Robertson, S. Fletcher, and S. Harvey, "Offshore Oil Spill Response in Dynamic Ice Conditions," Nuka Research and Planning Group.

[39] I. A. Buist, S. G. Potter, B. K. Trudel, S. R. Shelnutt, A. H. Walker, D. K. Scholz, P. J. Brandvik, J. Fritt-Rasmussen, A. A. Allen, and P. Smith, "In Situ Burning in Ice-Affected Waters: State of Knowledge Report," JIP24 October 2013.

[40] I. Singsaas, K.R. Sorheim, R. Lundmark Daae, B. Johanseb, and L. Solsberg, "Testing of Oil Skimmers Via Field Experiments in the Barents Sea," SINTEF & Counterspill Research Inc.5, 2010.

[41] Per Johan Brandvik, Janne fritt-Rasmussen, Roger Daniloff, Janne Lise Resby, and Frode leirvik, "Establishing, Testing and Verification of a Laboratory Burning Cell to Measure Ignitibility for In-Situ Burning of Oil Spills," in "Oil in Ice," SINTEF Materials and Chemistry, 2010.

[42] NORCOR, "The Interaction of Crude Oil with Arctic Sea Ice. Beaufort Sea Project. ," in "NORCOR Engineering and Research Ltd. (NORCOR).", Technical Report No. 27, Canada Department of the Environment, Victoria, BC, Canada.1975.

[43] D.F. Dickins and I. Buist, "Oil and Gas Under Sea Ice," Prepared by Dome Petroleum LtdCV-1, 1981, vol. I and II.

[44] H. M. Brown and R. H. Goodman, "In-situ Burning of Oil in Ice Leads," in *Arctic and Marine Oil Spill Program Technical Seminar, 9th Proceedings*, Edmonton, Alberta, 1986.

[45] N. K. Smith and A. Diaz, "In-place Burning of Crude Oil in Broken Ice- 1985 Testing at OHMSETT," *in Arctic and Marine Oilspill Program*, Ottawa, Canada, 1985.

[46] I. Buist and E. Twardus, "In-situ burning of uncontained oil slicks," in *Proceedings of the 7th Arctic and Marine Oil Spill Program (AMOP) Technical Seminar. Environment Canada*, 1984, pp. 127-154.

[47] I. Buist, "In Situ Burning for Oil Spills in Ice-Covered Waters," in *Proceedings of the Third INTERSPILL Conference and Exhibition*, 2004, no. 469.

[48] A. Bobra and M. Fingas, "The behaviour and fate of arctic oil spills," *Water science and technology*, vol. 18, no. 2, pp. 13-23, 1986.

[49] A. Fretheim, E. McLanahan, and S. Gudmundsdottir, "Arctic Council Arctic Marine Shipping Assessment (AMSA)," in *International Oil Spill Conference Proceedings (IOSC)*, 2011, vol. 2011, no. 1, p. abs427: American Petroleum Institute.

[50] S. Aggarwal, W. Schnabel, I. Buist, J. Garron, R. Bullock, R. Perkins, S. Potter, and D. Cooper, "Aerial application of herding agents to advance in-situ burning for oil spill response in the Arctic: A pilot study," *Cold Regions Science and Technology*, vol. 135, pp. 97-104, 2017.

[51] I. Buist, S. Potter, K. Trudel, A. H. Walker, D. Scholz, P. J. Brandvik, J. Fritt-Rasmussen, A. Allen, and P. Smith, "Report on In situ Burning in Ice-Affected Waters: A Technology Summary and Lessons from Key Experiments," Report from

Joint industry Programme on relevant scientific studies and laboratory and field experiments on th e use of in-situ burning in ice-affected offshore environments2013.

[52] N. Wu, T. Mosman, S. M. Olenick, and J. L. Torero, "Effect of Weathering on Piloted Ignition and Flash Point of a Slick of Oil," in *Arctic and Marine Oilspill Program (AMOP) Technical Seminar*, 1998.

[53] N. Mabile, "Controlled in-situ burning: Transition from alternative technology to conventional spill response option," *Proc. 35th AMOP Tech. Sem*, vol. 1, pp. 584-605, 2012.

[54] N. K. Smith and A. Diaz, "In-place Burning of Crude Oil in Broken Ice- 1985 Testing at OHMSETT," in *Arctic and Marine Oilspill Program*, Ottawa, Canada, 1985.

[55] H. M. Brown and R. H. Goodman, "In situ Burning of Oil in Ice Leads," in *Arctic and Marine Oil Spill Program Technical Seminar* vol. 9, ed, 1986.

[56] N. K. Smith and A. Diaz, "In-place Burning of Prudhoe Bay Oil in Broken Ice," in *Proceedings of the 1985 Oil Spill Conference,*, Washington D.C., 1985.

[57] N. K. Smith and A. Diaz., "In-place Burning of Crude Oil in Broken Ice " in *Proceeding of 1987 Oil Spill Conference*, Washington D.C., 1987, pp. 383-387: American Petroleum Institute.

[58] N. K. Diaz and A. Diaz, "In-place Burning of Prudhoe Bay Oil in Broken Ice," in *Proceedings of the 1985 Oil Spill Conference*, Washington D.C., 1985.

[59] D. S. Etkin, "Estimating cleanup costs for oil spills," in *International oil spill conference*, 1999, vol. 1999, no. 1, pp. 35-39: American Petroleum Institute.

[60] D. S. Etkin, "Worldwide analysis of marine oil spill cleanup cost factors," in *Arctic and marine oilspill program technical seminar*, 2000, vol. 1, pp. 161-174: Citeseer.

[61] A. R. Hall, "Pool Burning: a review," *Oxidation and Combustion Reviews*, vol. 6, pp. 169-225, 1973. Elsevier

[62] D. D. Evans, G. W. Mulholland, D. Gross, H. R. Baum, K. Saito, "Burning, Smoke Production and Smoke Dispersion From Oil Spill Combustion," in *Arctic and Marine Oilspill Program (AMOP) Technical Seminar 11th. Proceedings*, Ontario, Canada, 1988, pp. 41-87.

[63] L. van Gelderen, "In-Situ Burning of Crude Oil on Water: A study on the fire dynamics and fire chemistry in an Arctic context," PhD Dissertation, Technical University of Denmark, Department of Civil Engineering, 2017.

[64] I. Buist, "Window of Opportunity for In Situ Burning," in *In Situ Burning of Oil Spills Workshop Proceedings*, New Orleans, Louisiana, 1998.

[65] I. Buist, "Window-of-Opportunity for In Situ Burning," *Spill Science & Technology Bulletin,* vol. 8, no. 4, pp. 341-346., 2003.

[66] K.A. Murty, "Ignition of Liquid Fuels," The SFPE Handbook of Fire Protection Engineering; National Fire Protection Association, Quincy, MA, U.S.,1988.

[67] NIST, "Oil and Gas Technologies for the Arctic and Deepwater," Washington, DC: U.S. Congress, Office of Technology Assessment, OTA-O-270, 1985.

[68] EPPR, "Guide to Oil Spill Response in Snow and Ice Conditions. Emergency Prevention, Preparedness and Response " 2015.

[69] M. F. Fingas and B. P. Hollebone, "Review of behaviour of oil in freezing environments," *Marine Pollution Bulletin,* vol. 47, no. 9-12, pp. 333-340, 2003.

[70] W. G. Nelson and A. A. Allen, "The Physical Interaction and Cleanup of Crude Oil with Slush and Solid First Year Sea Ice," in *Proceedings of the Fifth Arctic and Marine Oilspill Program (AMOP) Technical Seminar,*, Edmonton, Canada, 1982, pp. 37-58.

[71] J. A. Fay, "Physical processes in the spread of oil on a water surface," in *International Oil Spill Conference,* 1971, vol. 1971, no. 1, pp. 463-467: American Petroleum Institute.

[72] E. Chen, "Arctic winter oil spill test," *Technical Bulletin,* vol. 68, p. 20, 1972.

[73] J. Glaeser, "A discussion of the future oil spill problem in the Arctic," in *International Oil Spill Conference*, 1971, vol. 1971, no. 1, pp. 479-484: American Petroleum Institute.

[74] M. Fingas and C. Brown, "Review of oil spill remote sensing," *Marine pollution bulletin,* vol. 83, no. 1, pp. 9-23, 2014.

[75] S. Vefsnmo and B. Johannessen, "Experimental oil spill in the Barents Sea. Drift and spread of oil in broken ice," Norsk Hydroteknisk Lab.1994.

[76] I. Singsaas, P. J. Brandvik, P. S. Daling, M. Reed, and A. Lewis, "Fate and behaviour of oils spilled in the presence of ice-a comparison of the results from recent laboratory, meso-scale flume and field tests," *Environmnet Canada,*, vol. 1, pp. 355-370, 1994.

[77] P. J. Brandvik and L.-G. Faksness, "Weathering processes in Arctic oil spills: Meso-scale experiments with different ice conditions," *Cold Regions Science and Technology,* vol. 55, no. 1, pp. 160-166, 2009.

[78] P. J. Brandvik and L. Faksness, "Weathering processes in Arctic oil spills: Meso-scale experiments with different ice conditions," *Cold Regions Science and Technology,* vol. 55, no. 1, pp. 160-166, 2009.

[79] L. van Gelderen, L. M. Malmquist, and G. Jomaas, "Vaporization order and burning efficiency of crude oils during in-situ burning on water," *Fuel,* vol. 191, pp. 528-537, 2017.

[80] I. Buist, K. Trudel, J. Morrison, and D. Aurand, "Laboratory studies of the properties of in-situ burn residues," in *International oil spill conference*, 1997, vol. 1997, no. 1, pp. 149-156: American Petroleum Institute.

[81] B. Trudel, I. Buist, D. Schatzke, and D. Aurand, "Laboratory studies of the properties of in-situ burn residues: chemical composition of residues," 1996.

[82] H. Farmahini Farahani, "A study on burning of crude oil in ice cavities," MS Thesis, Fire Protection Engineering, Worcetser Polytechnic Institute, 2014.

[83] M. Fingas, *Handbook of oil spill science and technology*. John Wiley & Sons, 2014.

[84] T. R. Buhite, "Cleanup of a cold weather terrestrial pipeline spill," in *International Oil Spill Conference*, 1979, vol. 1979, no. 1, pp. 367-369: American Petroleum Institute.

[85] X. Shi, P. Bellino, A. Simeoni, and A. Rangwala, "Experimental study of burning behavior of large-scale crude oil fires in ice cavities," *Fire Safety Journal,* vol. 79, pp. 91-99, 2016.

[86] P. W. Bellino, A.S. Rangwala, and M.R. Flynn, "A study of in situ burning of crude oil in an ice channel," *Proc. Combust. Inst.*, vol. 34, no. 2, pp. 2539-2546., 2013.

[87] H. Farmahini Farahani, X. Shi, A. Simeoni, and A. S. Rangwala, "A study on burning of crude oil in ice cavities," *Proc. Combust. Inst.*, vol. 35, no. 3, pp. 2699-2706., 2014.

[88] S. Potter, I. Buist, K. Trudel, D. Dickins, and E. Owens, "Spill response in the Arctic offshore," *Prepared for tthe American Petroleum Institute and the Joint Industry Programme on Oil Spill Recovery in Ice. American Petroleum Institute, Washington, DC,* 2012.

[89] I. Buist, J. McCourt, S. Potter, S. Ross, and K. Trudel, "In situ burning," *Pure and applied chemistry,* vol. 71, no. 1, pp. 43-65, 1999.

[90] J. L. Glaeser and G. P. Vance., "A Study of the Behavior of Oil Spills in the Arctic" Final Report to the USCG Office of Research & Development, Applied Technology Division, Groton, CT, U.S. Project Number 714708/A/001,002.," 1971.

[91] H. E. Huppert, R. S. J. Sparks, J. S. Turner, and N. T. Arndt, "Emplacement and cooling of komatiite lavas," *Nature,* vol. 309, no. 5963, pp. 19-22, 1984.

[92] H. Ishida, K. Sato, K. Hokari, and T. Hara, "Flame spread over fuel-spilled and/or snow-covered asphalt road," *Journal of Fire Sciences*, vol. 14, no. 1, pp. 50-66, 1996.

[93] P. W. Bellino, "A Study of Spreading and In Situ Burning of Oil in an Ice Channel," MS Thesis, Worcester Polytechnic Institute, 2012.

[94] X. Shi, R. T. Ranellone, H. Sezer, N. Lamie, L. Zabilansky, K. Stone, and A. S. Rangwala, "Influence of ullage to cavity size ratio on in-situ burning of oil spills in ice-infested water," *Cold Regions Science and Technology,* vol. 140, pp. 5-13, 2017.

[95] D. Drysdale, *An Introduction to Fire Dynamics*, 3rd ed. John Wiley & Sons Ltd, 2011.

[96] F. A. Williams, "Urban and wildland fire phenomenology," *Progress in Energy and Combustion Science,* vol. 8, no. 4, pp. 317-354, 1982.

[97] H. C. Hottel, "Review: Certain Laws Governing the Diffusive Burning of Liquids," *Fire Research Abstracts and Reviews,* vol. 1, pp. 41-43, 1959.

[98] A. Nakakuki, "Heat Transfer Mechanisms in Liquid Pool Fires," *Fire Safety Journal,* vol. 13, pp. 339-363., 1994.

[99] A. Nakakuki, "Heat Transfer in Small Scale Pool Fires," *Combustion and Flame* vol. 96, pp. 311-324, 1994.

[100] P. Joulain, "Convective and radiative transport in pool and wall fires: 20 years of research in Poitiers," *Fire Safety Journal,* vol. 26, no. 2, pp. 99-149, 1996.

[101] A. Hamins , S. Fischer , and T. Kashiwagi "A global model for predicting the burning rates of liquid pool fires," 1999.

[102] V. Babrauskas, "Estimating Large Pool Fires Burning Rates," *Fire Technology,* vol. 19, p. 251, 1983.

[103] E.M. Twardus and T. A. Brzustowski, "The burning of crude oil spilled on water," *Adchivum Combustionis, Polish Acad. Sci,* vol. 20, no. 1-2, pp. 49-60, 1981.

[104] J. P. Garo, H. Koseki, J.-P. Vantelon, and C. Fernandez-Pello, "Combustion of liquid fuels floating on water," *Thermal Science,* vol. 11, no. 2, pp. 119-140, 2007.

[105] M. Arai, K. Saito, and R. Altenkirch, "A Study of Boilover in Liquid Pool Fires Supported on Water Part I: Effects of a Water Sublayer on Pool Fires," *Combustion Science and Technology,* vol. 71, no. 1-3, pp. 25-40., 1990.

[106] E. S. Artemenko and V. I. Blinov, "Burning of liquid in vessels with change of level," *Combustion, Explosion, and Shock Waves,,* vol. 4, p. 39, 1968.

[107] V.I. Blinov and G. N. Khudiakov, "Diffusion Burning of Liquids," U.S. Army translation NIST No. AD2967621961.

[108] C. C. Ndubizu, Ramaker, D. E., Tatem, P. A. & Williams, F. W., "A model of freely burning pool fires," *Combustion Science and Technology*, vol. 31, p. 233, 1983.

[109] B. Z. Dlugogorski and M. Wilson, "Effect of Ullage on Properties of Small-scale Pool Fires," in *Asia-Oceania Association for Fire science and Technology*, Khabarovsk, 1995.

[110] A. Hamins, S. Fischer, and T. Kashiwagi, "Heat Feedback to the Fuel Surface in Pool Fires," *Combustion Science and Technology*, vol. 97, no. 1-3, pp. 37-62, 1994.

[111] A. Nakakuki, "Liquid fuel fires in the laminar flame region," *Combustion and Flame*, vol. 23, no. 3, pp. 337-346, 1974.

[112] A. Nakakuki, "Heat Transfer in Hot-Zone-Forming Pool Fires," *Combustion and Flame* vol. 109, pp. 353-369, 1997.

[113] M. Choi, A. Hamins, H. Rushmeier, and T. Kashiwagi, "Simultaneous optical measurement of soot volume fraction, temperature, and CO 2 in heptane pool fire," in *Symposium (International) on Combustion*, 1994, vol. 25, no. 1, pp. 1471-1480: Elsevier.

[114] M. Klassen, J. P. Gore, Y. Sivathanu, A. Hamins, and T. Kashiwagi, "Radiative heat feedback in a toluene pool fire," in *Symposium (International) on Combustion*, 1992, vol. 24, no. 1, pp. 1713-1719: Elsevier.

[115] L. Hu, S. Liu, and L. Wu, "Flame radiation feedback to fuel surface in medium ethanol and heptane pool fires with cross air flow," *Combustion and Flame*, vol. 160, no. 2, pp. 295-306, 2013.

[116] A. Hamins, S. Ficher, T. Kashiwagi, "Heat Feedback to the Fuel Surface in Pool Fires," *Combustion Science and Technology*, vol. 97, no. 1-3, pp. 37-62, 1994.

[117] A. T. Modak, "Thermal radiation from pool fires," *Combustion and Flame*, vol. 29, pp. 177-192, 1977.

[118] P. Joulain, "The Behavior of Pool Fires :State of the Artc and New Insights," *Symposium (International) on Combustion*, vol. 27, pp. 2691–2706, 1998.

[119] L. A. Gritzo, V. F. Nicolette, S. R. Tieszen, J. L. Moya, and J. Holen, "Heat transfer to the fuel surface in large pool fires," *Transport Phenomenon in Combustion*, 1995.

[120] J. L. Torero, S. M. Olenick, J. P. Garo, and J. P. Vantelon, "Determination of the Burning Characteristics of a Slick of Oil on Water," *Spill Science & Technology Bulletin*, vol. 8, no. 4, pp. 379-390, 2003.

[121] K. S. Mudan and P. A. Croce, " Fire hazard calculations for large open hydrocarbon fires " in *The SFPE Handbook of Fire Protection Engineering"* 2nd edition, 1995, pp. 3197-3240.

[122] L. A. Gritzo, V. F. Nicolette, S. R. Tieszen, J. L. Moya, J. Holen, *Heat transfer to the fuel surface in large pool fires* (Transport Phenomena in Combustion). Taylor and Francis Publishers, 1996.

[123] G. Cox, *Combustion Fundamentals of Fire*. Academic Press, London, 1995.

[124] M. G. Zabetakis, "Flammability characteristics of combustible gases and vapors," Bureau of Mines, Washington D.C., 1965.

[125] J. Burgoyne, A. Roberts, and P. Quinton, "The spread of flame across a liquid surface. I. The induction period," *Proceedings of the Royal Society of London. Series A. Mathematical and Physical Sciences,* vol. 308, no. 1492, pp. 39-53., 1968.

[126] R. Mackinven, J. Hansel, and I. Glassman, "Influence of laboratory parameters on flame spread across liquid fuels," *Combustion Science and Technology,* vol. 1, no. 4, pp. 293-306, 1970.

[127] I. Glassman and J.G. Hansel, *Fire Research Abstracts and Reviews,* vol. 10, pp. 217-234., 1968.

[128] H. D. Ross, "Ignition of and Flame Spread Over Laboratory-Scale Pools of Pure Liquid Fuels," *Prog. Energy Combust. Sci.,* vol. 20, pp. 17-63., 1994.

[129] I. Glassman and F. Dryer, "Flame Spreading Across Liquid Fuels," *Fire Safety Journal,* vol. 3 pp. 123 - 138., 1980/81.

[130] F. J. Miller and H. D. Ross, "Further observations of flame spread over laboratory-scale alcohol pools," in *Symposium (International) on Combustion*, 1992, vol. 24, no. 1, pp. 1703-1711.: Elsevier.

[131] R. Murad, J. Lamendola, H. Isoda, and M. Summerfield, " A Study of Some Factors Influencing the Ignition of a Liquid Fuel Pool " *Combustion and Flame,* vol. 1, no. 15, pp. 289-298., 1970.

[132] R. McKinven, J. G. Hensel, and I. Glassman, "Influence of laboratory parameters on flame spread over liquid surfaces," *Combustion Science and Technology,* vol. 1, pp. 293-306., 1970.

[133] A. Ito, D. Masuda , and K. Saito, "A Study of Flame Spread Over Alcohols Using Holographic Interferometry," *Combustion and Flame,* vol. 83, pp. 375-389., 1991.

[134] Y. Matsumoto and T. Saito, "Propagation of pool burning," *Journal of Japanese Society of Mechanical Engineers,* vol. 46, p. 998, 1980.

[135] D. N. Schiller and W. A. Sirignano, "Buoyant-Thermocapillary Flow with Nommiform Supra-Heating: I. Liquid-Phase Behavior," *J. Thermophysics,* vol. 6, no. 1, pp. 105-112., 1992.

[136] E. Degroote, "Control Parameters of Flame Spreading in a Fuel Container," *Journal of Thermal Analysis and Calorimetry,* vol. 87 no. 1, pp. 149–151, 2007.

[137] E. Degroote and P. L. G. Ybarra, "Flame Propagation Over Liquid Alcohols, Part II. Steady propagation regimes," *Journal of Thermal Analysis and Calorimetry,* vol. 80, pp. 549–553, 2005.

[138] E. Degroote and P. L. G. Ybarra, "Flame Propagation Over Liquid Alcohols Part III. Pulsating regime," *Journal of Thermal Analysis and Calorimetry,* vol. 80, pp. 555–558, 2005.

[139] E. Degroote and P. L. García Ybarra, "Flame Propagation Over Liquid Alcohols, Part I. Experimental results," *Journal of Thermal Analysis and Calorimetry,* vol. Vol. 80 no. 1, pp. 541–548, 2005.

[140] H. Tsuji and E. Osawa, "An experimental study on flame spread over liquid surfaces," in *Tenth Symposium (Japanese) on Combustion*, 1972, pp. 55-58.

[141] N. Wu, T. Mosman, S. M. Olenick, and J. L. Torero, "Effect of Weathering on Piloted Ignition and Flash Point of a Slick of Oil.," in *Arctic and Marine Oilspill Program (AMOP) Technical Seminar*, Ottawa, 1998.

[142] K. E. Torrance and R. L. Torrance, "Fire spread over liquid fuels: Liquid phase parameters," *Symposium (International) on Combustion,* vol. 15, no. 1, pp. 281-287., 1975.

[143] T. Yumoto, A. Takahashi, and T. Handa, "Combustion Behavior of Liquid Fuel in a Small Vessel: Effect of Convective Motion in the Liquid on Burning Rate of Hexane in the Early Stage of Combustion," *Combustion and Flame* vol. 30, pp. 33-43., 1997.

[144] A. Vali, D. S. Nobes, and L. W. Kostiuk, "Transport phenomena within the liquid phase of a laboratory-scale circular methanol pool fire," *Combustion and Flame,* vol. 161, no. 4, pp. 1076-1084., 2014.

[145] A. Vali, D. S. Nobes, and L. W. Kostiuk, "Characterization of flow field within the liquid phase of a small pool fire using particle image velocimetry technique," *Experimental Thermal and Fluid Science,* vol. 75, pp. 228-234., 2016.

[146] B. M. Carpenter and G. M. Homsy, "Combined buoyant-thermocapillary flow in a cavity," *Journal of Fluid Mechanics,* vol. 207, pp. 121-132, 1989.

[147] A. Bejan and C. Tien, "Laminar natural convection heat transfer in a horizontal cavity with different end temperatures," *Journal of Heat Transfer,* vol. 100, no. 4, pp. 641-647, 1978.

[148] A. Bejan, "A synthesis of analytical results for natural convection heat transfer across rectangular enclosures," *International Journal of Heat and Mass Transfer,* vol. 23, no. 5, pp. 723-726, 1980.

[149] J. Straub, "The role of surface tension for two-phase heat and mass transfer in the absence of gravity," *Experimental Thermal and Fluid Science,* vol. 9, no. 3, pp. 253-273., 1994.

[150] M. F. Schatz and G. P. Neitzel, "Experiments on thermocapillary instabilities," *Annual review of fluid mechanics,* vol. 33, no. 1, pp. 93-127., 2001.

[151] M. G. Braunsfurth and G. M. Homsy, "Combined thermocapillary-buoyancy convection in a cavity. Part II. An experimental study," *Physics of Fluids* vol. 9, no. 5, pp. 1277-1286., 1997.

[152] P. Gillon and G. M. Homsy, "Combined thermocapillary-buoyancy convection in a cavity: An experimental study," *Physics of Fluids (1994-present),* vol. 8, no. 11, pp. 2953-2963., 1996.

[153] B. M. CARPENTER and G. M. HOMSY, "Combined buoyant-thermocapillary flow in a cavity," *J. Fluid Mech.,* vol. 207 pp. 121-132, 1986.

[154] D. Schwabe and J. Metzger, "Coupling and separation of buoyant and thermocapillary convection," *Journal of Crystal Growth,* vol. 97, no. 1, pp. 23-33., 1989.

[155] J.-F. Mercier and C. Normand, "Buoyant-thermocapillary instabilities of differentially heated liquid layers," *Physics of Fluids (1994-present),* vol. 8, no. 6, pp. 1433-1445, 1996.

[156] T. Song, "Comparison of buoyancy and surface tension in a square cavity," *KSME Journal,* vol. 5, no. 1, pp. 10-15., 1991.

[157] D. Villers and J. Platten, "Coupled buoyancy and Marangoni convection in acetone: experiments and comparison with numerical simulations," *Journal of Fluid Mechanics,* vol. 234, pp. 487-510, 1992.

[158] E. Favre, L. Blumenfeld, and F. Daviaud, "Instabilities of a liquid layer locally heated on its free surface," *Physics of Fluids (1994-present),* vol. 9, no. 5, pp. 1473-1475, 1997.

[159] F. Preisser, D. Schwabe, and A. Scharmann, "Steady and oscillatory thermocapillary convection in liquid columns with free cylindrical surface," *Journal of Fluid Mechanics*, vol. 126, pp. 545-567, 1983.

[160] F. Daviaud and J. M. Vince, "Traveling waves in a fluid layer subjected to a horizontal temperature gradient," *Physical review E*, vol. 48, no. 6, p. 4432, 1993.

[161] C. Jones, "Hydrocarbons: Physical Properties and their Relevance to Utilisation, 2010.

[162] R.C.Reid, J.M. Praustinz, and B.E. Poling, *The Properties of Gasses & Liquids,*, 4th ed. McGraw-Hill, Inc, 1987.

[163] C. a. Sternling and L. Scriven, "Interfacial turbulence: hydrodynamic instability and the Marangoni effect," *AIChE Journal*, vol. 5, no. 4, pp. 514-523, 1959.

[164] R. Hosseini and M. Rahaeifard, "Experimental investigation and theoretical modeling of ice-melting processes," *Experimental Heat Transfer*, vol. 22, no. 3, pp. 144-162, 2009.

[165] K. Sefiane and C. A. Ward, "Recent advances on thermocapillary flows and interfacial conditions during the evaporation of liquids," *Advances in colloid and interface science*, vol. 134, pp. 201-223, 2007.

[166] D. N. Schiller and W. A. Sirignano, "Buoyant- Thermocapillary flow with nonuniform supra heating: II. Two phase behavior," *J. Thermophysics*, vol. 6, no. 1, pp. 113-120., 1992.

[167] N. Zhang, "Surface tension-driven convection flow in evaporating liquid layers," *Surface Tension-driven Flows and Applications, Research Signpost*, 2006.

[168] T. Doi and J. N. Koster, "Thermocapillary convection in two immiscible liquid layers with free surface," *Physics of Fluids A: Fluid Dynamics (1989-1993)*, vol. 5, no. 8, pp. 1914-1927, 1993.

[169] S. Ostrach, "Low-gravity fluid flows," *Annual Review of Fluid Mechanics*, vol. 14, no. 1, pp. 313-345., 1982.

[170] C. A. Schneider, W. S. Rasband, and K. W. Eliceiri, "NIH Image to ImageJ: 25 years of image analysis," *Nature methods*, vol. 9, no. 7, pp. 671-675., 2012.

[171] M. Raffel, C. E. Willert, S. Wereley, and J. Kompenhans, *Particle image velocimetry: a practical guide*. Springer, 2013.

[172] H. Farmahini Farahani, G. Jomaas, and A. S. Rangwala, "Effects of convective motion in n-octane pool fires in an ice cavity," *Combustion and Flame*, vol. 162, no. 12, pp. 4643-4648., 2015.

[173] D. Schwabe, A. Cramer, J. Schneider, S. Benz, and J. Metzger, "Experiments on the multi-roll-structure of thermocapillary flow in side-heated thin liquid layers," *Advances in Space Research,* vol. 24, no. 10, pp. 1367-1373., 1999.

[174] T. Inamura, K. Saito, and K. Tagavi, "A study of boilover in liquid pool fires supported on water. Part II: Effects of in-depth radiation absorption," *Combustion science and technology,* vol. 86, no. 1-6, pp. 105-119., 1992.

[175] A. Ito, K. Saito, and T. Inamura, "Holographic interferometry temperature measurements in liquids for pool fires supported on water," *Journal of heat transfer,* vol. 114, no. 4, pp. 944-949, 1992.

[176] G. Falkovich and A. Pumir, "Intermittent distribution of heavy particles in a turbulent flow," *Physics of Fluids* vol. 16, no. 7, pp. L47-L50., 2004.

[177] R. I. Emori and K. Saito, "A study of scaling laws in pool and crib fires," *Combustion science and technology,* vol. 31, no. 5-6, pp. 217-231, 1983.

[178] L. van Gelderen, J. Fritt-Rasmussen, and G. Jomaas, "Effectiveness of a chemical herder in association with in-situ burning of oil spills in ice-infested water," *Marine Pollution Bulletin,* vol. 115, no. 1, pp. 345-351., 2017.

[179] S. M. Pimputkar and S. Ostrach, "Convective effects in crystals grown from melt," *Journal of Crystal Growth,* vol. 55, no. 3, pp. 614-646., 1981.

[180] V. Polezhaev, "Hydrodynamics, heat and mass transfer during crystal growth," in *Growth and Defect Structures*: Springer, 1984, pp. 87-147.

[181] H. Farmahini Farahani, W. U. R. Alva, A. S. Rangwala, and G. Jomaas, "Convection-driven melting in an n-octane pool fire bounded by an ice wall," *Combustion and Flame,* vol. 179, pp. 219-227., 2017.

[182] A. Vali, D. S. Nobes, and L. W. Kostiuk, "Effects of altering the liquid phase boundary conditions of methanol pool fires," *Experimental Thermal and Fluid Science,* vol. 44, pp. 786-791., 2013.

[183] S. Chakraborty, S. Sarkar, and P. Dutta, "Scaling analysis of momentum and heat transport in gas tungsten arc weld pools," *Science and technology of welding and joining,* vol. 7, no. 2, pp. 88-94., 2002.

[184] N. Chakraborty, "Thermal transport regimes and effects of Prandtl number in molten pool transport in laser surface melting processes," *Numerical Heat Transfer, Part A: Applications,* vol. 53, no. 3, pp. 273-294., 2007.

[185] K. Takahashi, A. Ito, Y. Kudo, T. Konishi, and K. Saito, "Scaling analysis on pulsating flame spread over liquids," *International Journal of Chemical Engineering,* 2008.

[186] S. Kuwana, H. Tamizu, A. Ito, and H. Torikai, "Flame Spread over Liquid Fuel on a Water Layer-Basic Research on Tsunami Fire," *Open Journal of Safety Science and Technology,* vol. 7, no. 01, p. 11., 2017.

[187] M. R. Riazi and Y. A. Roomi, "Use of the refractive index in the estimation of thermophysical properties of hydrocarbons and petroleum mixtures," *Industrial & engineering chemistry research,* vol. 40, no. 8, pp. 1975-1984., 2001.

[188] Y. Okano, M. Itoh, and A. Hirata, "Natural and Marangoni convections in a two-dimensional rectangular open boat," *Journal of chemical engineering of Japan,* vol. 22, no. 3, pp. 275-281., 1989.

[189] K. Li, B. Xun, and W. Hu, "Some bifurcation routes to chaos of thermocapillary convection in two-dimensional liquid layers of finite extent," *Physics of Fluids,* vol. 28, no. 5, p. 054106., 2016.

[190] H. D. Ross and F. J. Miller, "Detailed Experiments of Flame Spread Across Deep Butanol Pools " *Symposium (International) on Combustion* vol. 26, pp. 1327–1334., 1996.

[191] G. Singh, S. Chander, and A. Ray, "Heat transfer characteristics of natural gas/air swirling flame impinging on a flat surface," *Experimental Thermal and Fluid Science,* vol. 41, pp. 165-176., 2012.

[192] D. N. Schiller, H. Ross, and W. A. Sirignano, "Computational predictions of flame spread over alcohol pools," in *31st Aerospace Sciences Meeting*, 1993, p. 825.

[193] H. A. Abderrahmane, M. Fayed, H. D. Ng, and G. H. Vatistas, "The Effect of Viscosity on the Rotating Waves and Polygonal Patterns within a Hollow Vortex Core," *Experimental Thermal and Fluid Science,* vol. 87, pp. 104–108., 2017.

[194] A. Bejan, *Convection heat transfer*, 4th ed. John wiley & sons, 2013.

[195] K. Torrance and R. Mahajan, "Fire spread over liquid fuels: liquid phase parameters," in *Symposium (International) on Combustion,* 1975, vol. 15, no. 1, pp. 281-287: Elsevier.

[196] L. van Gelderen and G. Jomaas, "The Parameters Controlling the Burning Efficiency of In-Situ Burning of Crude Oil on Water," in *40th AMOP Technical Seminar on Environmental Contamination and Response*, 2017.

[197] M. Fingas, "Review of the North Slope Oil properties relevant to environmental assessment and prediction," *Spill Science, Edmonton, Alberta, Canada*, 2010.

[198] L. Hu, "A review of physics and correlations of pool fire behaviour in wind and future challenges," *Fire Safety Journal*, 2017.

[199] D. D. Evans, G. W. Mulholland, H. R. Baum, W. D. Walton, and K. B. McGrattan, "In situ burning of oil spills," *Journal of research of the National Institute of Standards and Technology*, vol. 106, no. 1, p. 231, 2001.

[200] H. Pasdarshahri, G. Heidarinejad, and K. Mazaheri, "Large eddy simulation on one-meter methane pool fire using one-equation sub-grid scale model," in *MCS*, vol. 7, pp. 11-15, 2011.

[201] N. Pinel and C. Bourlier, "Unpolarized infrared emissivity of oil films on sea surfaces," in *Geoscience and Remote Sensing Symposium*, vol. 2, pp. II-85-II-88, 2009.

[202] J. R. Payne, G. D. Mcnabb Jr, and J. R. Clayton. Jr, "Oil-weathering behavior in Arctic environments," *Polar Research*, vol. 10, no. 2, pp. 631-662, 1991.

Appendix

Few pictures are presented here to show the setup of the Particle Image velocimetry study presented in chapter 4.

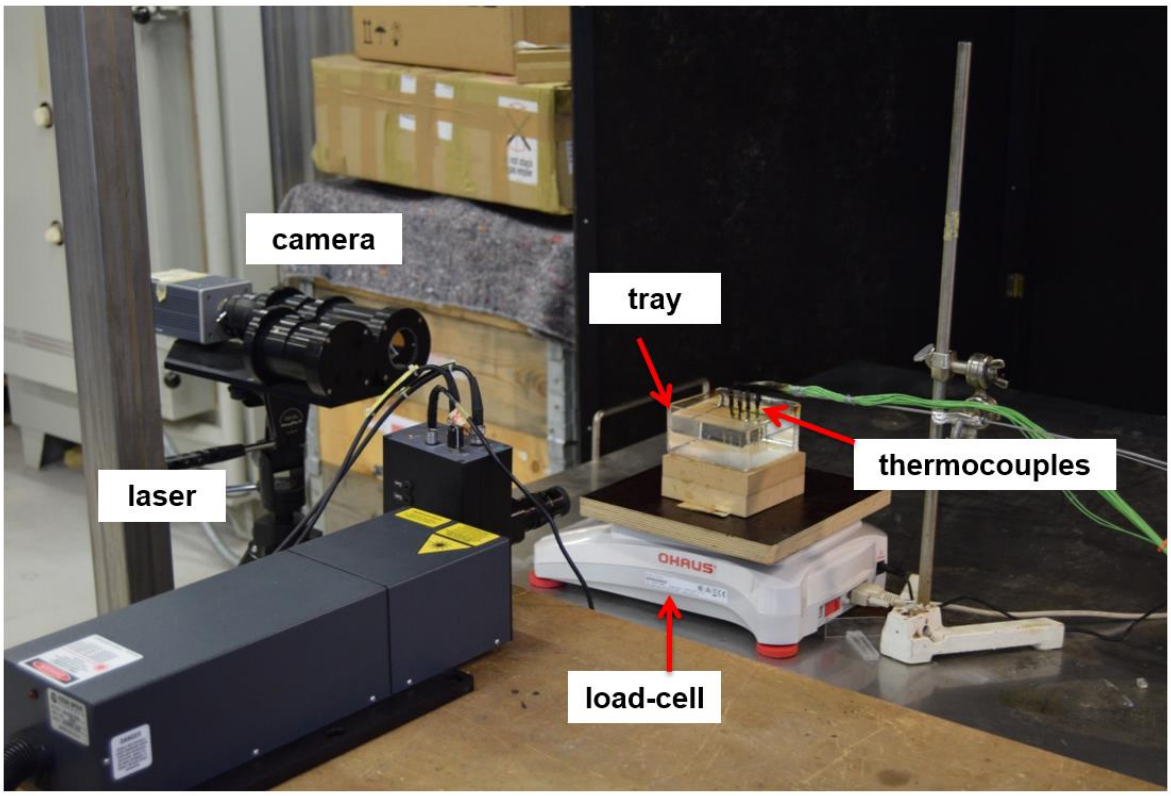

Figure A.1: A picture of PIV setup used in the study of chapter 4.

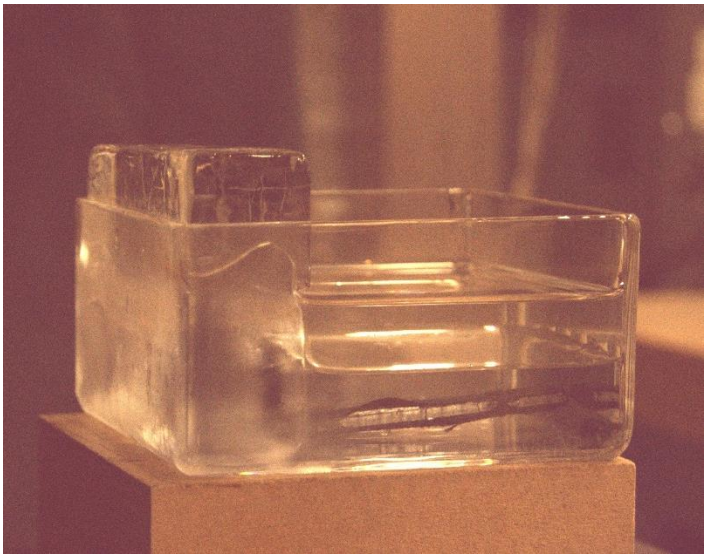

Figure A.2: The square glass containing n-octane and ice on the back wall.

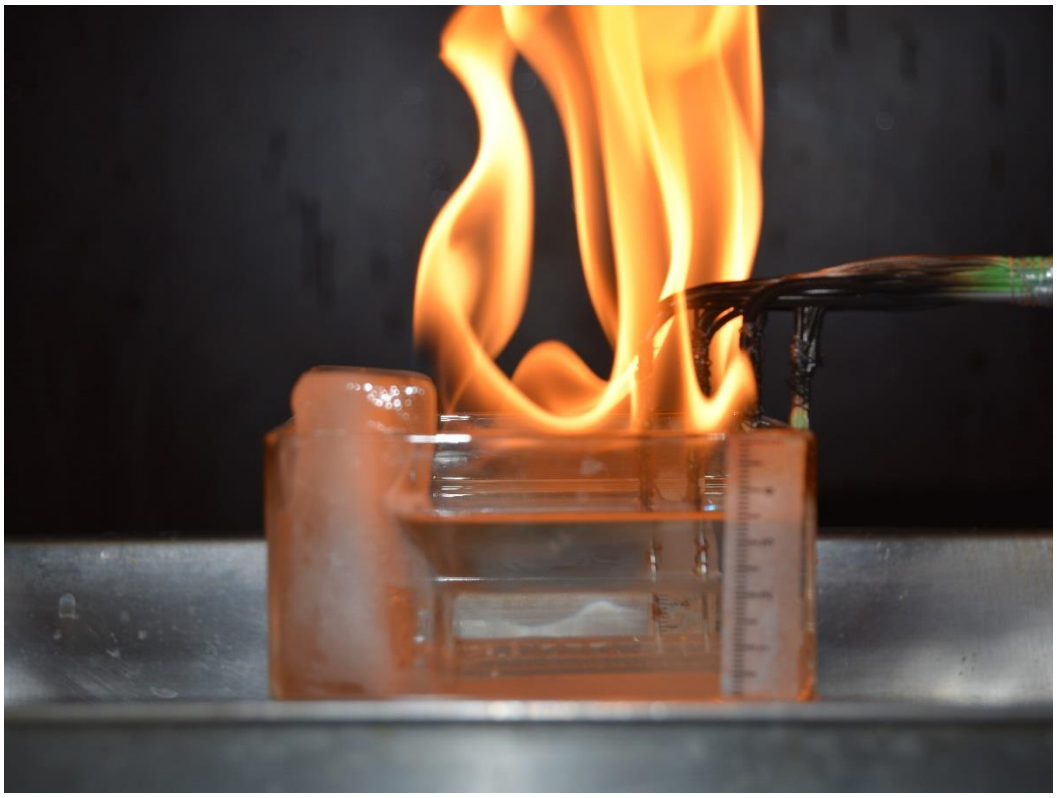

Figure A.2: The square glass containing n-octane burning and ice on the left wall.

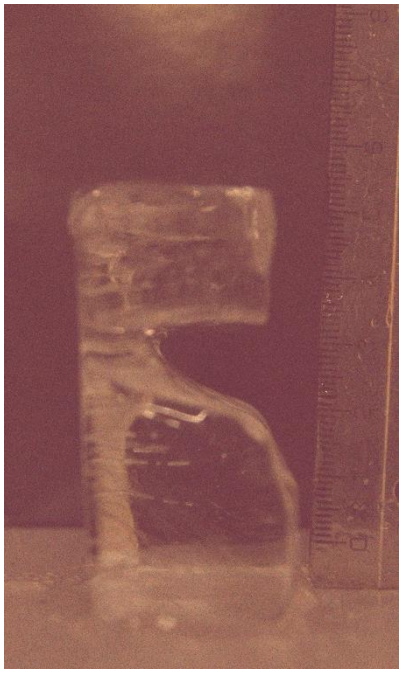

Figure A.4: The ice wall is removed halfway through one of the experiments.

The Matlab code for the least square regression method that was developed to define the parameters a, b_1, b_2, and b_3 of Equation 6.18.

```
% This code is written to find the proper values
%of the parameters in Equation 6.18 of the lateral cavity scaling%

clc
clear all
close all

%Information below are the initial diameter of the pool fire denoted as D
%and the intrusion length obtained from experiments denoted by L%

D =
[0.05,0.057,0.057,0.07,0.095,0.095,0.1,0.142,0.15,0.25,0.25,0.365,0.365,0
.365,1.10,1.05,1.03,1.00,1.00,1.50;];
L =
[0.05,0.05050,0.04750,0.03,0.03750,0.06500,0.04500,0.06,0.06,0.04500,0.06
,0.05500,0.07,0.08750,0.12,0.07,0.1,0.2,0.28,0.2;];

%To calculate the intrusion length by the correlation that is obtained
from
%the scaling analysis constants and the related
%properties of the liquid fuel and ice are defined here%

%constants:%
%thermal depth ,d, in m%
de = 0.004;
%heat feedback fraction%
Kai = 0.003;
```

```
%Flame Temperature in K%
Tf = 1200;
%density of air in kg/m^3%
airdensity = 1.225;
%Heat capacity of air in kJ/kg.K
aircp = 1.005;
%ambient Temperature in K%
Tamb = 293;
%acceleration due to gravity in m/s^2%
g = 9.8;
%characteristic length in m%
delta2 = 0.08;

% Now to calculate the first term of equation 6.18 called here as alpha%

%surface tension gradient is in kgm/Ks^2 %
SigmaT =
[0.0700,0.092600,0.108800,0.09260,0.0700,0.07,0.07,0.080,0.07000,0.070,0.
07,0.0700,0.070,0.070,0.070,0.0700,0.07000,0.0700,0.0700,0.0700;];
%Dynamic viscosity in kg/ms%
Mu =
[0.0010850,0.000542,0.000622,0.000542,0.010850,0.0010850,0.0108500,0.0080
,0.001085,0.01085,0.001085,0.001085,0.0010850,0.001085,0.0010850,0.001085
0,0.00108500,0.00108500,0.00108500,0.0010850];
%Thermal diffusivy in m/s^2%
Therdif = [6.60733e-08,8.66e-08,1.01326e-07,8.660e-08,6.60733e-
08,6.60733e-08,6.607330e-08,7.610e-08,6.607330e-08,6.60733e-08,6.607330e-
08,6.607330e-08,6.6073300e-08,6.607330e-08,6.6073300e-08,6.607330e-
08,6.60733e-08,6.60733e-08,6.60733e-08,6.60733e-08;];

alpha = SigmaT./(Mu.*Therdif);

% Now to calculate the second term called here as theta%
qx = Kai*1.27*airdensity*aircp*((Tamb*g*(Tf-Tamb))^0.5)*D.^0.5;
%Thermal conductivity of liquid fuel in kW/mK%
Kl =
[0.000132,0.0001272,0.0001421,0.00012720,0.000132,0.000132,0.000132,0.000
132,0.000132,0.000132,0.000132,0.000132,0.000132,0.0001320,0.000132,0.000
1320,0.0001320,0.0001320,0.0001320,0.000132;];

theta = (de.*qx./Kl);

% Now to calculate the third term called here as gamma%

%time of the experiments in seconds%
t=
[480,600,590,180,350,375,450,700,440,220,340,180,260,320,310,200,250,305,
370,230;];
%Density of ice in kg/m^3%
rhoice=
[916.7,916.7,916.7,916.7,916.7,916.7,916.7,916.7,916.7,916.7,916.7,916.7,
916.7,916.7,916.7,916.7,916.7,916.7,940.7,940.7,940.7;];
%Thermal conductivity of ice in kW/mK%
Kice=
[0.00222,0.00222,0.00222,0.00222,0.00222,0.00222,0.00222,0.00222,0.00222,
0.00222,0.00222,0.00222,0.00222,0.00222,0.00222,0.00222,0.00222,0.003,0.0
03,0.003;];
%Latent heat of fusion/melting of ice kJ/kg%
```

```
Lice=
[333.55,333.55,333.55,333.55,333.55,333.55,333.55,333.55,333.55,333.55,33
3.55,333.55,333.55,333.55,333.55,333.55,333.55,300.55,300.55,300.55;];


gamma = (Kice.*t)./(rhoice.*Lice);

%now, to calculate parameters a b1 b2 b3 as shown in chapter 6 we define
%the following regression parameters within a certain domain. Note: these
domains were changed and R^2 value was examined to obtain highest value
of R^2%

n = 20; % length of the array
a = linspace(0.2,0.5,n);
b = linspace(0.1,0.2,n);
c = linspace(1,1.5,n);
d = linspace(0.7,1,n);


for i = 1:length(a)
    for j = 1:length(b)
        for k = 1:length(c)
            for m = 1:length(d)

                Lc  =
a(i).*alpha.^b(j).*theta.^c(k).*gamma.^d(m)*((1/delta2)^0.333);
                 error(i,j,k,m) = sum(sqrt(((L-Lc).^2)));
            end
        end
    end
end


%% find the indexes that corresponds the minumum of the error%
[C,I] = min(error(:));
[I1,I2,I3,I4] = ind2sub(size(error),I);

amin = a(I1)
bmin = b(I2)
cmin = c(I3)
dmin = d(I4)

%The regression parameters that lead to lowest deviation from experiments
are identified and can be used to calculate the theoretical intrusion
length%
Lcmin = amin.*alpha.^bmin.*theta.^cmin.*gamma.^dmin*((1/delta2)^0.333);
Rsqured = floor((1-sum((L-Lcmin).^2)/sum((Lcmin-mean(L)).^2))*1000)/1000;

%The theoretical model now can be plotted against the experimental
results of intrusion length%

figure1 = figure;

% Create axes
axes1 = axes('Parent',figure1,...
    'Position',[0.13 0.11 0.775 0.750940695296523],...
    'LineWidth',2,...
    'FontSize',12);
```

```
box(axes1,'on');
hold(axes1,'all');

% Create multiple lines using matrix input to plot
plot1 = plot(D,[L;Lcmin],'Parent',axes1,'LineStyle','none');
set(plot1(1),'MarkerFaceColor',[0 0 1],'Marker','o',...
    'DisplayName','Experimental');
set(plot1(2),'MarkerFaceColor',[1 0 0],'Marker','square',...
    'DisplayName','Model');

% Create xlabel
xlabel(' Diameter (m)','FontSize',14);

% Create ylabel
ylabel('Intrusion length (m)','FontSize',14);

str = 'R^2 =  ';
str1 = mat2str(Rsqured);
strtitle = strcat(str,str1);
title(strtitle,'FontSize',14);

% Create legend
legend1 = legend(axes1,'show');
set(legend1,'EdgeColor',[1 1 1],'YColor',[1 1 1],'XColor',[1 1 1],...
    'Position',[0.162670427832628 0.743012951601915 0.21015514809591
0.0940695296523517]);
```